Chiral perturbation theory calculation of pion production in nucleon-nucleon collisions

DISSERTATION

zur
Erlangung des Grades
"Doktor der Naturwissenschaften"

an der Fakultät für Physik und Astronomie
der Ruhr-Universität Bochum

von
Arseniy Filin

aus
Moskau

Bochum 2014

b.w.

1. Gutachter	Prof. Dr. Evgeny Epelbaum
2. Gutachter	Prof. Dr. Fred Myhrer
Datum der Disputation	16.07.2014

Abstract

Understanding of near-threshold pion production is of significant importance since it allows a direct test of chiral EFT, probes NN dynamics at intermediate energies and provides access to isospin violation in few-nucleon processes.

It has been known since years that neutral pion production in $pp \to pp\pi^0$ is the most challenging process since the experimental cross-section in this channel is suppressed by more than an order of magnitude, as compared to the charged channels near threshold. The experimental evidence is fully in line with the chiral suppression of the leading production operators in this channel and the important role of higher order effects, especially chiral loops.

We present the results of the full pion production operator near threshold calculated up-to-and-including next-to-next-to-leading order (NNLO) in chiral effective field theory. We include explicit Delta degrees of freedom and demonstrate that they provide essential contribution required to understand neutral pion production data. Analysis of chiral loops at NNLO reveals new mechanisms which are important, but haven't been considered so far.

We perform a complete calculation of charge symmetry breaking effects for the reaction $pn \to d\pi^0$ at leading order in chiral perturbation theory. A new leading-order operator is included. From our analysis we extract $\delta m_N^{\rm str}$, the strong contribution to the neutron–proton mass difference. The value obtained, $\delta m_N^{\rm str} = (1.5 \pm 0.8\ (\text{exp.}) \pm 0.5\ (\text{th.}))$ MeV, is consistent with the result based on the Cottingham sum rule and modern Lattice simulations. This agreement provides a non–trivial test of our current understanding of the chiral structure of QCD.

The methods developed in this work can be helpful in the study of charge symmetry breaking in $dd \to \alpha\pi^0$.

Contents

Introduction

Strong interaction is one of four fundamental interactions in nature. It describes processes inside nucleus and its constituents. It reveals itself at very small distances of the order of 1–3 femtometers (fm). Depending on the energy scale, strong interactions have different manifestations.

At high energies, which can be reached, for example, in cosmic rays or in powerful accelerators, strong interactions can be described in terms of interactions between quarks and gluons. The theory which describes strong interactions in the Standard Model is called *quantum chromodynamics* (QCD). Due to asymptotic freedom [GW73, Pol73], QCD-equations at high energy can be solved perturbatively, leading to very accurate predictions.

At lower energies typical for a daily life (*e.g.* nuclei in the atoms of surrounding objects), one talks about strong interactions between hadrons: baryons and mesons. In this regime, which is called the regime of confinement, strong interactions are not yet well understood. QCD equations are still valid, but perturbative methods used to solve them at high energies are not applicable in this region. The solution of QCD in this energy regime requires development of special nonperturbative methods, such as lattice QCD, phenomenological models and effective field theories.

Understanding of low-energy interactions between nucleons — the lowest mass baryons — is very important for understanding nuclei and the surrounding matter, which is formed from nuclei. This is especially important given the fast progress in developments of nuclear lattice simulations a new method to study nuclei and their properties from the first principles on the lattice of the finite volume [EKLM11, EKL$^+$13, EKL$^+$14]. The key ingredient for this approach is the theory of nuclear forces, in particular the theory of NN interactions.

Nucleon-nucleon interactions are classified according to their range. Short-range interactions correspond to distances below 1 fm, intermediate-range correspond to 1–2 fm, and long-range to distances above 2 fm.

Nucleon-nucleon dynamics at low energy is significantly constrained by chiral symmetry of QCD. Thus, it is natural to use an *effective field theory* (EFT) framework based on chiral symmetry to study low-energy NN interactions [Wei90, ORvK94, ORvK96, EHM09, Epe06]. Chiral EFT produces model-independent predictions, which can be systematically improved by calculating higher order terms in low momentum expansion. Chiral EFT explicitly takes into account long- and intermediate-range interactions. Short-range effects are taken into account implicitly through a series of contact interactions with the corresponding low-energy constants. Chiral EFT was successfully applied to many processes, including pion-pion, pion-nucleon, and nucleon-nucleon interactions below pion production threshold.

The goal of this thesis is to make a step towards understanding of NN dynamics at intermediate energies where a pion can be produced. Pion production in nucleon-nucleon collisions is interesting for several reasons:

- The reaction $NN \to NN\pi$ is the first inelastic channel of NN interaction, thus it is essential for understanding intermediate-range NN dynamics.

- Despite extensive phenomenological and chiral EFT studies of $NN \to NN\pi$, mechanisms of pion production are still not really understood, see review articles [Han04, BHM14]. While various phenomenological models can describe data equally well using

different essentially short-range mechanisms, it is still unclear which particular mechanisms are important. Furthermore, the role of intermediate-range effects that contain important long-range contributions (such as two-pion-exchanges) was not studied at all in phenomenological calculations.

- Pion production is an extremely useful tool to study *charge symmetry breaking* (CSB) — a special kind of isospin violation in QCD. Specifically, in the $pn \to d\pi^0$ channel, CSB effects are very pronounced. Observables in this channel can be used to extract the important information about the proton-neutron mass difference, which is also a CSB effect.

- Pion production can be used as a test ground for chiral EFTs at the energies above pion mass. Since pion production involves relatively large momentum (required to produce a pion), a modification of the standard chiral expansion is needed to properly account for the new scale. The important goal is then to demonstrate that the modified expansion is convergent, that is that the theory has predictive power. It can be shown that this is indeed the case for $NN \to NN\pi$ [BHM14]. Thus, pion production can be used to develop methods to study reactions with a relatively large transferred momentum within chiral EFT framework.

- The process $NN \to NN\pi$ is also an important building block for many other low-energy processes like:

  - Three-nucleon forces since the leading short-range operator in, *e.g.*, $pd \to pd$ scattering provides also an important contribution to p-wave pion production [BHM14, BEH$^+$09, HvKM00, ENG$^+$02, EHM09, ME11, GQN09].
  - πd-scattering at low energies where $NN \to NN\pi$ drives the strength of the important dispersive correction due to $\pi d \to NN \to \pi d$ [LBH$^+$07, BHH$^+$11a, BHH$^+$11b].
  - CSB in $dd \to \alpha\pi^0$, the reaction which is not allowed in the isospin limit.

The reaction $NN \to NN\pi$ has been extensively studied both theoretically and experimentally over the past decades. However, the near-threshold regime is still not yet fully understood. After the first high-quality data for $pp \to pp\pi^0$ [MHN$^+$92] became available[1], it quickly became clear that the original models failed to reproduce the new data. For example, the model of Ref. [KR66] fell short by a factor of two for the reaction $pp \to d\pi^+$ and by an order of magnitude for $pp \to pp\pi^0$. Various attempts were made to identify the phenomenological mechanisms responsible for this discrepancy.

The first theoretical paper to explain quantitatively the cross section $pp \to pp\pi^0$ was Ref. [LR93]. The new contribution in [LR93] originated from the short ranged, irreducible currents constructed directly from the nucleon-nucleon potential. A phenomenological interpretation of this mechanism was provided in Ref. [HMG94], where the exchange of heavy mesons (mostly σ and ω) followed by a pion emission via a nucleon-antinucleon pair (the so-called z-mechanism) was calculated. The mechanism was also shown to provide the missing strength for $pp \to d\pi^+$ in Refs. [Hor93, Nis96]. An alternative mechanism is based on the

[1] Further experimental data can be found in, *e.g.*, the review article [Han04], with the latest measurements in Refs. [T$^+$12, D$^+$12, D$^+$13].

pion-nucleon rescattering diagram where the off-shell pion-nucleon amplitude plays a crucial role. It is well-known that the isoscalar pion nucleon scattering length is very small — see Refs. [BHH$^+$11b, BHH$^+$11a] for its most recent determination — as a result of a cancellation of individually sizable terms which have different energy dependences. It therefore appeared natural that in the off-shell kinematics relevant for the pion production reaction the amplitudes are significantly enhanced. This mechanism was also shown to be capable of describing the experimental data in both $pp \to pp\pi^0$ [HO95, HHR$^+$95] as well as $pp \to d\pi^+$ [HHH$^+$98] reactions. At this point there was no way to decide which of the mechanisms described captures the correct physics.

Since pion interactions are largely controlled by the chiral symmetry of the strong interaction, one might naturally expect that chiral perturbation theory (ChPT) provides the proper tool to resolve the above mentioned discrepancy. However, the use of the standard ChPT power counting, which is based on the assumption that all relevant momenta are effectively of the order of the pion mass, was not very successful. The first calculations in this framework were done at tree level up to N^{2}LO for both $pp \to pp\pi^0$ [CFMvK96, PMM$^+$96, SLMK97] as well as for $pp \to d\pi^+$ [dRMvK00, HHH$^+$98]. These studies revealed, in particular, that the discrepancy between theory and experiment increases for the neutral channel due to a destructive interference of the direct pion production and the isoscalar rescattering contributions at NLO in standard counting. In addition, some loop contributions at N^{2}LO were found in Refs. [DKMS99, APM01] to be larger than the NLO contribution, revealing a problem regarding the convergence of the standard ChPT power counting.

It was soon realized that the large initial nucleon momentum at threshold $|\vec{p}| = \sqrt{m_N m_\pi} \approx 360$ MeV, which is significantly larger than the pion mass $m_\pi \approx 140$ MeV, requires the modification of the standard power counting. The corresponding expansion parameter in the new scheme is

$$\chi = |\vec{p}|/\Lambda_\chi \simeq 0.4,$$

with Λ_χ being the chiral symmetry breaking scale of the order of 1 GeV. Here and in what follows, this power counting will be referred to as the *momentum counting scheme* (MCS). This modification was proposed in Refs. [CFMvK96, dRMvK00] while the proper way to treat this scale was first presented in Ref. [HvKM00] and implemented in Ref. [HK02], see Ref. [Han04, BHM14] for a review article. The MCS expansion is performed with two distinct parameters, namely the initial nucleon momentum $|\vec{p}|$ and the pion mass m_π, where $m_\pi/|\vec{p}| \sim |\vec{p}|/\Lambda_\chi$. Pion loop diagrams start to contribute at a given order in the expansion parameter, which can be identified based on the power counting, and, unlike the standard ChPT power counting, continue to contribute at all higher MCS orders.

Due to the fact that the Delta-nucleon mass splitting is numerically of the order of $|\vec{p}|$, the Delta-isobar should be explicitly included as a dynamical degree of freedom [CFMvK96]. This general argument was confirmed numerically in phenomenological calculations [Nis78, HHKS98, HHKS00], see also Refs. [CFMvK96, dRMvK00, HK02, BHH$^+$07] where the effect of the Δ in $NN \to NN\pi$ was studied within chiral EFT.

In the MCS, pion p-waves are given by tree level diagrams up to N^{2}LO and the corresponding calculations of Refs. [HvKM00, BEH$^+$09] showed a satisfactory agreement with the data. Meanwhile, for pion s-waves loop diagrams start to contribute individually already at NLO. However, they turned out to cancel completely both for the neutral [HK02] and charged [LBH$^+$06] pion production, a result which is reproduced in this thesis. To obtain this

result for charged pion production, it is crucial to consistently take into account a contribution related to nucleon recoil in the πN vertex as explained in detail in Ref. [LBH$^+$06]. As a by-product of the consistent treatment of nucleon recoil effects in Ref. [LBH$^+$06], the rescattering one-pion exchange amplitude at LO was found to be enhanced by a factor of 4/3 which was sufficient to overcome the apparent discrepancy with the data in the charged channel. The first attempts to study the subleading loop contributions were taken in Refs. [HW07, KSMK09]. The full N^{2}LO MCS calculation of s-wave pion production amplitudes have not been done yet.

Charge symmetry breaking in particle physics have been studied for a long time. The comprehensive reviews can be found in Refs. [MNS90, MOS06]. The sources of CSB are quark mass difference and electromagnetic effects. In pion production, CSB is of specific interest. In the channel $pn \to d\pi^0$ CSB causes an asymmetry of the differential cross section with respect to the interchange of the initial nucleons. In fact, no other types of isospin violation except for CSB contribute to the asymmetry in this reaction. In particular, there are no long-range electromagnetic effects (Coulomb interaction) between particles in this reaction. This allows one to get information about the quark mass difference from the asymmetry data, which makes this reaction so interesting.

The data on the forward-backward asymmetry exist thank to a precise measurement performed at TRIUMF [OKH$^+$03] which yielded $A_{fb} = (17.2 \pm 8(\text{stat.}) \pm 5.5(\text{sys.})) \times 10^{-4}$.

The first near-threshold phenomenological calculation of CSB in $pn \to d\pi^0$ was done in [Nis99][2], where the main mechanism was identified as $\pi\eta$ mixing.

The first chiral EFT studies Ref. [vKNM00] found that at leading order in chiral expansion the main mechanism corresponds to the pion rescattering operator with the CSB πN seagull vertex. The problem is that this mechanism leads to the significant overestimation of data by about the factor of four $A_{fb} = 69 \times 10^{-4}$. The difference between experiment and theory is much larger than the uncertainty of the chiral EFT calculation [vKNM00]. An update of the chiral EFT calculation was made in Ref. [BM10], but overestimation of the asymmetry remained.

In this thesis we will show that there is one more leading order contribution to the asymmetry in $pn \to d\pi^0$, not considered in previous studies and its inclusion brings the EFT calculation in agreement to the data already at leading order.[3]

In this thesis we pursue several goals. First, we want to perform a complete N^{2}LO analysis of isospin symmetric amplitudes of $NN \to NN\pi$ at threshold. Second, we want to investigate the role of the delta resonance in pion production up to N^{2}LO. These two calculations can accurately answer the question about the mechanisms of pion production in various channels, and clarify the role of intermediate-range effects in such reactions. They are also important building blocks for studying CSB effects. Finally, we want to perform a complete study of CSB effects in $pn \to d\pi^0$ at leading order. Matching our LO CSB calculation to data we extract the strong contribution to the proton-neutron mass difference and compare it to the corresponding result from lattice simulations [BOS07, BZD$^+$10, dDDF$^+$12] and dispersive studies [GL82, WLCM12].

[2] An extensive list of references about CSB in $pn \to d\pi^0$ at higher energies can be found in the review [MOS06].

[3] After publication of Ref. [FBE$^+$09] discussed in this Thesis, the complete leading order CSB operator was confirmed in Ref. [Bol11].

This thesis is organized as follows. In Chapter 1, the main concepts of chiral EFT and specialties of pion production are discussed. In Chapter 2, we present a complete $\mathrm{N^2LO}$ chiral EFT calculation of the pion production at threshold with only nucleons and pions as explicit degrees of freedom. Next, in Chapter 3, we calculate all additional corrections appearing in chiral EFT where the delta-isobar is included as an explicit degree of freedom up to $\mathrm{N^2LO}$. We also compare our results with phenomenological studies. In Chapter 4, we perform complete LO calculation of CSB effects in $pn \to d\pi^0$. Finally, in Conclusion, we formulate the main results of our study and present an outlook for future studies.

Chapter 1

Theory and methods

All calculations in this thesis are made in the framework of chiral EFT. In this chapter we give an introduction to the chiral EFT and discuss specific methods required to deal with pion production in nucleon-nucleon collisions. In particular, we focus on the following topics:

- *Chiral perturbation theory* (ChPT) — effective field theory of QCD which describes low-energy interactions of pions and nucleons.
- *Heavy baryon formulation* of ChPT (HBChPT) — a formalism to deal with nucleon propagators in loop-diagrams.
- Explicit inclusion of delta resonance — extension of ChPT to more general chiral EFT, in which delta resonance is considered as an explicit degree of freedom (in addition to pions and nucleons).
- *Momentum counting scheme* (MCS) — a special power counting which takes into account relatively large momentum required to produce a pion.
- *Hybrid approach* — a method to take into account non-perturbative NN interactions in the initial and final state.

1.1 Chiral perturbation theory (ChPT)

ChPT is a well established theory. A pedagogical introduction can be found in the book by Scherer and Schindler [SS12]. Other introduction articles and reviews can be found, for example, in Refs. [BKM95, Pic95, Sch03]. The latest review of different aspects of ChPT can be found in Ref. [Ber08]. In this section we summarize the basic principles of ChPT.

1.1.1 Strong interactions at low energies

At high energies the strong interactions are described with a high accuracy by Quantum Chromodynamics (QCD). The relevant degrees of freedom in the QCD Lagrangian are quarks and gluons. Observables are calculated using perturbation theory in the coupling constant α_s. At high energies the value of renormalized coupling α_s is very small, such that corresponding

QCD perturbation series converges fast. Such small coupling constant allows one to make accurate predictions for high energy observables using QCD Lagrangian.

At low energies, the value of renormalized coupling α_s becomes large. This makes the application of perturbation theory impossible. To make QCD-based calculations in the low-energy sector, several types of non-perturbative methods were developed.

Non-perturbative methods to study strong interactions at low-energies include lattice QCD, phenomenological models, and effective field theories.

Lattice QCD calculations are direct numerical solutions of QCD equations in discretized Euclidean space-time. This method allows one to obtain exact QCD results in the non-perturbative regime. This method has high computational complexity. In order to accurately simulate particles with small masses (such as pions), one has to use a very large lattices, which require huge computational resources. Lattice QCD already gives interesting results and in future, with advance of computational algorithms and technology, it could be used to study processes like pion production.

Phenomenological models are based on phenomenological Lagrangians. These models allow one to get a good description of data in a wide energy range. They can also provide useful insights. In particular, one can use them to estimate values of various coupling constants used in the EFT studies. However, the uncertainty and the model dependence of phenomenological calculations cannot be estimated reliably. One cannot unambiguously understand the mechanism of a particular process using such models, because it can happen that several different phenomenological models describe data equally well.

Chiral effective field theory — the method we use in this thesis — is based on the effective Lagrangian, which is consistent with all symmetries of QCD. At low energies one can organize systematic expansion in terms of small momenta. Chiral EFT allows one to understand the role of the chiral symmetry and the "pion cloud" in low-energy processes and predict observables with controlled uncertainty. However, this method can only be applied for energies which are much smaller than 1 GeV. Chiral Lagrangian contains unknown parameters, which should be fitted to data or calculated using lattice EFT. Once fixed, these parameters can be used to link different processes to each other or to predict new observables. These and other aspects of chiral EFT will be discussed in the next section.

1.1.2 Basic principles of ChPT

Any EFT is based on the ideas of symmetries and separation of scales. In this section we discuss these ideas applied to the specific example of EFT, namely, chiral perturbation theory (ChPT).

Before discussion of symmetries and scales, a remark about the degrees of freedom in chiral EFT should be made. In nature, quarks and gluons are never observed as free states (at least, under normal conditions). In the energy range accessible by experiment, they always form composite particles like mesons and baryons. This property of QCD is called *confinement*. At high energies the interactions between quarks become very weak, such that quarks can be considered as quasi-free particles. Due to this *asymptotic freedom*, in high-energy QCD-calculations, quarks and gluons are used as degrees of freedom. At low energies, as was mentioned before, the interaction between quarks and gluons becomes very strong, and the contributions of individual quarks cannot be tracked. For this reason, in low-energy EFT

calculations it is convenient to use mesons and baryons as *effective degrees of freedom*.

The main idea of any EFT is to use the symmetries of the underlying fundamental theory. In our case the fundamental theory is QCD. The Lagrangian of QCD describes the interaction of quarks and gluons and has certain symmetries. At high energies, this Lagrangian is used to calculate observables employing perturbation theory in coupling constant. At low energies perturbation theory does not converge, but the Lagrangian and its symmetries are still valid. The symmetries of the QCD Lagrangian constrain strong interactions even at low energies. These symmetry constraints can be used to make predictions for observables. EFT incorporates all relevant symmetries of the fundamental theory and allows to make predictions for observables at low energies.

The second idea behind EFT is a separation of scales. Dynamics of a low-energy process should not be affected by any heavy resonances. In QCD, the processes well below 1 GeV are only affected by the dynamics of the lightest quarks: up- and down-quarks, while the contributions from heavier quarks are negligible. It is important that the observed hadron spectrum at low energies has an energy gap between lightest resonance (pion at about 140 MeV) and the next resonance (rho-meson at about 700 MeV). This natural separation of scales suggests that at low energies pions should be considered as dynamic degrees of freedom and the dynamics associated with heavier resonances can be treated implicitly.

The smallness of the pion mass can be explained by the symmetries of QCD Lagrangian. Namely, if the masses of up- and down-quarks are equal to zero, the QCD Lagrangian has an extra symmetry — the *chiral symmetry*. However the ground state (vacuum) is not invariant under this transformation. This means that the chiral symmetry is spontaneously broken. According to the Goldstone theorem [Gol61], a spontaneously broken symmetry leads to the appearance of massless Goldstone bosons. But since u- and d-quarks are not exactly massless, chiral symmetry is also explicitly broken, and the Goldstone bosons receive a small mass. In QCD, pions are identified with Goldstone bosons of spontaneously broken chiral symmetry.

The ideas discussed above were used to construct the ChPT. In ChPT pions are the effective degrees of freedom[1]. The most general effective Lagrangian is constructed consistently with all symmetries of QCD including the chiral symmetry. Chiral symmetry breaking terms are accounted for as perturbation. According to Weinberg's theorem, the result obtained by using this Lagrangian will be the most general S-matrix consistent with Lorentz-invariance, analyticity, unitarity and all symmetries of QCD. Such S-matrix is equivalent to the result of QCD, but it includes unknown coefficients, which come from the effective Lagrangian.

Each term in the effective Lagrangian has an unknown numerical coefficient, which is not fixed by the symmetries of underlying theory. These coefficients are called low-energy constants (LECs). They parametrize high-energy (short-range) effects which are not included dynamically. Usually the values of LECs are determined by fitting to data, but they can be also calculated using lattice QCD simulations. LECs are, in general, dimensionful quantities. Since they parametrize the short-range physics they are expected to have the form a/Λ_χ^n, where a is a dimensionless number, Λ_χ is the chiral symmetry breaking scale, and n is a positive power which depends on the structure of particular Lagrangian term. The renormalized values of LECs are expected to be of natural size, which means that the dimensionless coefficient a should be of order of 1.

[1]Inclusion of the lightest baryons in EFT will be discussed in the next section.

Because the most general effective Lagrangian has infinite number of terms, chiral EFT requires a special estimation procedure — *power counting*. In order to make practical calculations one has to design a method to distinguish more important Lagrangian terms from less important ones. More precisely, one needs a method to estimate and classify terms according to the size of their contributions to observables.

Power counting relies on the separation of scales. To illustrate the power counting for the Lagrangian, let's consider an example of generic Lagrangian term for pion-pion interaction. Each term in the effective Lagrangian consists of one low-energy constant and some combination of pion fields, derivatives of pion fields and pion masses. The LEC gives a contribution of order $1/\Lambda_\chi^n$, pion fields produce dimensionless contributions, and the derivatives of pion fields will generate a pion momentum, which we denote by p. As a result, in the numerator of each Lagrangian term there is always a small-scale quantity of order of p (to some power) and in the denominator there is a large scale Λ_χ^n. Due to separation of scales, the typical momenta p is much smaller than Λ_χ, and thus the natural expansion parameter is the ratio of small and large scales $\chi = p/\Lambda_\chi \ll 1$. Using this expansion parameter, the Lagrangian terms can be easily classified according to the number of p/Λ_χ suppressions. To denote terms of different importance the following notation is used. The effective Lagrangian terms with minimal number of small-scale quantities are called *leading-order* or *lowest-order* Lagrangian (LO). Terms with one extra (compared to LO) insertion of the small scale are called *next-to-leading-order* Lagrangian (NLO), terms with two extra small scale insertions (again, compared to LO) are called *next-to-next-to-leading* order $\mathrm{N^2LO}$, and so on. In this way, the power counting scheme allows one to estimate importance of any effective Lagrangian term by counting the number of p/Λ_χ suppressions.

Power counting is also required for Feynman diagrams, because even from the leading-order Lagrangian one can construct an infinite number of Feynman diagrams (*e.g.* with pion loops). To select which diagrams give the most important contribution to the amplitude, the power counting is defined for diagrams in a similar way as for individual Lagrangian terms. To estimate the whole diagram, each of its constituents is estimated. Vertices are estimated in the same way as Lagrangian terms[2]. Pion propagators give the factor p^{-2}. And each loop-integral gives the factor of $p^4/(4\pi f_\pi)^2$ due to loop integration. The factor $(4\pi f_\pi)$ is typically associated with the large scale Λ_χ. Product of estimations of all parts of the diagram gives the total estimation of the diagram. As well as the Lagrangian, diagrams are classified according to the number of p/Λ_χ-suppressions, and the naming convention for diagrams is the same: diagrams with minimal number of p/Λ_χ-suppressions are called LO, diagrams with one suppression are called NLO, and so on.

Using power counting for Feynman diagrams, one classify them according to their contribution to observables. This gives a perturbation series not in a coupling constant, but rather in low momenta. Perturbation series allows one to estimate the uncertainty due to omitted higher-order terms. It also allows one to calculate higher order terms to increase the accuracy, *i.e.* results of chiral EFT are systematically improvable.

There are several counting schemes, which differ in some details. The most commonly used one is the so-called *Weinberg counting* scheme [Wei79]. In this scheme, all momenta p are taken to be of order of the pion mass m_π and diagrams are counted exactly in the same

[2] Except that p is not always taken of order of m_π, but depends on the kinematics of particular diagram. This issue will be discussed in sec. 1.4.

way as Lagrangian terms. Weinberg's scheme is applicable to problems with a single small scale.

A slightly different counting scheme, which we will use in this thesis, is the *momentum counting scheme* (MCS). It is designed to deal with two small scales[3]. In MCS, all vertices are still taken from the usual ChPT Lagrangian, although the momentum scale p is not always identified with pion mass. Both these small scales must be correctly taken into account when estimating the order of diagrams.

Power counting is essential for renormalization of EFT. In general, EFT is not renormalizable, because one cannot renormalize an infinite number of coupling constants (LECs) in the effective Lagrangian. However, it is possible to renormalize EFT up to a given order in power counting [GL84]. Up to any given order there are only finite number of Lagrangian terms and corresponding coupling constants. One can thus perform standard renormalization procedure. In this way, the EFT is *renormalizable order-by-order*.

In the next sections we describe the construction of effective Lagrangian for pion-pion interactions and inclusion of the lightest baryons in the effective field theory.

1.1.3 Pion-pion interactions

Chiral perturbation theory was first formulated to describe low-energy meson-meson interactions, such as pion-pion scattering. In this section we provide basic information about the effective chiral Lagrangian which is relevant to our study.

For our study we use an SU(2) formulation of chiral perturbation theory. In this formulation, u- and d-quarks are considered as light, and all other quarks as heavy. In principle, there is also an SU(3) formulation of ChPT, where s-quark is also considered to be light. However, the formalism of SU(3) theory is more complicated, and the convergence is slower [BKM95]. Since the study of pion production is already related to slow convergence due to relatively large momentum involved in the reaction, it is reasonable to use SU(2) formulation of ChPT to study pion production.

ChPT is based on the effective Lagrangian. This Lagrangian should satisfy all symmetries of the underlying theory. To construct the effective Lagrangian one can first write down all possible building blocks with well-defined transformation properties and symmetries, and then take all possible combinations of building blocks, which satisfy symmetries required by the underlying theory (QCD).

We start with a brief description of the building blocks of chiral Lagrangian for meson-meson interactions. Systematic review of Lagrangian construction procedure can be found in Refs. [Kra90, BK99]. The effective chiral Lagrangian includes SU(2) matrix $U(x)$. Pion fields $\boldsymbol{\pi} = (\pi_1, \pi_2, \pi_3)$ are connected non-linearly with the U-field

$$U(x) = \sqrt{1 - \frac{\boldsymbol{\pi}(x)^2}{f_\pi^2}} + i\frac{\boldsymbol{\tau}\cdot\boldsymbol{\pi}(x)}{f_\pi} = 1 + i\frac{\boldsymbol{\tau}\cdot\boldsymbol{\pi}}{f_\pi} - \frac{\boldsymbol{\pi}^2}{2f_\pi^2} - \frac{\boldsymbol{\pi}^4}{8f_\pi^4} + \cdots , \tag{1.1}$$

where f_π is a pion decay constant in chiral limit and $\boldsymbol{\tau} = (\tau_1, \tau_2, \tau_3)$ are Pauli matrices. It is

[3] In pion production there are two small scales: m_π and $\sqrt{m_\pi m_N}$, where m_N stands for the nucleon mass. Extended discussion of this topic is provided in the MCS section.

also convenient to introduce matrix $u(x)$

$$u(x) = \sqrt{U(x)} = 1 + i\frac{\boldsymbol{\tau}\cdot\boldsymbol{\pi}}{2f_\pi} - \frac{\boldsymbol{\pi}^2}{8f_\pi^2} + i\frac{(\boldsymbol{\tau}\cdot\boldsymbol{\pi})^3}{16f_\pi^3} + \cdots . \tag{1.2}$$

The expressions (1.1) and (1.2) correspond to one particular pion field representation called *sigma-gauge*. The choice of pion field representation is not unique. Other possible pion field representations can be found, for example, in [HW07]. Observables are, however, invariant under change of pion field parametrization.

Due to nonzero masses of light quarks, the chiral symmetry is explicitly broken. To take this effect into account the chiral Lagrangian also includes a mass term, which is related to the matrix $\chi = 2B_0 s$, where s is the SU(2) quark mass matrix and B_0 is a quantity proportional to SU(2) quark condensate in the chiral limit. Neglecting isospin breaking corrections (effects coming from the mass difference of the u and d quarks and their electromagnetic interactions) one can write $\chi = m_\pi^2 1_I$, where 1_I is the unit matrix in the isospin space and m_π is a physical pion mass.[4] In this section we consider only isospin symmetric Lagrangian. Isospin violating terms are presented in Chapter 4.

Leading-order pion-interaction Lagrangian includes the following building blocks: the chiral vielbein u_μ, and mass term χ_+

$$u_\mu = i\left(\partial_\mu u\, u^\dagger + u^\dagger \partial_\mu u\right), \tag{1.3}$$

$$\chi_+ = u^\dagger \chi u^\dagger + u \chi^\dagger u. \tag{1.4}$$

The lowest order pion-pion Lagrangian has the form

$$\mathcal{L}^{(2)}_{\pi\pi} = \frac{f_\pi^2}{4}\langle u^\mu u_\mu\rangle + \frac{f_\pi^2}{4}\langle\chi_+\rangle, \tag{1.5}$$

where $\langle\cdots\rangle$ denotes a trace in the isospin space Using explicit expression (1.2) for $u(x)$ we get the Lagrangian density for the pion propagator and the leading four-pion vertex (in the sigma-gauge):

$$\mathcal{L}^{(2)}_{\pi\pi} = \frac{1}{2}(\partial_\mu\boldsymbol{\pi}\cdot\partial^\mu\boldsymbol{\pi}) - \frac{1}{2}m_\pi^2\boldsymbol{\pi}^2 + \frac{1}{2f_\pi^2}(\boldsymbol{\pi}\cdot\partial^\mu\boldsymbol{\pi})(\boldsymbol{\pi}\cdot\partial_\mu\boldsymbol{\pi}) - \frac{m_\pi^2}{8f_\pi^2}\boldsymbol{\pi}^4 + \cdots , \tag{1.6}$$

where the dots stand for terms with six or more pion fields.

The next higher-order mesonic Lagrangian $\mathcal{L}^{(4)}_{\pi\pi}$ is not relevant for our study, because it starts to contribute at much high orders.

1.1.4 Pion-nucleon interactions

Chiral EFT can be extended to include interactions of pions with nucleons [BKM95]. The construction procedure of the Lagrangian is similar to the pure mesonic case. This procedure

[4] In general, one should use bare pion mass before all renormalization procedures are carried out. But in our study all renormalization corrections to pion mass start to contribute at very high orders. Thus we use physical pion mass in all relations throughout this work.

is described in the reference [FMMS00], where the pion-nucleon covariant Lagrangian was constructed up to $\mathcal{L}_{\pi N}^{(4)\mathrm{rel}}$.

To describe interactions of pions with nucleons one should introduce nucleons as an explicit degree of freedom. One introduces the isodoublet representation of the nucleon

$$\Psi = \begin{pmatrix} p \\ n \end{pmatrix}, \tag{1.7}$$

where p stands for the proton and n for the neutron. It is also convenient to introduce following building blocks: the chiral connection Γ_μ and the covariant derivative D_μ of the baryon field

$$\Gamma_\mu = \frac{1}{2}\left(u^\dagger\,\partial_\mu u + u\,\partial_\mu u^\dagger\right), \tag{1.8}$$

$$D_\mu = \partial_\mu + \Gamma_\mu. \tag{1.9}$$

The most general leading-order relativistic pion-nucleon Lagrangian reads [GSS88]

$$\mathcal{L}_{\pi N}^{(1)\mathrm{rel}} = \bar{\Psi}\left(i\not{D} - m_N + \frac{g_A}{2}\not{u}\gamma_5\right)\Psi, \tag{1.10}$$

where g_A denotes the axial-vector coupling of the nucleon and m_N denotes mass of the nucleon.

The next-to-leading order pion-nucleon Lagrangian has the following form:

$$\begin{aligned}\mathcal{L}_{\pi N}^{(2)\mathrm{rel}} = \bar{\Psi}\Big(& c_1\langle\chi_+\rangle - c_2\frac{1}{8m_N^2}\left(\langle u_\mu u_\nu\rangle\left\{D^\mu, D^\nu\right\} + \mathrm{h.c.}\right) \\ & + c_3\frac{1}{2}\langle u^\mu u_\mu\rangle + c_4\frac{i}{4}[u_\mu, u_\nu]\sigma^{\mu\nu} + \cdots\Big)\Psi,\end{aligned} \tag{1.11}$$

where the dots stand for terms not relevant for our calculation (isospin breaking and interactions with external sources). The coefficients c_i are low-energy constants. They are dimensionful and expected to be of order of $1/\Lambda_\chi$. And $\sigma^{\mu\nu} = i[\gamma^\mu, \gamma^\nu]/2$ is proportional to the commutator of two Dirac matrices.

For this work we need $\mathcal{L}_{\pi N}^{(1)\mathrm{rel}}$ and several terms from $\mathcal{L}_{\pi N}^{(2)\mathrm{rel}}$. Terms from covariant Lagrangian $\mathcal{L}_{\pi N}^{(3)\mathrm{rel}}$ produce diagrams which are of a higher order than we consider in this work.[5]

Inclusion of nucleons as dynamic degrees of freedom introduces a new scale m_N. This scale doesn't vanish in the chiral limit and leads to additional difficulties with power counting. In particular, the four-momentum of a nucleon will appear in the numerator in loop-integrals. This four-momentum momentum includes the nucleon mass and is therefore much larger than the small scale. One cannot organize convergent series with the expansion parameter $m_N/\Lambda_\chi \sim 1$. A special method is required.

Several approaches were developed to define convergent chiral EFT with nucleons. They include heavy-baryon formalism (HBChPT) [JM91], infrared regularization [BL99], and extended on-mass-shell regularization [SGS04].

In this thesis we use heavy baryon formalism. It allows one to transform the pion-nucleon Lagrangian in a way that heavy nucleon mass contributions are moved from propagators into vertices. This method is discussed in the next section.

[5]Note, however, that after carrying out the heavy baryon expansion (discussed in the next section), there will be terms in $\mathcal{L}_{\pi N}^{(3)\mathrm{HB}}$ relevant for our calculation. They emerge from $1/m_N$-expansion of $\mathcal{L}_{\pi N}^{(1)\mathrm{rel}}$ and $\mathcal{L}_{\pi N}^{(2)\mathrm{rel}}$.

1.2 The heavy baryon formulation of ChPT

To define convergent chiral EFT for pion-nucleon systems, one needs to specify a procedure to deal with nucleon propagators in loop-integrals. Without such a procedure, multi-loop diagrams with nucleons will not be suppressed. Historically, the first solution to deal with baryons in chiral EFT was proposed by [JM91] and is called *heavy baryon* formulation of CHPT (HBChPT). It exploits the fact that nucleons can be treated nonrelativistically in low-energy reactions. This allows one to separate small dynamical parts from the nucleon four-momenta and the nucleon field, and treat them perturbatively.

In HBChPT, the total four-momentum P_μ of the nucleon is separated into two terms:

$$P_\mu = m_N v_\mu + p_\mu, \tag{1.12}$$

where v is a nucleon four-velocity ($v^2 = 1$), and p_μ is a small residual nucleon momentum, which satisfies the relation $v \cdot p \ll m_N$. The first term $m_N v_\mu$ corresponds to the large nucleon mass, which doesn't affect dynamics significantly, while the second term p_μ corresponds to small nucleon momenta which governs its dynamics.

The covariant baryon field is also separated into the "light" component $N_v(x)$ and the "heavy" component $h_v(x)$ using the projection operators $(1 \pm \not{v})/2$

$$N_v(x) = \exp(im_N\, v \cdot x)\frac{1+\not{v}}{2}\Psi(x), \tag{1.13}$$

$$h_v(x) = \exp(im_N\, v \cdot x)\frac{1-\not{v}}{2}\Psi(x). \tag{1.14}$$

The light component is considered explicitly, while the heavy one is integrated out. The contribution of the heavy field generates additional Lagrangian terms which are suppressed as $1/m_N^n$, with n ranging from 1 to ∞. In this way, the contribution of the heavy part of baryon field is pushed to $1/m_N$-suppressed vertices. In this work, we refer to all $1/m_N^n$-terms as *recoil corrections* (for any n, not necessary $n = 1$). Heavy baryon expansion allows one to organize consistent power counting with the expansion parameter being $|\vec{p}|/m_N$.

The Dirac algebra is simplified considerably in the heavy baryon formalism. Instead of all gamma-matrices and their combinations, there are only two nontrivial operators, namely the four-velocity v^μ and the covariant spin-operator S_μ, defined as

$$S_\mu = \frac{i}{2}\gamma_5\sigma_{\mu\nu}v^\nu\,. \tag{1.15}$$

To regularize loop-diagrams in this study we use the dimensional regularization scheme. For this purpose we should keep all relations in general d-dimensional space-time. In d-dimensional space-time, the operators v and S obey the following simple relations

$$S \cdot v = 0\,, \quad \{S_\mu, S_\nu\} = \frac{1}{2}\left(v_\mu v_\nu - g_{\mu\nu}\right)\,, \quad S^2 = \frac{1-d}{4}, \quad v^2 = 1\,, \tag{1.16}$$

where $g_{\mu\nu}g^{\mu\nu} = d$. In addition to the relations (1.16), in the physical four-dimensional space-time, one can define the commutator of two spin-operators in terms of four-dimensional Levi-Civita tensor

$$[S_\mu, S_\nu] = i\epsilon_{\mu\nu\gamma\delta}v^\gamma S^\delta \quad \text{only if} \quad d = 4, \tag{1.17}$$

where we use the convention $\epsilon^{0123} = -1$ (or equivalently $\epsilon_{0123} = 1$).

To calculate the constant part of the divergent loop diagrams correctly it is important to work in d-dimensional space-time until the renormalization procedure is complete. The reason for that is that loop diagrams in dimensional regularization scheme contain divergent $1/(d-4)$-terms, which can produce additional finite contribution when multiplied with the factor d coming from spin coefficients.

After all renormalization procedures are carried out, spin operators can be further simplified. Namely, one can reduce the operators S to the three-dimensional form, represented by Pauli matrices. Examples of such reduction are shown below:

$$S_1 \cdot k_1 = -\frac{1}{2}\vec{\sigma}_1 \cdot \vec{k}_1, \tag{1.18}$$

$$4\,[S_{2\mu}, S_{2\nu}]\, S_1^\nu k_1^\mu = 4i\varepsilon^{\alpha\mu\nu\beta} v_\alpha k_{1\mu} S_{1\nu} S_{2\beta} = i\vec{k}_1 \cdot (\vec{\sigma}_1 \times \vec{\sigma}_2), \tag{1.19}$$

where $\vec{\sigma}$ is a three-vector of Pauli matrices, and the indices 1 or 2 of the operators S and $\vec{\sigma}$ are nucleon labels.

After performing the heavy baryon reduction of the covariant pion-nucleon Lagrangian, one gets

$$\mathcal{L}_{\pi N}^{(1)\mathrm{HB}} = \bar{N}_v \left(iv \cdot D + g_A\, S \cdot u\right) N_v, \tag{1.20}$$

where explicit degrees of freedom are only light components of the baryon field.

In a similar fashion, the next-to-leading Lagrangian is reduced to

$$\begin{aligned}
\mathcal{L}_{\pi N}^{(2)\mathrm{HB}} &= \bar{N}_v \left(\frac{1}{2m_N}(v \cdot D)^2 - \frac{1}{2m_N} D \cdot D - \frac{i\, g_A}{2m_N} \{S \cdot D,\, v \cdot u\} \right) N_v \\
&\quad + \bar{N}_v \left(c_1 \langle \chi_+ \rangle + \left(c_2 - \frac{g_A^2}{8m_N} \right) (v \cdot u)^2 + c_3 u \cdot u \right. \\
&\quad \left. + \left(c_4 + \frac{1}{4m_N} \right) [S^\mu, S^\nu]\, u_\mu u_\nu \right) N_v + \cdots ,
\end{aligned} \tag{1.21}$$

Note that in addition to the c_i-terms, the heavy baryon NLO Lagrangian contains $1/m_N$-corrections. The $1/m_N$-corrections in the first line correspond to the nucleon recoil corrections to the LO Lagrangian, while the $1/m_N$-corrections in the second and third line are contributions of the heavy part of the baryon field (anti-nucleon contribution).

In a similar way, the N^{2}LO pion-nucleon Lagrangian contains terms from the covariant N^{2}LO Lagrangian proportional to the LECs d_i as well as $1/m_N$- and $1/m_N^2$-corrections to the LO and NLO Lagrangians. Terms proportional to d_i are not relevant for our study since they start to contribute at much higher orders. We will, however, need several $1/m_N$- and $1/m_N^2$-corrections from N^{2}LO Lagrangian. These terms are listed in the Appendix A.

Although the expressions in terms of the matrix u are convenient for the construction of the Lagrangian, in order to derive the Feynman rules, all Lagrangians should be expanded in terms of pion fields. Expanded Lagrangians are provided in the Appendix A.

1.3 Explicit inclusion of the Delta resonance

In standard baryon ChPT, only pions and nucleons are considered as explicit degrees of freedom. All other resonances of the nucleon (such as Delta, Roper, etc) are considered

heavy and taken into account implicitly through low-energy constants (LECs). However, the lightest nucleon resonance — delta-isobar — has a very low excitation energy. The delta-nucleon mass difference is only about two pion masses. This is particularly important for the pion production process, where the initial nucleon momentum (required to produce a pion) is numerically of the same order as the delta-nucleon mass difference. In addition, if the delta is only included in the theory through LECs, the values of LECs required to describe a given process can become unnaturally large. This can lead to slow convergence of the theory. Thus, it might be advantageous to consider dynamical long-range effects of delta resonance in chiral EFT.

The solution is to extend baryon ChPT to more general chiral EFT which includes delta explicitly. This EFT includes all the diagrams with pion-nucleon interactions from the baryon ChPT[6], and, in addition, it includes new diagrams with explicit deltas.

The construction of chiral EFT with explicit delta using Rarita–Schwinger formalism [RS41] was done in the work by Hemmert [Hem96, HHK98][7]. Here we present the main ideas of this formalism and expressions required for our study.

The inclusion of the delta-resonance into an effective field theory is analogous to the inclusion of the nucleons. The heavy-baryon formalism can also be applied to the nucleon and delta simultaneously. Due to the inclusion of delta, an additional numerically small parameter enters the calculation, namely the delta-nucleon mass difference:

$$\delta = m_\Delta - m_N. \tag{1.22}$$

Note that this quantity doesn't vanish in the chiral limit. It is nevertheless possible to define a consistent power counting scheme by assigning this new scale to one of the small scales in the problem. This issue is discussed in Chapter 3.

To properly take into account the spin-3/2 and isospin-3/2 components of the delta, the special spin and isospin operators should be introduced. One should also take care to project out unphysical states with spin-1/2 which appear in this formalism [Hem96, HHK98]. For this purpose the spin-3/2 and isospin-3/2 transition operators ($\mathbb{S}$ and $\mathbf{T}$) are introduced. In d-dimensional space-time they have the following normalization:

$$\mathbb{S}_\mu \mathbb{S}^\dagger_\nu = g_{\mu\nu} - v_\mu v_\nu - \frac{4}{1-d} S_\mu S_\nu, \quad T_i T^\dagger_j = \frac{1}{3}\left(2\delta_{ij} - i\epsilon_{ijk}\,\tau_k\right), \quad i,j = 1,2,3.$$

After carrying out all renormalization procedures, the combinations of spin operators $\mathbb{S}$ inside bilinears constructed from the nucleon fields can be further simplified by reducing them to three-dimensional Pauli matrices:

$$\mathbb{S}_\mu \mathbb{S}^\dagger_\nu p^\mu q^\nu \to \frac{1}{3}(\vec{\sigma}\cdot\vec{p})(\vec{\sigma}\cdot\vec{q}) - \vec{p}\cdot\vec{q}, \tag{1.23}$$

where $\vec{\sigma} = (\sigma_1, \sigma_2, \sigma_3)$ are Pauli matrices.

[6]The values of LECs will be different in these two theories and should be fitted to data in each case separately.

[7]Note that conventions used in this thesis is slightly different from those of Ref. [HHK98]. Namely, we use sigma-gauge for pion field parametrization, instead of exponential gauge in [HHK98]. And we place spin/isospin projection operators into $\pi N\Delta$ and $\pi\Delta\Delta$ vertices, but not into delta propagators.

Using these operators, the effective Lagrangian for pion-nucleon-delta interactions expanded in pion fields in the sigma-gauge can be written as:

$$\begin{aligned}\mathcal{L}_{\pi N\Delta} &= -\Psi^\dagger_\Delta(iv\cdot\partial-\delta)\Psi_\Delta+\frac{g_1}{f_\pi}\Psi^\dagger_\Delta\,\mathbb{S}^{\dagger\mu}S^\beta\mathbb{S}_\mu\,T_i\boldsymbol{\tau}\cdot\partial_\beta\boldsymbol{\pi}T_i\Psi_\Delta\\ &\quad-\frac{1}{4f_\pi^2}\Psi^\dagger_\Delta\Big[(\dot{\boldsymbol{\pi}}\times\boldsymbol{\pi})\cdot T_i^\dagger\boldsymbol{\tau}T_i+2i\Big((\mathbf{T}^\dagger\cdot\boldsymbol{\pi})(\mathbf{T}\cdot\dot{\boldsymbol{\pi}})-(\mathbf{T}^\dagger\cdot\dot{\boldsymbol{\pi}})(\mathbf{T}\cdot\boldsymbol{\pi})\Big)\Big]\Psi_\Delta\\ &\quad-\frac{h_A}{2f_\pi}\Big[N^\dagger\mathbf{T}\cdot\Big(\partial^\mu\boldsymbol{\pi}+\frac{1}{2f_\pi^2}\boldsymbol{\pi}(\boldsymbol{\pi}\cdot\partial^\mu\boldsymbol{\pi})\Big)\,\mathbb{S}_\mu\,\Psi_\Delta+h.c.\Big]\\ &\quad+\frac{h_A}{2m_Nf_\pi}\Big[iN^\dagger\mathbf{T}\cdot\dot{\boldsymbol{\pi}}\;\mathbb{S}\cdot\partial\Psi_\Delta+h.c.\Big]+\cdots,\end{aligned}\tag{1.24}$$

where Ψ_Δ is a light component of the delta field in heavy-baryon formulation, g_1 is the leading $\pi\Delta\Delta$ coupling constant, and $h_A\equiv 2g_{\pi N\Delta}$ is the leading $\pi N\Delta$ coupling constant. Covariant form of this Lagrangian can be found in the Refs. [Hem96, HHK98].

1.4 Momentum counting scheme for the pion production process

A power counting scheme is an essential part of the chiral EFT, required to classify Lagrangian terms and Feynman diagrams according to their importance. A counting scheme relies on the importance of different scales involved in the process. In most processes that were studied in chiral EFT, the only small scale is the pion mass m_π. In contrast, the pion production process involves a second small scale, related to relatively large initial momentum required to produce a pion. To deal with two small scales in pion production reactions the *momentum counting scheme* (MCS) was designed.

Historically the first power counting scheme used in chiral EFT was the Weinberg power counting scheme [Wei79]. In this scheme all small scale parameters[8] are estimated to be of order of the pion mass. All large parameters like the scale associated with loops $4\pi f_\pi$ and the nucleon mass m_N are treated as the heavy scale Λ_χ. This leads to the Weinberg expansion parameter $\chi_{\rm W}=m_\pi/\Lambda_\chi$. To estimate the order of the Lagrangian term or the order the diagram one only has to count the number of the small-scale quantities in the corresponding term or diagram. Each additional inclusion of the small scale gives a suppression by the factor $\chi_{\rm W}$. Weinberg's counting works very well for processes with small transferred momenta: for example, $\pi\pi$-scattering [Wei79, GL84, CGL01], πN-Scattering [FM01a], few-nucleon processes [ORvK94, ORvK96, BBH$^+$00, EGM98, EGM05, Epe06, ENG$^+$02], $\gamma d\to\pi NN$ [LBH$^+$05, LBE$^+$07], and $\pi d\to\gamma NN$ [GP06]. For these low-energy processes the explicitly calculated amplitudes are in a good agreement with the counting estimations.

First studies of pion production in HBChPT formalism were also made using Weinberg's power counting [CFMvK96, PMM$^+$96, HHH$^+$98]. It was, however, shown that Weinberg's counting give inaccurate estimations for some diagrams. The source of the problem was already pointed out in [CFMvK96], where it was noted that the pion production process includes a new scale, namely, the initial momentum of nucleons, which is larger than the pion

[8] Small-scale parameters can include pion mass, momenta of pions, residual momenta of heavy baryons, and the delta-nucleon mass difference. Exact set of small parameters depends on the particular process.

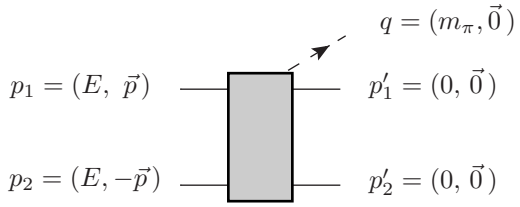

Figure 1.1: The kinematics of the reaction $NN \to NN\pi$ in the heavy baryon formalism. Nucleon mass is subtracted from the momentum of each nucleon (*i.e.* $p_1 = P_1 - m_N\, v$, where P_1 is the full four-momentum of the first nucleon; see Eq. 1.12). Threshold values for energy and three-momenta are shown in brackets.

mass. This idea was further developed in [dRMvK00, HvKM00, HK02], see also Ref. [Han04] for a review article. In this section we give an introduction to momentum counting scheme including recent developments.

One of the main specifics of pion production, compared to other processes studied in ChPT, is its kinematics, more precisely, the large transferred momenta. The kinematics of the pion production reaction is shown in Fig. 1.1. To produce a pion at threshold, the kinetic energy of each nucleon should be $E = m_\pi/2$. The corresponding three-momenta can be easily estimated in the non-relativistic limit:

$$E \simeq \frac{\vec{p}^{\,2}}{2m_N} \quad \Rightarrow \quad |\vec{p}\,| \simeq \sqrt{m_\pi m_N}. \tag{1.25}$$

The exact value of three-momenta can be found from the nucleon on-mass-shell condition $P^2 = m_N^2$, which leads to

$$|\vec{p}\,| = \sqrt{E^2 + 2m_N E} = \sqrt{m_\pi^2/4 + m_\pi m_N}. \tag{1.26}$$

However, for power counting estimations the simpler estimate Eq. (1.25) is sufficient.

In the production process, the momentum $\vec{p}$ is transferred from one nucleon to another. This transferred momentum is several times larger than the pion mass, but still much smaller than the large scale Λ_χ. Effectively, this is a second small scale in the problem (in addition to the small scale m_π). In total, there are two different small scales in pion production process. The momentum counting scheme allows for a more accurate estimation of Feynman diagrams by distinguishing these two small scales.

Because of the two small scales, one can expect to end up with two expansion parameters[9]: $\chi_1 = |\vec{p}\,|/\Lambda_\chi \simeq \sqrt{m_\pi/m_N}$ and $\chi_2 = m_\pi/\Lambda_\chi \simeq m_\pi/m_N$. However, due to the simple relation between these expansion parameters ($\chi_2 = \chi_1^2$), it is convenient to introduce a single expansion parameter corresponding to the ratio $|\vec{p}\,|/m_N$. Thus, the expansion parameter in MCS is

$$\chi_{\rm MCS} = \frac{\text{small scale}}{\text{large scale}} \simeq \frac{|\vec{p}\,|}{\Lambda_\chi} \simeq \frac{|\vec{p}\,|}{m_N} \simeq \sqrt{\frac{m_\pi}{m_N}}, \tag{1.27}$$

[9] In MCS the large scale Λ_χ is associated with nucleon mass m_N, because both are of order of 1 GeV.

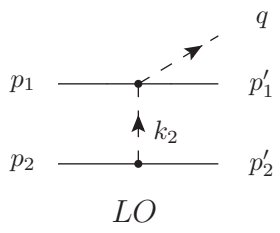

Figure 1.2: Rescattering diagram constructed from the leading-order vertices. According to the MCS estimation Eq. (1.29) it contributes to the amplitude at LO.

where the larger one of two small scales is used. Note that the ratio of two small scales[10] $m_\pi/|\vec{p}|$ is also equal to $\chi_{\rm MCS}$.

The MCS expansion parameter ($\chi_{\rm MCS} \simeq 0.4$) is larger than the one in Weinberg scheme ($\chi_{\rm W} \simeq 0.15$), so the convergence of the perturbation series in MCS is expected to be slower. Slower convergence of chiral expansion is one of the motivations to calculate higher orders in MCS studies.

Feynman diagrams in MCS are estimated in a special way. Unlike standard ChPT, in momentum counting scheme the expansion parameter for diagrams doesn't exactly coincide with the expansion of the Lagrangian. While the Lagrangian is classified using the Weinberg expansion parameter χ_W, Feynman diagrams in MCS are estimated using the larger expansion parameter $\chi_{\rm MCS} \simeq \sqrt{\chi_W}$.

The main point of the MCS is the proper identification of the small scales in the Feynman diagrams. By using the proper kinematics for a particular diagram, one can identify which momenta are of order m_π and which are of order of $|\vec{p}|$. This method allows one to make accurate estimations of pion production diagrams.

In MCS, to estimate a particular diagram, one has to write down the expression for this diagram using the Feynman rules and then use the reaction kinematics to estimate different dimensionful quantities in the expression. The rules to assign a proper small scale to typical structures are following:

$$\begin{aligned} S\cdot p_i \to |\vec{p}| \qquad & p_i^2 \to \vec{p}^{\,2} \qquad & v\cdot p_i \to m_\pi \\ S\cdot p_i' \to m_\pi \qquad & p_i'^2 \to m_\pi^2 \qquad & v\cdot p_i' \to m_\pi \\ S\cdot q \to 0 \qquad & q^2 \to m_\pi^2 \qquad & v\cdot q \to m_\pi, \end{aligned} \tag{1.28}$$

where $i = 1$ or 2 denotes the first or the second nucleon. Note that terms proportional to $(S\cdot q)$ are neglected, because they do not contribute to the amplitude at threshold. Low-energy constants are estimated in a usual way as $1/\Lambda_\chi^n$, where the power n is given by the dimension of the LEC. Additional care is required to estimate the running momenta inside the loops.

To illustrate the main features of the MCS we provide exemplary estimations of typical tree-level and loop diagrams.

Let's first estimate the size of the rescattering diagram involving only leading-order vertices (Fig. 1.2). To make an MCS estimation, we use both: Feynman-rules and the kinematics. In

[10] This ratio enters, for example, the estimation of leading rescattering diagram Eq. (1.29).

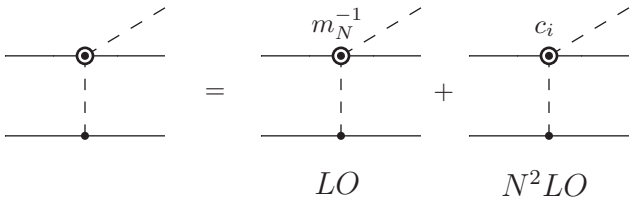

Figure 1.3: Rescattering diagram constructed from subleading $\pi N \to \pi N$ vertex (and leading πNN vertex) can be separated into two parts. One part involves $1/m_N$-corrections to the leading $\pi N \to \pi N$ vertex and contributes at LO MCS (Eq. 1.30). The second part involves subleading $\pi N \to \pi N$ vertex proportional to LECs c_i. This part contributes at N^{2}LO (Eq. 1.31). The kinematics is the same as in Fig. 1.2.

this diagram, pion emission from second nucleon gives the factor $S\cdot k_2/f_\pi$, where $k_2 = p_2 - p_2'$. The pion propagator gives $1/k_2^2$, and the Weinberg–Tomozawa (WT) vertex gives $v\cdot q/f_\pi^2$. Combining all factors together and using rules (1.28) we get

$$\frac{S\cdot k_2}{f_\pi}\frac{1}{k_2^2}\frac{v\cdot q}{f_\pi^2} \sim \frac{1}{f_\pi^3}\frac{m_\pi}{|\vec{p}|} \sim \frac{1}{f_\pi^3}\chi_{\rm MCS} \to \text{LO}. \tag{1.29}$$

Given that it is not possible to construct a diagram with estimation lower than $\chi_{\rm MCS}/f_\pi^3$, the diagram (Fig. 1.2) contributes at leading order.

Let's consider the rescattering diagram with subleading $\pi N \to \pi N$ vertex shown in the Fig. 1.3. Subleading $\pi N \to \pi N$ vertex consists of two parts. The first part includes terms proportional to the LECs c_i. This part comes from the NLO covariant Lagrangian. The second part includes the $1/m_N$-corrections to the LO vertex. These corrections appear from heavy baryon expansion of LO covariant Lagrangian. We will consider these two contributions as two separate diagrams. For this purpose we introduce the notation shown in the r.h.s. in Fig. 1.3. Naively, one can expect the contributions to the amplitude of both parts of the vertex to be of the same order, because both parts are from the NLO Lagrangian. However, due to the kinematics of pion production reaction, these parts contribute differently. To demonstrate this, we consider both diagrams individually.

Consider first a rescattering diagram with $1/m_N$-correction to leading WT vertex (first graph in the right-hand side in Fig. 1.3). Pion emission from nucleon 2 and pion propagator yield exactly the same contributions $S\cdot k_2/f_\pi$ and $1/k_2^2$ as discussed for LO diagram (Fig. 1.2), and the $1/m_N$-correction to the leading WT vertex gives $(k_2+q)\cdot(p_1+p_1')/(f_\pi^2 m_N) \sim p_1^2/(f_\pi^2 m_N)$. Combining all factors and using counting rules (1.28) we get

$$\frac{S\cdot k_2}{f_\pi}\frac{1}{k_2^2}\frac{(k_2+q)\cdot(p_1+p_1')}{f_\pi^2 m_N} \sim \frac{1}{f_\pi^3}\frac{|\vec{p}|}{m_N} \sim \frac{1}{f_\pi^3}\chi_{\rm MCS} \to \text{LO}. \tag{1.30}$$

We see the striking result: the diagram involving (subleading) $1/m_N$-correction to the WT vertex yields an additional LO contribution. This was first noted in Ref. [LBH$^+$06], where it was explicitly shown that the LO diagram in Fig. 1.3 gives additional $\sim 30\%$ contribution to the pion production amplitude, which is essential to reproduce the correct total cross section in $pp \to d\pi^+$. This example illustrates that MCS allows one to correctly estimate

$1/m_N$-corrections, which can be "enhanced" in the pion production kinematics. In other words, due to the presence of several scales, leading and sub-leading vertices of the chiral Lagrangian can contribute to the pion production amplitude at the same order. This may rise a question of how important $(1/m_N)^2$-vertex-corrections could be? It turns out that the kinematic enhancement can promote recoil correction only slightly, due to the suppression provided by powers of nucleon mass in the denominator.

Let's consider the rescattering diagram involving subleading $\pi N \to \pi N$ vertices proportional to c_i (the right one in Fig. 1.3). Estimations of πNN vertex and pion propagator are exactly the same as in previous two cases. The estimation of the remaining $\pi N \to \pi N$ vertex is done using the corresponding Feynman rules. Depending on the particular LEC c_i $(i = 1, \ldots, 4)$ one obtains the following estimation:

$$\frac{S\cdot k_2}{f_\pi}\frac{1}{k_2^2}\frac{1}{f_\pi^2}\begin{cases} c_1 m_\pi^2 \\ c_2 v\cdot k_2 v\cdot q \\ c_3 k_2\cdot q \\ c_4 S\cdot k_2\, S\cdot q \end{cases} = \frac{1}{f_\pi^3}\frac{1}{|\vec{p}|}\begin{cases} m_\pi^2/\Lambda_\chi \\ m_\pi^2/\Lambda_\chi \\ m_\pi^2/\Lambda_\chi \\ 0 \end{cases} = \frac{1}{f_\pi^3}\begin{cases} \chi^3_{\rm MCS} \\ \chi^3_{\rm MCS} \\ \chi^3_{\rm MCS} \\ 0 \end{cases} \to {\rm N^2LO}, \tag{1.31}$$

where, in addition to the counting rules (1.28), we used the estimation for LECs $c_i \sim 1/\Lambda_\chi \sim 1/m_N$. In this example we see that the diagram with subleading $\pi N \to \pi N$ vertices proportional to c_i is quite suppressed compared to LO.

So far we have considered the rescattering diagrams with leading and subleading $\pi N \to \pi N$ vertices. We found that the rescattering diagram with the leading vertices is of LO, while the rescattering diagram with subleading vertices has two parts contributing at different orders. The part proportional to $1/m_N$-corrections is also LO, but the one proportional to LECs c_i is $\rm N^2LO$.

To summarize, in the pion production kinematics, diagrams involving subleading $1/m_N$ vertices can be enhanced compared to similar diagrams involving vertices proportional to LECs. Finally, we note that the issue with the enhanced $1/m_N$-corrections is specific to the HBChPT formalism and doesn't appear in the covariant formulation of baryon ChPT where all recoil effects are contained in the LO vertex itself.

Lets consider an estimation of loop-diagrams in MCS. The crucial point in such estimations is assigning a proper scale to the running loop momenta. The scale of loop momenta may drastically change the order of the diagram. The method to assign a scale to the loop momenta is the following. If the loop integral contains the momenta of order of $|\vec{p}|$, which cannot be eliminated by a shift of variables, then the integration momenta of this loop is of order of $|\vec{p}|$. If all quantities of order $|\vec{p}|$ can be removed from the loop integral by a variable shift, then the loop momenta is of order of m_π.

The example of the diagram with relatively large running momenta is shown in Fig. 1.4(a). In this diagram the loop integral contains one nucleon propagator and two pion propagators. The structure of the loop-integral is given by

$$\frac{1}{f_\pi^5}\int\frac{d^4l}{(2\pi)^4}\frac{(S_2\cdot\tilde{l})(S_2\cdot\ l)(S_1\cdot\tilde{l})}{(l^2-m_\pi^2+i0)(\tilde{l}^2-m_\pi^2+i0)(-v\cdot l+i0)}, \tag{1.32}$$

where $\tilde{l} = l + p_1 - p_1' - q \simeq l + p_1$. There is no possibility to remove momenta $|\vec{p}|$ from the loop-integral. Thus, the scale of running momenta is $|\vec{p}|$. Complete estimation of the diagram

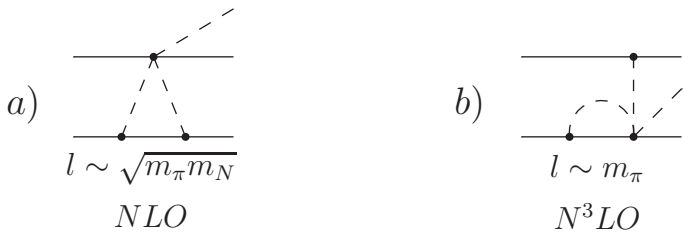

Figure 1.4: Exemplary one-loop diagrams with different running loop momenta. Both diagrams are constructed from exactly the same vertices, however due to different structure of the loop-integrals, the diagram (a) starts to contribute at NLO MCS, while the diagrams (b) starts at $\mathrm{N^3LO}$.

1.4(a) gives:

$$\frac{1}{f_\pi^3}\frac{l^4}{(4\pi f_\pi)^2}\frac{k^2 l}{l^5} \sim \frac{1}{f_\pi^3}\chi^2_{\mathrm{MCS}} \to \mathrm{NLO}, \tag{1.33}$$

where we used $k \sim |\vec{p}|$ and $4\pi f_\pi \sim m_N$.

Example of the diagram with small running momenta is shown in Fig. 1.4(b). In this diagram, the loop consists of single nucleon propagator and single pion propagators. The structure of the loop-integral is given by

$$\frac{S\cdot k_1}{f_\pi}\frac{1}{k_1^2}\frac{S\cdot k_1}{f_\pi}\frac{1}{f_\pi^3}\int\frac{d^4l}{(2\pi)^4}\frac{(S_2\cdot l)}{(l^2-m_\pi^2+i0)(-v\cdot l+i0)}, \tag{1.34}$$

where $k_1 = p_1 - p_1'$. This loop-integral doesn't involve large momenta $|\vec{p}|$, thus the running momenta l is of order of m_π. MCS estimation of this diagram gives:

$$\frac{1}{f_\pi^3}\frac{1}{(4\pi f_\pi)^2}\frac{l^5}{l^3} \sim \frac{1}{f_\pi^3}\chi^4_{\mathrm{MCS}} \to \mathrm{N^3LO}, \tag{1.35}$$

where we used $l \sim m_\pi$.

These two examples (Fig. 1.4) show that diagrams constructed from exactly the same set of vertices and containing identical number of loops, can contribute at different MCS order.

Theory with explicit delta requires additional counting rules, related to the scale introduced by the delta-nucleon mass difference. Inclusion of delta-nucleon mass difference in the MCS is discussed in the Chapter 3.

1.5 General pion production amplitude at threshold

The most general form of the threshold amplitude (where the pion is in an s-wave relative to a NN S-wave final state) for the pion-production reaction $N_1(\vec{p}) + N_2(-\vec{p}) \to N + N + \pi$ in the center-of-mass frame can be written as [FBE+12] :

$$M_{th}(NN \to NN\pi) = \mathcal{A}\,(\vec{\sigma}_1 \times \vec{\sigma}_2)\cdot\vec{p}\;\boldsymbol{\tau}_+\cdot\boldsymbol{\phi}^* + \mathcal{B}\;(\vec{\sigma}_1+\vec{\sigma}_2)\cdot\vec{p}\;(-i)\,\boldsymbol{\tau}_\times\cdot\boldsymbol{\phi}^*\,, \tag{1.36}$$

where $\boldsymbol{\tau}_+ = \boldsymbol{\tau}_1 + \boldsymbol{\tau}_2, \boldsymbol{\tau}_\times = i\,\boldsymbol{\tau}_1 \times \boldsymbol{\tau}_2$ and $\vec{\sigma}_{1,2}$ and $\boldsymbol{\tau}_{1,2}$ are the spin and isospin operators of nucleons 1 and 2. This expression incorporates the selection rules for the NN states. The final

pion's isospin state is denoted by $\boldsymbol{\phi}$, e.g. $\boldsymbol{\phi} = (0,0,1)$ for π^0-production and $\boldsymbol{\phi} = (1,i,0)/\sqrt{2}$ for π^+-production. For example, the amplitude $\mathcal{A}$ corresponds to the production of an s-wave pion accompanied with the final state spin-singlet S-wave NN interaction ($pp \to pp\pi^0$), while $\mathcal{B}$ corresponds to the spin triplet NN final state ($pp \to d\pi^+$).

It is convenient to write down the threshold reaction amplitudes in the form where the relevant spin-angular structure of the initial and final nucleon pairs are shown explicitly [11]

$$\begin{aligned} \mathcal{M}_{pp\to pp\pi^0} &= 4i\mathcal{A}(\vec{\mathcal{S}}\cdot\hat{p})\mathcal{I}'^{\dagger}, \\ \mathcal{M}_{pp\to d\pi^+} &= -2\sqrt{2}i\mathcal{B}\,(\vec{\mathcal{S}}\times\hat{p}\,)\cdot\vec{\varepsilon}\,. \end{aligned} \tag{1.37}$$

Here, $\vec{\varepsilon}$ is the deuteron polarization vector, $\hat{p}$ is the unit vector of the initial relative momenta of two nucleons, and $\vec{\mathcal{S}} = \chi_2^T\sigma_y\vec{\sigma}\chi_1/\sqrt{2}$, and $\mathcal{I}'^{\dagger} = \chi_{1'}^{\dagger}\sigma_y\chi_{2'}^{*}/\sqrt{2}$ denote the normalized spin structures of the initial spin-triplet and final spin-singlet states, respectively.

One of the main goals of this thesis is to derive the contributions to $\mathcal{A}$ and $\mathcal{B}$ that originate from all diagrams up to N^{2}LO MCS.

1.6 Method to calculate the full pion production amplitude

Calculation of the full amplitude of pion production reactions is not trivial for several reasons. In addition to the relatively large transferred momentum and related convergence issues (discussed in Section 1.4), an additional complication arises due to nucleon-nucleon interactions in the initial and final states.

The reaction $NN \to NN\pi$ involves nucleon-nucleon states both in the initial and in the final states. Nucleon-nucleon interactions are non-perturbative due to the presence of bound or virtual states in the NN system. To reproduce a virtual or a bound state (and the behavior of the NN phase shifts), one has to iterate NN interactions an infinite number of times. In the language of Feynman diagrams, this means that one has to calculate an infinite number of diagrams which are of the same importance. This specifics doesn't allow one to treat NN interactions perturbatively.

1.6.1 Hybrid approach for pion production

One scheme to deal with non-perturbative few-nucleon interactions in ChPT was proposed by Weinberg [Wei90, Wei91, Wei92]. In Ref. [Wei92] he formulated a method, called *the hybrid approach*, to calculate few-nucleon reactions with external probes in ChPT. In the same article he applied this method to study the elastic pion-deuteron scattering ($\pi NN \to \pi NN$). In this thesis we use the hybrid approach to study pion production ($NN \to NN\pi$).

In the hybrid approach, the full amplitude is divided into three pieces: initial state interaction (ISI), irreducible pion production operator (IPPO), and the final state interaction (FSI). This division is illustrated in the Fig. 1.5. Each piece is calculated using appropriate methods. The production operator is calculated perturbatively in chiral EFT framework. Initial- and final-state interactions are calculated using non-perturbative methods. Ideally, ISI and FSI should be calculated based on the chiral NN potential. But at the energies of pion production threshold, no chiral NN wave functions are available at the moment. For this reason,

[11] The connection of the amplitudes $\mathcal{A}$ and $\mathcal{B}$ to the observables is given in, e.g., Ref. [BEH$^+$09]

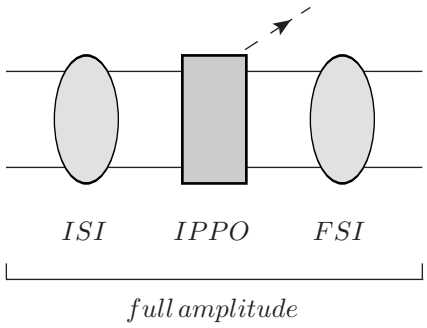

Figure 1.5: The hybrid approach to calculate full pion production amplitude. Full amplitude is obtained by convoluting irreducible pion production operator (IPPO) with initial-state NN-interactions (ISI) and final-state NN-interactions (FSI). IPPO is calculated perturbatively in chiral EFT. ISI and FSI are taken from phenomenological models.

ISI and FSI are taken from calculations based on phenomenological potentials. The usage of phenomenological NN interactions explains the name "hybrid" used for this approach[12]. Finally, to get the full amplitude all pieces are convoluted together. In the following sections we consider individual parts of the full amplitude.

1.6.2 Irreducible pion production operator

The pion production operator is the main part of the pion production amplitude. It is calculated perturbatively in the chiral EFT formalism. The full amplitude is obtained by convoluting the production operator with the ISI and FSI. Since all NN interactions are taken into account by the convolution procedure, the production operator should itself not contain any parts of NN interactions. The production operator is called *irreducible* if it does not contain any NN cuts, and *reducible* when it contains one or more such cuts. To make consistent hybrid calculation, only irreducible production operators should be considered. This is important to avoid *double counting* — a situation when the same contribution is included twice: first in the production operator and second in the NN interactions. To get a correct full amplitude, only irreducible production operators should be convoluted with the ISI and FSI.

In most cases, reducibility of a production operator can be easily identified from the topology of the corresponding Feynman diagram. If one can cut two nucleon lines to separate the diagram into two pieces, the diagram is called reducible, if this is not possible, the diagram is called irreducible. Examples of reducible and irreducible diagrams are shown in Fig. 1.6, where the diagram on the left is reducible, because it contains the two-nucleon cut (even two of them). The diagram on the right is irreducible, since there are no NN cuts. From these two diagrams only the irreducible (right) one, should be calculated as a part of the production operator and convoluted with the ISI and FSI.

In some cases, an additional care is required to identify reducibility. Namely, some dia-

[12] At the time of the study [Wei92] there were no chiral NN wave functions available even at very small energies, typical for πd-scattering. This explains the motivation behind the hybrid approach.

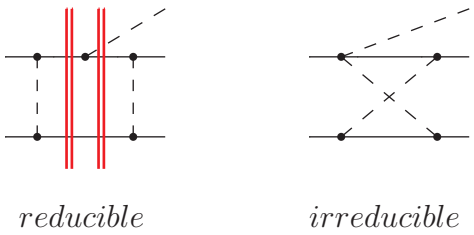

Figure 1.6: Examples of reducible and irreducible pion production operators. Double line denotes the two-nucleon cut.

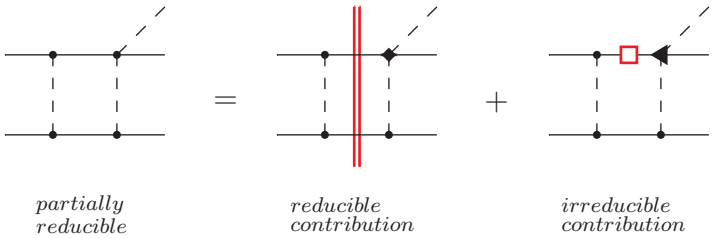

Figure 1.7: The box diagram contains both reducible and irreducible contributions. In the box diagram, the leading $\pi N \to \pi N$ vertex can be decomposed into two parts (see Appendix C). The part denoted by diamond is proportional to the outgoing pion mass and gives reducible contribution. The second part denoted by triangle is proportional to nucleon momenta and exactly cancels adjacent nucleon propagator (denoted by red square). Double (red) line denotes two-nucleon cut.

grams with the two-nucleon cut, may involve irreducible contributions due to four-momentum-dependent vertices[13] [LBH$^+$06]. An example of a partially irreducible diagram is the box diagram (Fig. 1.7 left). This diagram contains the momentum-dependent $\pi N \to \pi N$ vertex, which (as explained in Appendix C) can be separated into three parts. The first part (denoted as diamond in Fig. 1.7) proportional to the outgoing pion momentum generates a reducible contribution (central diagram in Fig. 1.7). The second part (denoted as triangle in Fig. 1.7) proportional to internal nucleon momenta exactly cancels the nucleon propagator denoted by red square in Fig. 1.7. Thus, the corresponding part of this diagram doesn't contain any NN cuts and generates an irreducible contribution, which should be included in the total IPPO. The third part (not shown) is proportional to external nucleon momenta. If the external nucleon is on-shell, this part is exactly zero. If the nucleon is off-shell, the contribution of this part corresponds to a multi-loop high-order correction [LBH$^+$06]. The irreducible contribution of the box diagram plays a crucial role to obtain a correct one-loop NLO-correction to the full pion production amplitude [LBH$^+$06]. To identify all irreducible contributions relevant to a particular process, the reducible diagrams with four-momentum dependent vertices have to be examined carefully for the appearance of irreducible contributions.

One more reducibility issue is related to the so called "direct" pion production operators

[13]Note that in heavy baryon formulation four-momentum-dependent vertices show up as time-dependent ones.

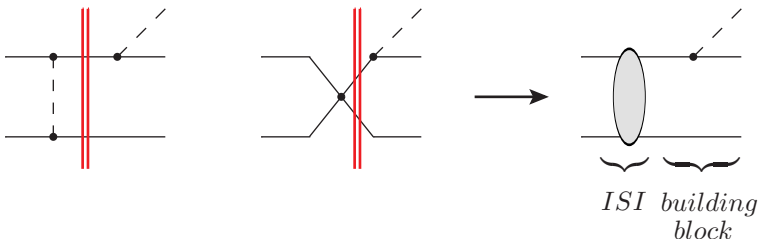

Figure 1.8: Direct pion production operators and the way to include them in the hybrid approach. Left and center: two-nucleon cuts in the "direct" pion production operators. Right: the way to include direct pion production process into the hybrid calculation. Double line denotes two-nucleon cut.

(left and central diagrams in Fig. 1.8). These diagrams do have two-nucleon cuts. However, if one removes the one-pion-exchange (or NN contact interaction) from these diagrams, the remaining part is a disconnected (and off-shell) operator. Due to this behavior, it is not immediately clear whether these diagrams are reducible or not. Several ideas on how to get an irreducible contribution from the "direct" diagrams were discussed in [BM11, Bol11] within different approximations. In the present work we consider "direct" diagrams as reducible. The "direct" contribution to the full amplitude in our approach should be calculated as a convolution of the "building block", corresponding to the "direct" pion production from one nucleon, with the ISI or FSI (right diagram in Fig. 1.8). The "building block" itself is not an independent irreducible pion production operator. It must always be convoluted with the ISI or FSI to get a contribution to the full amplitude.

Since pion production requires important contribution from diagrams with delta resonance degree of freedom, it is useful to generalize the formalism described to include explicitly $N\Delta$ intermediate states, see section 3.1 for further discussions.

1.6.3 Nucleon-nucleon wave functions

Ideally, both the production operator and NN wave functions should be calculated in the same ChPT framework. However, to produce a pion, the initial momenta of the nucleons should be quite large. At the moment, no ChPT calculations of the NN interactions near pion production threshold are available. This motivates to resort to the hybrid approach and use modern phenomenological NN potentials, instead of ones based on the chiral potentials.

Phenomenological NN models can accurately describe NN observables in the pion production threshold region. However, a fully consistent theoretical uncertainty estimate will be possible only when chirally motivated NN wave functions will become available. Since there are many different phenomenological potentials available, one can estimate the model dependence by calculating the full amplitude using convolutions with NN interactions from different models. The spread in the results should not exceed the estimations based on the chiral order to which to which the pion production operator is evaluated.

Chapter 2

Pion production operator in chiral perturbation theory

The isospin symmetry requires that different pion production reaction channels at threshold can be expressed in terms of two s-wave isospin amplitudes. In total, there are three possible s-wave pion production channels: $pp \to d\pi^+$, $pp \to pp\pi^0$, and $pn \to d\pi^0$. All of them have interesting features.

The channels $pp \to d\pi^+$ and $pp \to pp\pi^0$ are known for the so-called cross section puzzle. Namely, while one can naively expect the total cross sections (TCS) in both channels to be of the same order, the data shows a drastic difference.[1] At near threshold energy of $T_{\rm lab} = 293.5$ MeV [AS$^+$03], the total cross section of charged pion production is $\sigma_{\rm tot}(pp \to d\pi^+) \simeq 43\,\mu b$. In contrast, the cross section of neutral pion production is only $\sigma_{\rm tot}(pp \to pp\pi^0) \simeq 3\,\mu b$, which is an order of magnitude smaller than in the charged channel. To understand this difference one has to consider the mechanisms behind both processes. The overview of the various production mechanisms contributing to these processes is given in Table 2.1.

In the $pp \to d\pi^+$ channel, the dominant contribution to the total cross section (TCS) is provided by the LO rescattering diagram (Fig. 1.2). It was shown [LBH$^+$06] that the LO rescattering diagram together with its LO recoil correction reproduces TCS in this channel within the calculation uncertainty. It was also demonstrated that at NLO all loop contributions cancel out exactly [LBH$^+$06], thus providing no additional contribution. The estimated uncertainty of the NLO MCS calculation [LBH$^+$06] is about $2\chi^2_{\rm MCS} \sim 30\%$ in the total cross section. The N^{2}LO calculation will allow one to reduce the uncertainty down to $2\chi^3_{\rm MCS} \sim 13\%$ in the TCS.

In the $pp \to pp\pi^0$ channel, the mechanisms are quite different. The LO rescattering diagram as well as its recoil corrections are forbidden, because the leading pion nucleon vertex (Weinberg–Tomozawa vertex) is of isovector origin, and thus, it cannot contribute to the neutral pion production in $pp \to pp\pi^0$ channel since there are no charge exchanges. The remaining LO mechanism — direct pion production (Fig. 1.8) — gives a very small contribution after the convolution with the ISI and FSI. (This suppression happens due to the momentum mismatch between the initial and final state nucleons [Han04].) Furthermore,

[1] Note that the cross sections of some two-body reactions is normally significantly bigger than those of three-body channels due to the phase space. However, even after correcting for the phase-space factors the difference between cross sections of $pp \to d\pi^+$ and $pp \to pp\pi^0$ is still large.

Table 2.1: Diagrams contributing to the pion production operator up to N^2LO MCS and a qualitative estimation of their contributions to different pion production channels. First row shows the MCS order, second row shows the diagrams which start to contribute at that order, and the last two rows indicate the role of the diagrams to different pion production channels. The notation and expressions for the vertices are given in the Appendix B.

MCS order	LO	NLO	N^2LO
diagrams	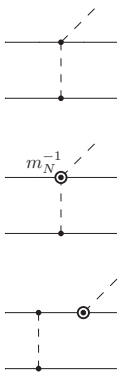	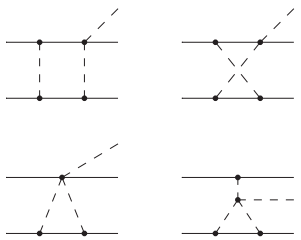 + ⋯	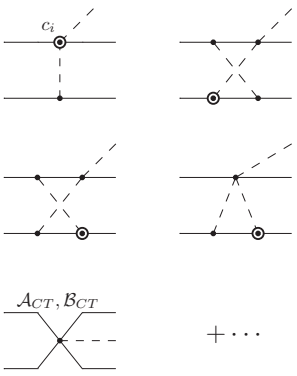 + ⋯
contr. to $pp \to d\pi^+$	big [LBH$^+$06]	zero (full cancellation) [LBH$^+$06]	expected to be small, provides only a small correction to large LO terms [calculated in this work]
contr. to $pp \to pp\pi^0$	negligible [CFMvK96] [PMM$^+$96]	zero (full cancellation) [HK02]	expected to be small, but important in this channel [calculated in this work]

loop contributions at NLO cancel out exactly [HK02]. Thus, in the $pp \to pp\pi^0$ channel, the net effect of the LO and NLO diagrams appears to be very small. As a consequence, the cross section is mostly governed by the N^2LO mechanisms. This specifics of the reaction $pp \to pp\pi^0$ allows one to investigate the role of subleading mechanisms of pion production once a systematic N^2LO calculation is performed.

Understanding of isospin symmetric pion production, as outlined above, is not only interesting by its own, but also appears as a necessary prerequisite for investigation of charge symmetry breaking in $pn \to d\pi^0$. In the isospin symmetric world the differential cross section of this reaction would be symmetric under interchange of initial proton and neutron. However, in real world, the differential cross section is not symmetric due to *charge symmetry breaking* (CSB) — a specific isospin breaking effect. We investigate CSB in $pn \to d\pi^0$ in Chapter 4.

Another motivation for high-accuracy calculation of the pion production operator is provided by studies of few-nucleon processes. Some few-nucleon processes include pion production as a building block. For example, in the isospin forbidden $dd \to \alpha\pi^0$ reaction one can study charge symmetry breaking using measurements of the total cross section. Any non-zero TCS in this reaction is a manifestation of CSB [SBA$^+$03, GHN$^+$04, NFG$^+$06, FMM09]. The reac-

tion $NN \to NN\pi$ is a building block for $dd \to \alpha\pi^0$. For this reason, the calculation of the CS and CSB pion production operators to a high accuracy would be an important step to study CSB in $dd \to \alpha\pi^0$.

Thus, a high-accuracy calculation of pion production operator at threshold is important to understand the mechanisms behind neutral pion production, study charge symmetry breaking in QCD and develop new methods to study large-momentum-transfer processes using chiral EFT.

In this chapter we derive the pion production operator at threshold up-to-and-including N^{2}LO MCS. We identify the mechanisms responsible for neutral pion production and show importance of the intermediate-range effects, which were not considered in phenomenological studies so far. We also develop an efficient method to calculate loop corrections to the amplitude, which can be further used in other chiral EFT studies.

To derive the production operator we use a heavy-baryon formulation of chiral perturbation theory (HBChPT). To estimate Feynman diagrams we employ the momentum counting scheme (MCS). This counting scheme takes into account the relatively large momenta inherent to pion production reactions. Unlike the standard Weinberg's power counting, the MCS correctly estimates pion production diagrams with heavy-baryon recoil corrections and diagrams with loops.

To calculate loop corrections to the production operator we develop an efficient method, based on the identification of common structures in Feynman diagrams. This method (which is discussed in Section 2.2) allows one to detect numerous cancellations between diagrams before carrying out the loop integration. In addition, we derive relations between propagators and momentum-dependent vertices in ChPT. These relations (which are given in the Appendix C) allow one to easily identify relevant irreducible contributions and help to spot cancellations between various diagrams. These methods and relations depend neither on the heavy baryon formulation, nor on the counting scheme and can be used in the wide range of chiral EFT studies.

This chapter is organized as follows. In Section 2.1 we present all possible tree-level contributions up-to-and-including N^{2}LO MCS. In Section 2.2 we consider loop diagrams to the same order. We discuss renormalization or loop diagrams in Section 2.2.5 and give a summary in Section 2.3.

2.1 Tree-level operators

Tree-level contributions to pion production operators can be of several types (Fig. 2.1): rescattering operators, direct pion production operators, and five-point contact operators. In the rescattering operators (Fig. 2.1a), a pion is emitted from one nucleon and rescattered from another nucleon. In the direct pion production (Fig. 2.1b), a pion is emitted from a single nucleon. Five-point contact operators (Fig. 2.1c) refer to $NN \to NN\pi$ contact terms. Below we consider all these types of tree-level operators in detail.

2.1.1 Rescattering operators

The general topology of the rescattering operator is shown in Fig. 2.1a. The rescattering operator consists of a πNN vertex, a pion propagator, and a $\pi\pi NN$ vertex. All combinations

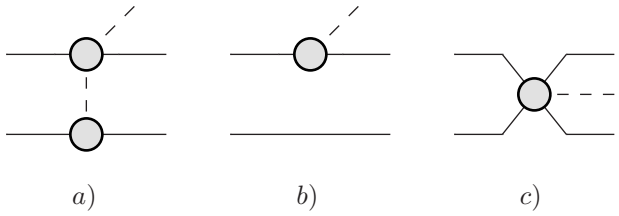

Figure 2.1: General topologies of the tree-level diagrams. Rescattering operator (a), direct pion production (b), and five-point contact operator (c). Solid lines denote nucleons, dashed lines — pions, circles refer to any LO, NLO, or N^{2}LO vertices from chiral Lagrangian.

of vertices that give contributions relevant for our N^{2}LO MCS calculation are shown in the box in Fig. 2.2.

At leading order (LO) there are two diagrams: diagram Fig. 2.2a is constructed completely from leading vertices, and diagram Fig. 2.2b includes $1/m_N$-correction to the $\pi\pi NN$ vertex. These diagrams are of the same order due to the kinematics of pion production (see Section 1.4 for discussion). The total LO contribution from these two diagrams is given by

$$iM^{\rm LO}_{\rm resc} = iM^{\rm LO}_{\rm resc.(a)} + iM^{\rm LO}_{\rm resc.(b)} = \frac{g_A}{2f_\pi^3}\frac{v\cdot q}{k_2^2 - m_\pi^2 + i0}(S_2\cdot k_2)\tau_\times^a + (1\leftrightarrow 2), \qquad (2.1)$$

where the superscript a (a=1,2,3) refers to the isospin quantum number of the outgoing pion field. An isovector combination of Pauli matrices $\tau_\times^a$ is defined as $\tau_\times^a = i(\boldsymbol{\tau}_1\times\boldsymbol{\tau}_2)^a$, the transferred momentum is denoted by $k_2 = p_2 - p_2'$, and four-vectors v^μ and S^μ are defined in Section 1.2. The symbol $(1\leftrightarrow 2)$ refers to the fact that there are additional diagrams of the same kind with nucleons one and two being interchanged. Other symmetrization factors are introduced by partial wave projection during convolution with NN wave functions.

The rescattering operator at N^{2}LO contains corrections suppressed by $1/m_N$ due to the vertices from $\mathcal{L}^{(2)}_{\pi N}$ and also corrections $\propto 1/m_N^2$ from $\mathcal{L}^{(3)}_{\pi N}$. We call these amplitude operators $M^{\rm N^2LO}_{\rm rescat1}$ and $M^{\rm N^2LO}_{\rm rescat2}$, respectively. The explicit expressions read:

$$\begin{aligned} iM^{\rm N^2LO}_{\rm rescat1} &= \frac{g_A}{f_\pi^3}\frac{(S_2\cdot k_2)\tau_2^a}{k_2^2 - m_\pi^2 + i0}\left[4c_1 m_\pi^2 - v\cdot q\, v\cdot k_2\left(2c_2 + 2c_3 - \frac{g_A^2}{4m_N}\right)\right] \\ &\quad -\frac{g_A}{f_\pi^3}\frac{(v\cdot q)\,\tau_\times^a}{k_2^2 - m_\pi^2 + i0}\frac{S_2\cdot(p_2+p_2')}{4m_N}(v\cdot k_2) + (1\leftrightarrow 2), \qquad (2.2) \\ iM^{\rm N^2LO}_{\rm rescat2} &= \frac{g_A}{f_\pi^3}\frac{v\cdot q}{k_2^2 - m_\pi^2 + i0}\Bigg\{ -\tau_2^a\,(S_2\cdot k_2)\frac{k_2\cdot(p_1+p_1')}{m_N^2}\left(m_N c_2 - \frac{g_A^2}{16}\right) \\ &\quad +\tau_\times^a\,(S_2\cdot k_2)\left[\frac{\vec{p}_1^{\,2} + \vec{p}_1^{\,\prime 2}}{16m_N^2} + \frac{1 + g_A^2 + 8m_N c_4}{8m_N^2}\left([S_1\cdot k_2, S_1\cdot(p_1+p_1')] + \frac{k_2^2}{2}\right)\right] \\ &\quad -\frac{\tau_\times^a}{8m_N^2}\left[(S_2\cdot p_2')p_2^2 - (S_2\cdot p_2)p_2'^2\right]\Bigg\} + (1\leftrightarrow 2), \qquad (2.3) \end{aligned}$$

where $[S_{1\mu}, S_{1\nu}] = S_{1\mu}S_{1\nu} - S_{1\nu}S_{1\mu}$. The first two terms in the curly bracket in Eq.(2.3) are due to the corrections to the $\pi\pi NN$ vertex from $\mathcal{L}^{(3)}_{\pi N}$ while the last one stands for the

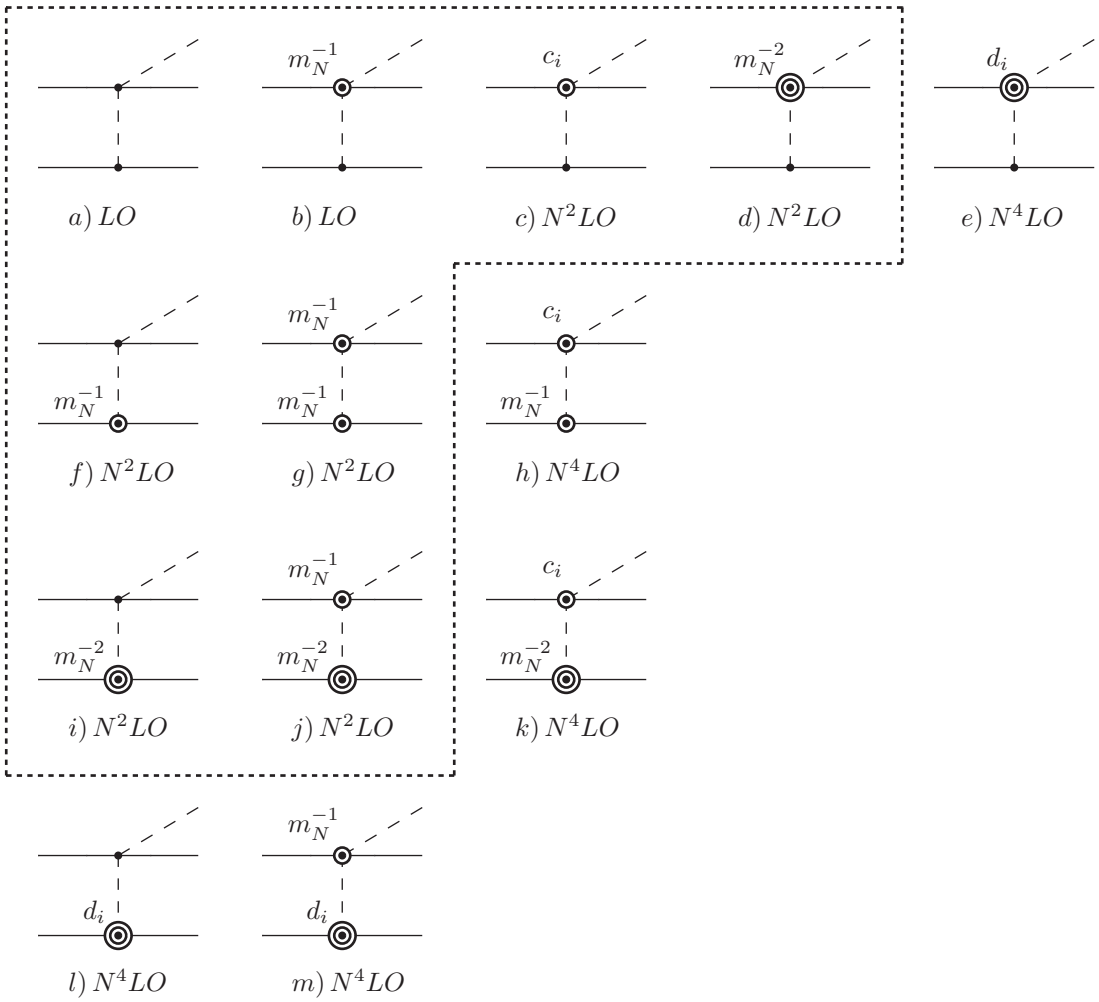

Figure 2.2: Various rescattering diagrams and corresponding MCS estimations. Diagrams in the same column (row) have the same vertex on the upper (lower) nucleon line. Diagrams relevant for N^{2}LO calculation are outlined. Diagrams with MCS order higher than N^{4}LO are not shown. Solid, circled and double-circled dots denote vertices from $\mathcal{L}_{\pi N}^{(1)\mathrm{HB}}$, $\mathcal{L}_{\pi N}^{(2)\mathrm{HB}}$, and $\mathcal{L}_{\pi N}^{(3)\mathrm{HB}}$ HBChPT Lagrangians, respectively. c_i and d_i refer to parts of the vertices proportional to the corresponding LECs while m_N^{-1} and m_N^{-2} denote parts of the vertices proportional to the inverse nucleon mass (recoil corrections). Recoil corrections to the LECs c_i are also denoted as m_N^{-2}. The notation and expressions for the vertices are given in the Appendix B.

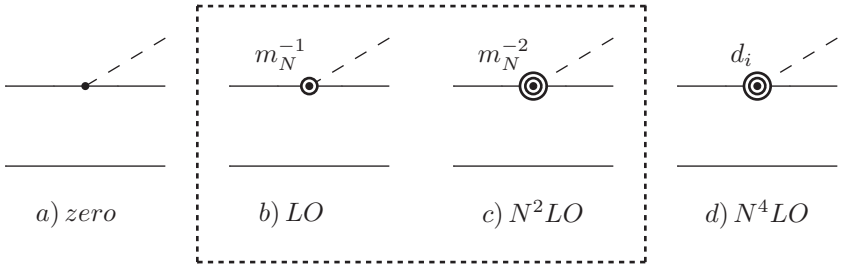

Figure 2.3: Various direct pion production diagrams and the corresponding MCS estimations. Diagrams relevant for N^2LO calculation are outlined. Diagrams with MCS order higher than N^4LO are not shown. Diagram (a) does not contribute to the s-wave pion production at threshold, because it is proportional to the three-momentum of the outgoing pion. Solid, circled, and double-circled dots denote vertices from $\mathcal{L}_{\pi N}^{(1)\mathrm{HB}}$, $\mathcal{L}_{\pi N}^{(2)\mathrm{HB}}$, and $\mathcal{L}_{\pi N}^{(3)\mathrm{HB}}$ HBChPT Lagrangians, respectively. d_i refers to the part of the vertices proportional to corresponding LECs, while m_N^{-1} and m_N^{-2} denote parts of the vertices proportional to inverse nucleon mass (recoil corrections). The notation and expressions for the vertices are given in the Appendix B.

correction to the πNN vertex at the same order. Both amplitudes $M_{\mathrm{rescat1}}^{\mathrm{N^2LO}}$ and $M_{\mathrm{rescat2}}^{\mathrm{N^2LO}}$ contribute to the isoscalar ($\mathcal{A}$) and isovector ($\mathcal{B}$) amplitudes defined in Section 1.5.

2.1.2 Direct pion production

The general topology of the direct pion production is shown in Fig. 2.1b. Direct pion production is not a usual pion production operator but rather a building block for the full amplitude. Direct pion production emerges from disconnected diagrams (sometimes called one-body or single-nucleon diagrams). The corresponding amplitude is always off-shell. It only "makes sense" when convoluted with initial- or final-state NN interaction. To get the counting estimate, the direct pion production operator should be convoluted with one-pion-exchange between initial or final nucleons. Notice that to obtain full amplitude, one has to convolute this operator with the full NN interaction between initial or final nucleons.

Contributions from direct pion production which are relevant for our N^2LO calculation are shown in the box in Fig. 2.3. The leading πNN vertex (Fig. 2.3a) does not contribute to the pion production at threshold, because this vertex is proportional to the outgoing pion three-momentum, which vanishes at threshold. The subleading πNN vertex ($1/m_N$-correction to the leading one) gives the LO MCS contribution to the amplitude (Fig. 2.3b). The sub-sub-leading πNN vertex, proportional to $1/m_N^2$, gives additional N^2LO MCS contribution (Fig. 2.3c). Finally, the contribution of the sub-sub-leading πNN vertices, proportional to LECs d_i, are of higher order, than N^2LO (Fig. 2.3d). The total contribution from direct pion production up-to-and-including N^2LO is given by

$$\begin{aligned} iM_{\mathrm{dir}} &= \frac{g_A}{f_\pi}\tau_1^a\, v\cdot q\;\delta(\vec{p}_2-\vec{p}_2{}') \\ &\times\left[-\frac{1}{2m_N}S_1\cdot(p_1+p_1')+\frac{1}{4m_N^2}\left(v\cdot p_1(S_1\cdot p_1)+v\cdot p_1'(S_1\cdot p_1')\right)\right]+(1\leftrightarrow 2). \end{aligned} \tag{2.4}$$

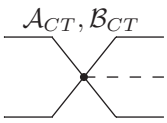

Figure 2.4: Five-point ($NN \to NN\pi$) contact interaction, which starts to contribute at N^{2}LO. It has two contributions: $\mathcal{A}_{CT}$ contributes to the neutral pion production, and $\mathcal{B}_{CT}$ to the charged pion production.

As already stressed above, to get the contributions to the full amplitude, the building block (2.4) should be convoluted with initial and final state NN interactions.

2.1.3 Five-point contact operator

The general topology of the five-point contact operators is shown in Fig. 2.1c. Each five-point contact operator consists of a single $NN \to NN\pi$ vertex proportional to the corresponding low-energy constant. At N^{2}LO MCS there are, in total, two five-point contact operators relevant for s-wave pion production. They have different spin-isospin structures and can be chosen in such a way that one of them contributes only to the amplitude $\mathcal{A}$ and another only to $\mathcal{B}$ (see Eq. (1.5)). The contributions to the amplitude of these two contact terms are denoted by $\mathcal{A}_{\rm CT}$ and $\mathcal{B}_{\rm CT}$.

Low-energy constants of the five-point contact interactions have two parts: the divergent part is required for renormalization of N^{2}LO loop diagrams while the finite (renormalized) part parametrizes the short-range physics. The divergent part can be fixed from the full N^{2}LO operator calculation according to the renormalization procedure. This is done in Section 2.2.5. The finite (renormalized) part should be fitted to the data after carrying out the convolution with the wave functions.

Both finite and divergent parts change if an additional degrees of freedom are added to the effective Lagrangian. This case will be considered in Chapter 3, where the delta-resonance is included as an explicit degree of freedom.

The separation of LEC into finite and divergent parts is renormalization-scheme-dependent. While a particular choice does not affect observables, it is important to maintain consistent definitions in all calculation. We discuss renormalization in Section 2.2.5.

2.2 One-loop operators

To calculate high-accuracy pion production operator at threshold one has to consider loop diagrams. Loop diagrams start to contribute to s-wave pion production at NLO MCS. In this section[2] we calculate the loop corrections to pion production operator at threshold up-to-and-including N^{2}LO MCS.

[2]The content of this chapter is published in [FBE$^+$12].

2.2.1 One-loop diagrams and power counting

The counting of loop diagrams in MCS requires some discussion. The order of a loop diagram in MCS is highly dependent on the structure of a particular diagram. This is in contrast to the standard Weinberg's counting, where all loop diagrams constructed from leading vertices are of the same order.

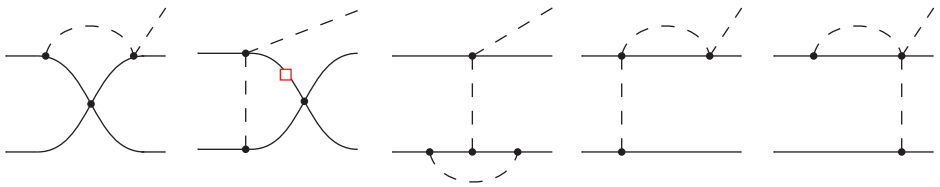

Figure 2.5: Examples of diagrams which are of the higher order than $\mathrm{N^2LO}$. Loop integrals in all these diagrams include several nucleon propagators and only one pion propagator. In this case, large momenta p are not involved in the loop or can be removed by shifting of integration variables. This leads to a suppression compared to diagrams with two pion propagators in the loop, where the scale p cannot be removed from the integral.

As discussed in Section 1.4, the order of loop diagram in MCS depends strongly on the scale of the running loop momentum l. The size of the scale l depends on the structure of the loop integral. Loop integrals with only one pion propagator do not involve large momenta p, since it can always be removed by the shift of variables. Hence, the corresponding diagrams are highly suppressed. Examples of suppressed diagrams are shown in Fig. 2.5. In contrast, the loop integrals with two pion propagators always involve large momenta p which cannot be removed, and the corresponding diagrams give important contributions. Diagrams with two pion propagators in the loop are typically two-pion-exchange (TPE) diagrams. Thus, only TPE loop diagrams give important contributions to s-wave pion production at threshold. This fact dramatically reduces the number of loop diagrams which should be calculated at $\mathrm{N^2LO}$ MCS. All loop diagrams relevant for $\mathrm{N^2LO}$ calculation are listed in Fig. 2.6.

Even TPE diagrams alone require extensive calculation, because there are about 14 diagrams and, in addition, the recoil corrections in each vertex of each diagram should be taken into account. While brute-force calculation of all of the $\mathrm{N^2LO}$ TPE diagrams is possible, it can be tedious and error-prone. To simplify the calculation and to make cancellation patterns more apparent, we first divide all TPE diagrams into several groups, where each group has a common structure. Then, we factor out this structure and consider only the remaining different subgraphs.

The most efficient way to group the diagrams is to consider the structure of the second nucleon line. There are three possible structures for the second nucleon line. The first one corresponds to two πNN-vertices and one nucleon propagator. All diagrams of this structure are proportional to g_A^3 and shown in the second line in Fig. 2.6. The second structure involves the leading WT vertex. Diagrams with this structure are proportional to g_A and shown in the first line in Fig. 2.6. Finally, the third possible structure emerges from the c_i-vertices. Diagrams with this structure are proportional to $c_i g_A$ and are shown in the third line in Fig. 2.6. It turns out that after factorizing out the common structure from any of these groups, the remaining subgraphs correspond to the $\pi N \to \pi\pi N$ process. To obtain the total

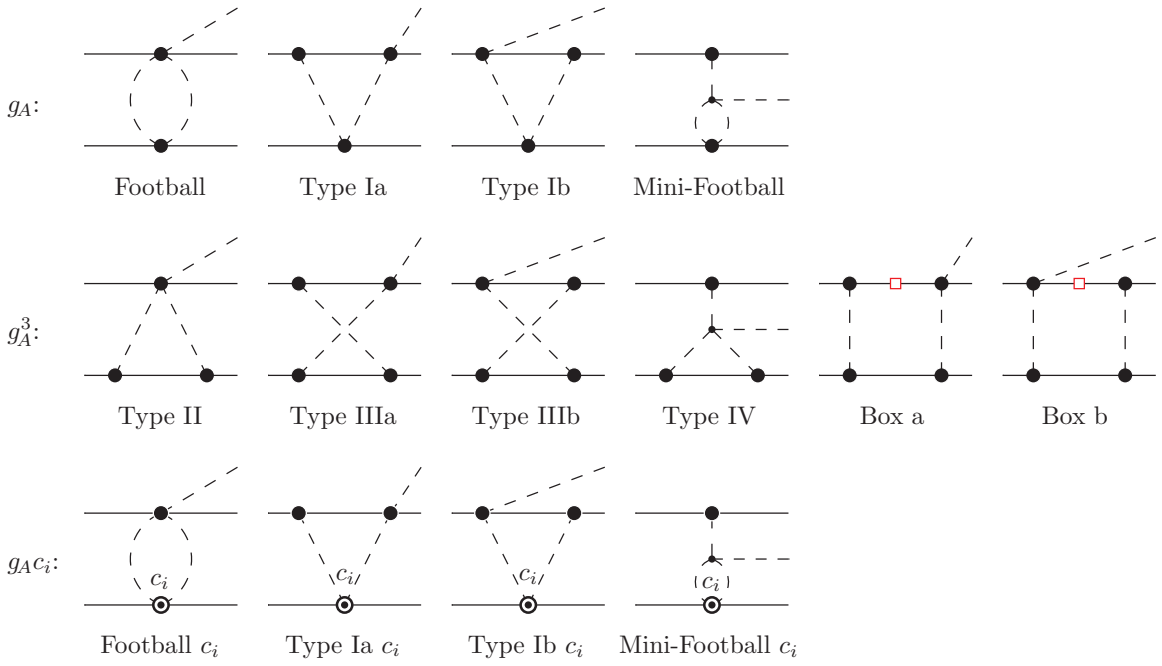

Figure 2.6: Loop diagrams (without delta) that contribute to $NN \to NN\pi$ up to N^{2}LO in MCS. Big dots correspond to the sum of leading vertex and the corresponding $1/m_N$-correction. Other notation and expression for vertices can be found in Appendix B.

contribution of the group we first sum up all $\pi N \to \pi\pi N$ subgraphs, and then plug the sum back into the common structure. Since the set of $\pi N \to \pi\pi N$ subgraphs is the same for all three groups, we only need to calculate the sum once. It also turns out that numerous cancellations happen among these $\pi N \to \pi\pi N$ subgraphs, thus the sum has a very simple form. Consequently, total result from TPE diagrams is also very short and simple. We discuss individual groups in the next sections.

2.2.2 Calculation of diagrams proportional to g_A^3

The diagrams of the g_A^3-group in Fig. 2.6 have a common structure illustrated in Fig. 2.7.

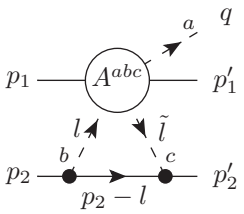

Figure 2.7: The general structure of g_A^3-diagrams.

The loop diagram in Fig. 2.7 is integrated over the momentum $l = (l_0, \vec{l})$. We also use the

short-hand notation

$$\tilde{l} = l + k_1 - q \ ,$$

with $k_1 = p_1 - p_1'$. Pion isospin indices a, b, and c are defined as shown in Fig. 2.7. The circle containing the vertex operator A^{abc} produces an outgoing pion with isospin index a off nucleon 1. This operator is different for each diagram and its explicit form is derived in Appendix F.1, where also the detailed structure of each g_A^3-diagram is given.

The invariant amplitude for each relevant diagram proportional to g_A^3 can be written as

$$iM_{g_A^3} = \int \frac{d^4 l}{(2\pi)^4} \, B_2(l, \tilde{l}) \ \tau_2^c \tau_2^b \ A^{abc}_{g_A^3}, \tag{2.5}$$

where $B_2(l, \tilde{l})$ is the common operator structure associated with nucleon 2 in Fig. 2.7. The operator $B_2(l, \tilde{l})$ involves two pion propagators, two πNN-vertices and the nucleon propagator. The explicit form of $B_2(l, \tilde{l})$ can be read off from the diagram in Fig. 2.7:

$$\begin{aligned} B_2(l, \tilde{l}) \ &= \ \frac{i}{l^2 - m_\pi^2 + i0} \, \frac{i}{\tilde{l}^2 - m_\pi^2 + i0} \, \frac{i}{p_{20} - l_0 - (\vec{p}_2 - \vec{l})^2/(2m_N) + i0} \\ &\quad \times \frac{g_A}{f_\pi} \left(-S_2 \cdot \tilde{l} + \frac{S_2 \cdot (p_2 + p_2' - l) v \cdot \tilde{l}}{2m_N} \right) \frac{g_A}{f_\pi} \left(S_2 \cdot l - \frac{S_2 \cdot (2p_2 - l) v \cdot l}{2m_N} \right) . \end{aligned} \tag{2.6}$$

Note that $B_2(l, \tilde{l})$ contains no isospin indices as all isospin operators are included in Eq. (2.5). Since the structure of $B_2(l, \tilde{l})$ is the same for all considered g_A^3-diagrams, we concentrate our discussion on the structure of the operator $A^{abc}_{g_A^3}$ in Eq. (2.5), see Appendix F.1 for details. Note that the amplitude, Eq. (2.5) is not yet properly symmetrized with respect to the nucleon labels. Below we will first discuss the emergence of the partial cancellation amongst the various pion loop diagrams on the basis of the decomposition illustrated in Fig. 2.7. In Sec. 2.2.4 the non-vanishing remainder will be given in a symmetrized form.

Pion s-wave contributions $\propto g_A^3$

In Appendix F.1 we derive the expressions for each of the six g_A^3-diagrams which contribute to near-threshold s-wave pion production from two nucleons. The results of these calculations are summarized in Table 2.2 where, for the sake of convenience, we have introduced the following short-hand notation for the isospin structures:

$$\tau_+ = (\boldsymbol{\tau}_1 + \boldsymbol{\tau}_2)^a, \qquad \tau_- = (\boldsymbol{\tau}_1 - \boldsymbol{\tau}_2)^a, \qquad \tau_\times = i(\boldsymbol{\tau}_1 \times \boldsymbol{\tau}_2)^a. \tag{2.7}$$

The left column in Table 2.2 shows the spin structures that emerge from these diagrams, the next six columns show the contributions from the individual diagrams to the given spin structure, whereas the last two columns summarize the net effect of all diagrams and the MCS order, respectively. When we add together the resulting expressions for the six diagrams we confirm the finding of Ref. [LBH$^+$06] that the sum of the NLO contributions from all diagrams vanishes, see the first two rows of operators in Table 2.2. Moreover, since the sum of the operators in the first two rows of Table 2.2 is exactly zero, the corresponding spin-momentum structures $S_1 \cdot l$ and $S_1 \cdot \tilde{l}$ will not contribute also at N^{2}LO and all higher orders. In addition,

all nucleon recoil corrections $\propto 1/(2m_N)$ to the individual diagrams at N^{2}LO also cancel in the sum. The reason for that cancellation is completely analogous to the cancellation that happens at NLO. In fact, only those parts of the g_A^3-diagrams that cannot be reduced to the topology of the diagram II in Fig. 2.6 give a non-zero contribution to the transition amplitude. Thus, only very few N^{2}LO contributions to the pion production amplitude survive, as seen in Table 2.2. The non-vanishing terms appear from the two cross-box diagrams and diagram IV.

Since the sum of the $A_{g_A^3}^{abc}$-operators from the different diagrams starts to contribute at N^{2}LO, we keep only the leading part of the operator $B_2(l,\tilde{l})$. Adding up the contributions from all six g_A^3 diagrams we arrive at the following result:

$$\begin{aligned} iM_{g_A^3}^{\mathrm{N^2LO}} &= i\frac{g_A^3}{4f_\pi^5}\int\frac{d^4l}{(2\pi)^4}\,\frac{S_2\cdot\tilde{l}}{l^2-m_\pi^2+i0}\,\frac{S_2\cdot l}{\tilde{l}^2-m_\pi^2+i0}\,\frac{1}{-v\cdot l+i0} \\ &\quad\times\Big\{(-2\tau_+ +\tau_\times)\frac{2v\cdot q}{-v\cdot l+i0}(S_1\cdot\tilde{l})+(-2\tau_+ -\tau_\times)\frac{2v\cdot q}{-v\cdot l+i0}(S_1\cdot l) \\ &\quad -8\tau_\times(S_1\cdot k_1)\frac{(l+\tilde{l})\cdot q}{k_1^2-m_\pi^2+i0}\Big\}, \end{aligned} \tag{2.8}$$

where for the nucleon propagator in Eq. (2.6) we dropped p_{20} and all recoil terms of order $\mathcal{O}(m_\pi)$ compared to the lower-order $l_0\equiv v\cdot l\sim|\vec{l}|\sim p$ term. Rearranging the isospin structure we arrive at three independent integrals to be evaluated for s-wave pion production:

$$\begin{aligned} iM_{g_A^3}^{\mathrm{N^2LO}} &= -i\frac{g_A^3}{4f_\pi^5}\Big\{4(v\cdot q)\tau_+ S_2^\mu S_2^\nu S_1^\lambda\int\frac{d^4l}{(2\pi)^4}\,\frac{\tilde{l}_\mu l_\nu(l+\tilde{l})_\lambda}{(l^2-m_\pi^2+i0)(\tilde{l}^2-m_\pi^2+i0)(-v\cdot l+i0)^2} \\ &\quad -2(v\cdot q)\tau_\times S_2^\mu S_2^\nu(S_1\cdot k_1)\int\frac{d^4l}{(2\pi)^4}\,\frac{\tilde{l}_\mu l_\nu}{(l^2-m_\pi^2+i0)(\tilde{l}^2-m_\pi^2+i0)(-v\cdot l+i0)^2} \\ &\quad +8q^\lambda\tau_\times\frac{S_2^\mu S_2^\nu(S_1\cdot k_1)}{k_1^2-m_\pi^2+i0}\int\frac{d^4l}{(2\pi)^4}\,\frac{\tilde{l}_\mu l_\nu(l+\tilde{l})_\lambda}{(l^2-m_\pi^2+i0)(\tilde{l}^2-m_\pi^2+i0)(-v\cdot l+i0)}\Big\} \end{aligned} \tag{2.9}$$

Employing dimensional regularization and an integration method outlined in Appendix G, Eq. (2.9) can be brought into the more transparent form:

$$\begin{aligned} iM_{g_A^3}^{\mathrm{N^2LO}} &= \frac{g_A^3(v\cdot q)}{f_\pi^5}\Big\{\tau_+ i\varepsilon^{\mu\nu\alpha\beta}k_{1\mu}S_{1\nu}v_\alpha S_{2\beta}\left[-I_{\pi\pi}(k_1^2)\right] \\ &\quad +\tau_\times(S_1\cdot k_1)\left[-\frac{19}{24}I_{\pi\pi}(k_1^2)+\frac{5}{9}\frac{1}{(4\pi)^2}\right]\Big\}, \end{aligned} \tag{2.10}$$

where we have only kept the lowest order parts of the integrals which give contributions to the amplitude at N^{2}LO. The pion loop diagrams generate ultraviolet divergent terms, which are contained in the following integral:

$$I_{\pi\pi}(k_1^2) = -i\int\frac{d^4l}{(2\pi)^4}\,\frac{1}{l^2-m_\pi^2+i0}\,\frac{1}{(l+k_1)^2-m_\pi^2+i0} \tag{2.11}$$

The divergences are to be absorbed by the five-point $NN\to NN\pi$ LECs as we will discuss in Sec. 2.2.5.

Table 2.2: Interference pattern of NLO and N^{2}LO s-wave contributions from the individual g_A^3 diagrams. The Table shows the contributions to the vertex $\tau_2^c\tau_2^b\ A^{abc}_{g_A^3}$ defined in Eq.(2.5) and Fig. 2.7. These contributions are given separately for the different spin-momentum structures of the vertex $A^{abc}_{g_A^3}$, shown in the leftmost column. The notation for the isospin structures is defined in Eq.(2.7).

	Type II	Type IIIa	Type IIIb	Type IV	Box a	Box b	Sum	Order
$S_1\cdot l$	$-4\tau_+-4\tau_-+2\tau_\times$	0	$-2\tau_+-\tau_\times$	$6\tau_++6\tau_-$	$-2\tau_--\tau_\times$	0	0	NLO, N^{2}LO
$S_1\cdot \tilde{l}$	$4\tau_++4\tau_-+2\tau_\times$	$2\tau_+-\tau_\times$	0	$-6\tau_+-6\tau_-$	0	$2\tau_--\tau_\times$	0	NLO, N^{2}LO
$S_1\cdot l\,\frac{v\cdot\tilde{l}}{2m_N}$	$-2\tau_++2\tau_-$	$2\tau_+-\tau_\times$	0	0	0	$-2\tau_-+\tau_\times$	0	N^{2}LO
$S_1\cdot \tilde{l}\,\frac{v\cdot l}{2m_N}$	$2\tau_+-2\tau_-$	0	$-2\tau_+-\tau_\times$	0	$2\tau_-+\tau_\times$	0	0	N^{2}LO
$S_1\cdot (p_1+p_1')\,\frac{v\cdot l}{2m_N}$	$4\tau_++4\tau_--2\tau_\times$	0	$2\tau_++\tau_\times$	$-6\tau_+-6\tau_-$	$2\tau_-+\tau_\times$	0	0	N^{2}LO
$S_1\cdot (p_1+p_1')\,\frac{v\cdot \tilde{l}}{2m_N}$	$-4\tau_+-4\tau_--2\tau_\times$	$-2\tau_++\tau_\times$	0	$6\tau_++6\tau_-$	0	$-2\tau_-+\tau_\times$	0	N^{2}LO
$S_1\cdot l\frac{2v\cdot q}{-v\cdot l+i0}$	0	0	$-2\tau_+-\tau_\times$	0	0	0	$-2\tau_+-\tau_\times$	N^{2}LO
$S_1\cdot \tilde{l}\frac{2v\cdot q}{-v\cdot l+i0}$	0	$-2\tau_++\tau_\times$	0	0	0	0	$-2\tau_++\tau_\times$	N^{2}LO
$S_1\cdot k_1\frac{q\cdot(l+\tilde{l})}{k_1^2-m_\pi^2+i0}$	0	0	0	$-8\tau_\times$	0	0	$-8\tau_\times$	N^{2}LO

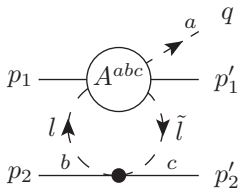

Figure 2.8: The general structure of g_A-diagrams.

2.2.3 Calculation of diagrams proportional to g_A

We evaluate the g_A-diagrams following a similar strategy we used when evaluating the g_A^3-diagrams. The invariant amplitude for each diagram proportional to g_A can be written as

$$iM_{g_A} = \int\frac{d^4l}{(2\pi)^4}\,D_2(l,\tilde{l})\;\varepsilon^{bcd}\tau_2^d\;A^{abc}_{g_A}, \tag{2.12}$$

where $D_2(l,\tilde{l})$ is a common operator structure which is associated with nucleon 2 in Fig. 2.8.

This structure involves the WT vertex at the second nucleon and the two pion propagators:

$$D_2(l,\tilde{l}) = \frac{i}{l^2-m_\pi^2+i0}\;\frac{i}{\tilde{l}^2-m_\pi^2+i0}\;\frac{v\cdot(l+\tilde{l})}{4f_\pi^2}. \tag{2.13}$$

Note that we have only written the leading WT-vertex contribution in $D_2(l,\tilde{l})$, Eq. (2.13), since the sum of the $A^{abc}_{g_A}$-operators starts to contribute at N^{2}LO only, as can be seen from Table 2.3. This is in a full analogy to the sum of the $A^{abc}_{g_A^3}$-operators, which also only starts to contribute at N^{2}LO, where, as discussed just before Eq. (2.8), the recoil $(1/m_N)$ corrections in $B_2(l,\tilde{l})$, Eq. (2.6), only contribute at higher order. In other words, the corrections to $D_2(l,\tilde{l})$, that is the recoil correction to the leading WT interaction term contributes at a higher order than what is considered in this work.

Table 2.3: Interference pattern of s-wave contributions from the individual g_A diagrams. The Table shows the contributions to the vertex $\varepsilon^{bcd}\tau_2^d A_{g_A}^{abc}$ defined in Fig. 2.8 and Eq.(2.12). The contributions are given separately for different spin-momentum structures of the vertex $A_{g_A}^{abc}$, shown in the leftmost column. The notation for the isospin structures is defined in Eq.(2.7).

	Football	Type Ia	Type Ib	MiniFB	Sum	Order
$S_1\cdot l$	$-2\tau_\times$	$-\tau_+ + \tau_- + \tau_\times$	$\tau_+ - \tau_- + \tau_\times$	0	0	NLO, N^{2}LO
$S_1\cdot \tilde{l}$	$-2\tau_\times$	$-\tau_+ + \tau_- + \tau_\times$	$\tau_+ - \tau_- + \tau_\times$	0	0	NLO, N^{2}LO
$S_1\cdot l\,\frac{v\cdot\tilde{l}}{2m_N}$	$2\tau_+ - 2\tau_-$	$-\tau_+ + \tau_- + \tau_\times$	$-\tau_+ + \tau_- - \tau_\times$	0	0	N^{2}LO
$S_1\cdot \tilde{l}\,\frac{v\cdot l}{2m_N}$	$-2\tau_+ + 2\tau_-$	$\tau_+ - \tau_- - \tau_\times$	$\tau_+ - \tau_- + \tau_\times$	0	0	N^{2}LO
$S_1\cdot (p_1{+}p_1')\,\frac{v\cdot l}{2m_N}$	$2\tau_\times$	$\tau_+ - \tau_- - \tau_\times$	$-\tau_+ + \tau_- - \tau_\times$	0	0	N^{2}LO
$S_1\cdot (p_1{+}p_1')\,\frac{v\cdot \tilde{l}}{2m_N}$	$2\tau_\times$	$\tau_+ - \tau_- - \tau_\times$	$-\tau_+ + \tau_- - \tau_\times$	0	0	N^{2}LO
$S_1\cdot l\frac{2v\cdot q}{-v\cdot l+i0}$	0	0	$2\tau_+ - 2\tau_- + 2\tau_\times$	0	$2\tau_+ - 2\tau_- + 2\tau_\times$	N^{2}LO
$S_1\cdot \tilde{l}\frac{2v\cdot q}{-v\cdot l+i0}$	0	$2\tau_+ - 2\tau_- - 2\tau_\times$	0	0	$2\tau_+ - 2\tau_- - 2\tau_\times$	N^{2}LO
$S_1\cdot k_1\frac{q\cdot(l+\tilde{l})}{k_1^2-m_\pi^2+i0}$	0	0	0	$8\tau_\times$	$8\tau_\times$	N^{2}LO

Pion s-wave contributions $\propto g_A$

The operator expressions for each individual diagram of the g_A-type contributing to s-wave pion production can be found in Appendix F.2. In a complete analogy with the g_A^3-diagrams, we summarize in Table 2.3 the contributions of the individual diagrams and their net effect for different spin structures. In distinction to the g_A^3-graphs, the diagrams of this topology do not appear, contrary to naive MCS expectations, at NLO, see Appendix F.2.1 for a more detailed discussion. Similarly to the g_A^3-type contributions, only a few of the N^{2}LO terms survive after cancellation in the sum. Again, only those parts of the diagrams Ia, Ib and "mini-football" that cannot be reduced to the topology of the "football" diagram in Fig. 2.6, give a non-zero contribution to the transition amplitude. The results are shown in Table 2.3, and the sum of these g_A contributions gives the following transition amplitude:

$$\begin{aligned} iM_{g_A}^{\mathrm{N^2LO}} &= i\frac{g_A}{8f_\pi^3}\int\frac{d^4l}{(2\pi)^4}\,D_2(l,\tilde{l})\,\Big\{(2\tau_+ - 2\tau_- - 2\tau_\times)\frac{2v\cdot q}{-v\cdot l+i0}S_1\cdot\tilde{l} \\ &\quad +(2\tau_+ - 2\tau_- + 2\tau_\times)\frac{2v\cdot q}{-v\cdot l+i0}S_1\cdot l + 8\tau_\times\; S_1\cdot k_1\frac{q\cdot(l+\tilde{l})}{k_1^2-m_\pi^2+i0}\Big\}. \end{aligned} \tag{2.14}$$

Upon performing simplifications, the total result for the g_A-contribution to the transition amplitude in Eq. (2.14) can be brought into the form

$$\begin{aligned} iM_{g_A}^{\mathrm{N^2LO}} &= -i\frac{g_A}{8f_\pi^5}\Big\{(\tau_+ - \tau_-)(v\cdot q)\int\frac{d^4l}{(2\pi)^4}\,\frac{v\cdot(l+\tilde{l})S_1\cdot(l+\tilde{l})}{(l^2-m_\pi^2+i0)(\tilde{l}^2-m_\pi^2+i0)(-v\cdot l+i0)} \\ &\quad -\tau_\times(v\cdot q)(S_1\cdot k_1)\int\frac{d^4l}{(2\pi)^4}\,\frac{v\cdot(l+\tilde{l})}{(l^2-m_\pi^2+i0)(\tilde{l}^2-m_\pi^2+i0)(-v\cdot l+i0)} \\ &\quad +2\tau_\times(S_1\cdot k_1)\frac{1}{k_1^2-m_\pi^2+i0}\int\frac{d^4l}{(2\pi)^4}\,\frac{v\cdot(l+\tilde{l})q\cdot(l+\tilde{l})}{(l^2-m_\pi^2+i0)(\tilde{l}^2-m_\pi^2+i0)}\Big\}. \end{aligned} \tag{2.15}$$

The first term in Eq. (2.15) does not contribute at N^{2}LO, since at this order the term $v\cdot(l+\tilde{l})\approx 2v\cdot l$ in the numerator cancels with the nucleon propagator $-v\cdot l+i0$. The resulting integral

vanishes due to the symmetry of the integrand. Specifically, the integral is to be invariant under the shift of variables ($l \to -\tilde{l}, \tilde{l} \to -l$). Indeed, the denominator of this integrand is invariant under this transformation whereas the numerator changes its sign. Therefore, the first term in Eq. (2.15) is equal to zero. Finally, keeping only the lowest-order terms as appropriate at N^{2}LO and using the expressions for the loop integrals outlined in Appendix G, we arrive at the final result:

$$iM_{g_A}^{\mathrm{N^2LO}} = \frac{g_A}{f_\pi^5}\tau_\times (v\cdot q)(S_1\cdot k_1)\left[\frac{1}{6}I_{\pi\pi}(k_1^2) - \frac{1}{18}\frac{1}{(4\pi)^2}\right] , \tag{2.16}$$

where the UV-divergent integral $I_{\pi\pi}(k_1^2)$ is defined in Eq. (2.11).

Pion s-wave contributions $\propto g_A c_i$

We now turn to the contribution emerging from the diagrams of Fig. 2.6 with the c_2 and c_3-vertices in the off-shell pion kinematics at nucleon 2. We obtain the following expression for the amplitude:

$$\begin{aligned} iM_{g_A,c_i}^{\mathrm{N^2LO}} &= -i\frac{g_A}{2f_\pi^5}(\tau_+ + \tau_-)(S\cdot k_1) \\ &\times \int \frac{d^4l}{(2\pi)^4}\,\frac{c_3(l\cdot\tilde{l}) + (c_2 - g_A^2/8m_N)(v\cdot l)(v\cdot\tilde{l})}{(l^2 - m_\pi^2 + i0)(\tilde{l}^2 - m_\pi^2 + i0)}\,\left\{2 + \frac{1}{2} + \frac{1}{2} - 3\right\} = 0\,, \end{aligned} \tag{2.17}$$

where the numbers in the curly bracket correspond to the individual contributions of the g_A-diagrams, as they appear in Fig. 2.6, in order. Again, while the individual diagrams do contribute at N^{2}LO, their sum turns out to yield a vanishing result. We, therefore, conclude that there are no loop amplitudes $\propto c_i$ to the order we are working.

2.2.4 Summary of the two-pion exchange diagrams

Until now we have evaluated the expressions for the production operator assuming that the pion is produced off nucleon 1. We now add the contribution emerging from interchanging the nucleon labels. We use $k_1 = -k_2 + q$ and employ the approximate relation $k_1^2 \simeq k_2^2$ with higher-order terms being ignored. Throughout, we also ignore operators leading to p-wave pion production. We then obtain from Eqs. (2.16) and (2.10) the following complete (i.e. symmetrized with respect to the nucleon labels) expressions:

$$iM_{g_A}^{\mathrm{N^2LO}} = \frac{g_A\ (v\cdot q)}{f_\pi^5}\tau_\times (S_1+S_2)\cdot k_1\left[\frac{1}{6}I_{\pi\pi}(k_1^2) - \frac{1}{18}\frac{1}{(4\pi)^2}\right] , \tag{2.18}$$

$$\begin{aligned} iM_{g_A^3}^{\mathrm{N^2LO}} &= \frac{g_A^3\ (v\cdot q)}{f_\pi^5}\Big\{\tau_+ i\varepsilon^{\alpha\mu\nu\beta}v_\alpha k_{1\mu}S_{1\nu}S_{2\beta}\left[-2I_{\pi\pi}(k_1^2)\right] \\ &\quad +\tau_\times (S_1+S_2)\cdot k_1\left[-\frac{19}{24}I_{\pi\pi}(k_1^2) + \frac{5}{9}\frac{1}{(4\pi)^2}\right]\Big\}. \end{aligned} \tag{2.19}$$

Employing dimensional regularization and setting $d = 4 - \varepsilon$, the integral $I_{\pi\pi}(k_1)$ entering the above expressions can be written in the form

$$\begin{aligned} I_{\pi\pi}(k_1^2) &= \frac{\mu^\varepsilon}{i} \int \frac{d^{(4-\varepsilon)}l}{(2\pi)^{(4-\varepsilon)}} \frac{1}{[l^2 - m_\pi^2 + i0][(l+k_1)^2 - m_\pi^2 + i0]} \\ &= -2L - \frac{1}{(4\pi)^2} \left[\log\left(\frac{m_\pi^2}{\mu^2}\right) - 1 + 2F_1\left(\frac{k_1^2}{m_\pi^2}\right) \right], \end{aligned} \tag{2.20}$$

where the function $F_1(x)$ is defined via

$$F_1(x) = \frac{\sqrt{4 - x - i0}}{\sqrt{x}} \arctan\left(\frac{\sqrt{x}}{\sqrt{4 - x - i0}}\right), \tag{2.21}$$

and the UV divergency appears as a simple pole in the function L:

$$L = \frac{1}{(4\pi)^2} \left[-\frac{1}{\varepsilon} + \frac{1}{2}\left(\gamma_E - 1 - \log(4\pi)\right) \right]. \tag{2.22}$$

Note that both $M_{g_A}^{\mathrm{N^2LO}}$ and $M_{g_A^3}^{\mathrm{N^2LO}}$ are proportional to the outgoing pion energy $v \cdot q \simeq m_\pi$, *i.e.* both operator amplitudes vanish at threshold in the chiral limit.

2.2.5 Renormalization procedure

Our N^{2}LO calculation involves divergent loop diagrams, which require proper renormalization to get the physical result. Renormalization procedure introduces additional vertices, called counter terms, which absorb infinite parts of divergent loop diagrams. In this section we show that the only relevant renormalization correction in our N^{2}LO calculation is the five-point contact interaction, discussed in the previous section. All other renormalization corrections contribute at higher orders.

To understand why renormalization effects are suppressed let's first consider divergent loop diagrams which should be renormalized by renormalization corrections to Z_N, Z_π, g_A, f_π, m_π, and m_N. Several examples of such diagrams are shown in Fig. 2.9. All these diagrams are highly suppressed in MCS, because the only small scale in the corresponding loop integrals is m_π. (Large momentum p either does not enter the loop integrals or can be removed by a shift of variables). MCS estimation procedure for these kind of diagrams is explained in Sec. 1.4. Renormalization corrections which absorb the corresponding ultraviolet divergencies are also of higher order. It can also be understood by carefully counting the involved scales. Since renormalization corrections, by construction, do not depend on the kinematics, the only small scale which can appear in these corrections is m_π. The small scale m_π is accompanied in these corrections by the loop-factor $(4\pi f_\pi)^{-2} \sim m_N^{-2}$, thus producing a significant suppression in terms of the MCS expansion parameter $\sqrt{m_\pi/m_N}$.

Thus, in the N^{2}LO MCS calculation, one can ignore all effects related to renormalization of masses, fields (Z-factors), coupling constants and most of the LECs. The only quantities, which should be renormalized are the five-point $NN \to NN\pi$ LECs. All other LECs, masses, and couplings can be taken as renormalized (physical) values, because the corresponding renormalization corrections are of the order higher than N^{2}LO.

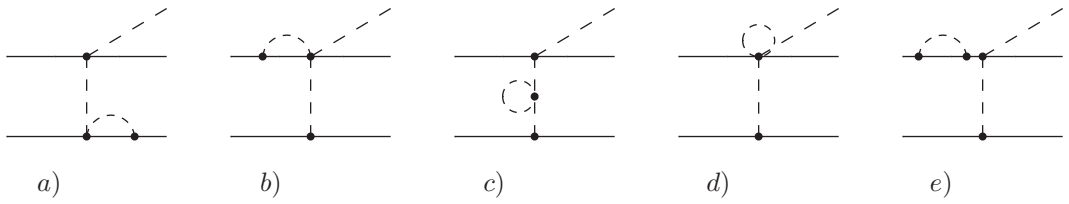

Figure 2.9: Exemplary loop diagrams, which contribute to higher order than N^{2}LO. The corresponding renormalization corrections also appear at orders higher than N^{2}LO.

At N^{2}LO, we only have to consider the TPE loop diagrams. The UV divergences appearing in the corresponding integrals are to be absorbed into five-point $NN \to NN\pi$ LECs $\mathcal{A}_{\rm CT}$ and $\mathcal{B}_{\rm CT}$ introduced in Sec. 1.5. The contributions of the loops to the amplitudes $\mathcal{A}$ and $\mathcal{B}$, see Eq. (1.36), can be separated into singular and finite parts

$$\begin{aligned} \mathcal{A} &= \frac{m_\pi}{(4\pi f_\pi)^2 f_\pi^3}(\tilde{\mathcal{A}}_{\rm singular} + \tilde{\mathcal{A}}_{\rm finite}), \\ \mathcal{B} &= \frac{m_\pi}{(4\pi f_\pi)^2 f_\pi^3}(\tilde{\mathcal{B}}_{\rm singular} + \tilde{\mathcal{B}}_{\rm finite}), \end{aligned} \tag{2.23}$$

where

$$\tilde{\mathcal{A}}_{\rm singular} = g_A^3 (4\pi)^2 L, \qquad \tilde{\mathcal{B}}_{\rm singular} = -\frac{g_A}{6}\left(\frac{19}{4}g_A^2 - 1\right)(4\pi)^2 L\ . \tag{2.24}$$

Here, we have used that at threshold $\vec{k}_1 = \vec{p}$ and $v\cdot q = m_\pi$. Notice that the above decomposition into singular and finite pieces is, clearly, scheme-dependent. Analogously, the amplitudes given by the $4N\pi$ Lagrangian contact terms which are given in e.g., Ref. [CFMvK96] are written as:

$$\mathcal{A}_{\rm CT} = \frac{m_\pi}{(4\pi f_\pi)^2 f_\pi^3}(\tilde{\mathcal{A}}^r_{\rm CT}(\mu) + (4\pi)^2\beta_{\mathcal{A}} L), \quad \mathcal{B}_{\rm CT} = \frac{m_\pi}{(4\pi f_\pi)^2 f_\pi^3}(\tilde{\mathcal{B}}^r_{\rm CT}(\mu) + (4\pi)^2\beta_{\mathcal{B}} L)\ . \tag{2.25}$$

The singular parts of the amplitudes in Eq. (2.25) cancel the singularities of the amplitudes in Eq. (2.23), emerging from the loops. The resulting finite expressions for the scattering amplitudes are given in terms of the renormalized LECs of Ref. [CFMvK96] as:

$$\begin{aligned} \mathcal{A}^r_{\rm CT} &= \frac{m_\pi}{(4\pi f_\pi)^2 f_\pi^3}\tilde{\mathcal{A}}^r_{\rm CT} = -(d_1' + 2e_1 - 2e_2)\frac{m_\pi}{4 m_N f_\pi}, \\ \mathcal{B}^r_{\rm CT} &= \frac{m_\pi}{(4\pi f_\pi)^2 f_\pi^3}\tilde{\mathcal{B}}^r_{\rm CT} = -(d_1' + 2e_1)\frac{m_\pi}{4 m_N f_\pi}. \end{aligned} \tag{2.26}$$

The magnitudes of the amplitudes $\mathcal{A}^r_{\rm CT}$ and $\mathcal{B}^r_{\rm CT}$ can be estimated using the values of the LECs determined in Refs. [CFMvK96, dRMvK00, vKMR96] where the short-ranged production mechanisms were assumed to originate from z-diagrams with σ and ω exchanges (see explicit expressions for these exchanges in Refs. [CFMvK96, KSMK09]). Given the estimates in Ref. [vKMR96], we find $d_1' + 2e_1 - 2e_2 \simeq -7.5/f_\pi^2 m_N$ and $d_1' + 2e_1 \simeq -3.5/f_\pi^2 m_N$, and using $m_N \simeq 4\pi f_\pi$ we obtain $\mathcal{A}^r_{\rm CT} \simeq 2\, m_\pi/(m_N^2 f_\pi^3)$ and $\mathcal{B}^r_{\rm CT} \simeq 1\, m_\pi/(m_N^2 f_\pi^3)$ which results in $\tilde{\mathcal{A}}^r_{\rm CT} \simeq 2$ and $\tilde{\mathcal{B}}^r_{\rm CT} \simeq 1$.

We take these numbers to estimate the size of typical N^{2}LO contributions. Therefore, these estimates allow us to infer the importance of the pion–nucleon loop contributions to the $NN \to NN\pi$ reactions at threshold. In particular, we can compare this estimate with the finite parts of the loops given by Eqs. (2.18) and (2.19) (where $v \cdot p \sim m_\pi \ll |\vec{p}|$).

$$\begin{aligned} \tilde{\mathcal{A}}_{\rm finite} &= -\frac{g_A^3}{2}\left[1 - \log\left(\frac{m_\pi^2}{\mu^2}\right) - 2F_1\left(\frac{-\vec{p}^{\,2}}{m_\pi^2}\right)\right], \\ \tilde{\mathcal{B}}_{\rm finite} &= -\frac{g_A}{6}\left[-\frac{1}{2}\left(\frac{19}{4}g_A^2 - 1\right)\left(1 - \log\left(\frac{m_\pi^2}{\mu^2}\right) - 2F_1\left(\frac{-\vec{p}^{\,2}}{m_\pi^2}\right)\right) + \frac{5}{3}g_A^2 - \frac{1}{6}\right]. \end{aligned} \tag{2.27}$$

Choosing $\mu = 4\pi f_\pi$ with $f_\pi = 92.4$ MeV and $g_A = 1.32$, we find $\tilde{\mathcal{A}}_{\rm finite} = -2.9$ and $\tilde{\mathcal{B}}_{\rm finite} = 1.4$. We, therefore, conclude that contributions of the finite parts of the loops are comparable in size with $\tilde{\mathcal{A}}^r_{\rm CT}$ and $\tilde{\mathcal{B}}^r_{\rm CT}$. This confirms our power counting and shows that pion loops contributions, not considered in previous analyses, are indeed significant. One should, however, keep in mind that this result was obtained for the particular regularization scheme as explained above. In general, the finite parts of the loops $\tilde{\mathcal{A}}_{\rm finite}$ and $\tilde{\mathcal{B}}_{\rm finite}$ can be further decomposed into the *short-* and *long*-range parts. The former one is just a (renormalization-scheme dependent) constant to which all terms in Eq. (2.27) but F_1 contribute. On the other hand, long-range parts of the loops are scheme-independent. By expanding the function $F_1(-\vec{p}^{\,2}/m_\pi^2)$, Eq. (2.21), which is the only long-range piece in (2.27), in the kinematical regime relevant for pion production, i.e. $(\vec{p}^{\,2}/m_\pi^2) \gg 1$, up to the terms at N^{2}LO one obtains

$$\begin{aligned} \tilde{\mathcal{A}}^{\rm long}_{\rm finite} &= -\frac{g_A^3}{2}\log\left(\frac{m_\pi^2}{\vec{p}^{\,2}}\right) + \mathcal{O}\left(\frac{m_\pi^2}{\vec{p}^{\,2}}\right), \\ \tilde{\mathcal{B}}^{\rm long}_{\rm finite} &= \frac{g_A}{12}\left(\frac{19}{4}g_A^2 - 1\right)\log\left(\frac{m_\pi^2}{\vec{p}^{\,2}}\right) + \mathcal{O}\left(\frac{m_\pi^2}{\vec{p}^{\,2}}\right). \end{aligned} \tag{2.28}$$

Numerical evaluation of these terms gives $\tilde{\mathcal{A}}^{\rm long}_{\rm finite} = 2.2$ and $\tilde{\mathcal{B}}^{\rm long}_{\rm finite} = -1.5$. The scheme-independent long range part of N^{2}LO pion loops appears to be as large as the resulting short-range amplitudes, $\tilde{\mathcal{A}}^r_{\rm CT}$ and $\tilde{\mathcal{B}}^r_{\rm CT}$, which are given by the meson-exchange mechanism, proposed in Refs. [LR93, HMG94, Hor93, Nis96] to resolve the discrepancy between phenomenological calculations and experimental data. Hence, the importance of the N^{2}LO pion loop effects, not included in the previous studies, raises serious doubts on the physics interpretation behind the phenomenologically successful models of Refs. [LR93, HMG94, Hor93, Nis96].

2.3 Chapter summary

In this chapter we have calculated the pion production operator at threshold up-to-and-including N^{2}LO MCS.

We have shown that the intermediate-range two-pion-exchange effects give important contribution to the production operator. This can question mechanisms used in phenomenological calculations, where data description was obtained without these contributions.

The obtained production operator has a simple form and gives rise to different applications. It can be used to calculate total cross sections in s-wave pion production channels. It also represents the important ingredient for the study of charge symmetry breaking in $pn \to d\pi^0$,

and extraction of the strong contribution to the proton-neutron mass difference from the cross section asymmetry data in $pn \to d\pi^0$. This operator is also an important building block to study CSB in $dd \to \alpha\pi^0$.

To calculate loop corrections to the production operator we developed an efficient method, based on identification of common structures in Feynman diagrams. This method allowed us to detect numerous cancellations between diagrams before carrying out the loop integration. In addition, we derived relations between propagators and momentum-dependent vertices in ChPT. These relations allowed us to identify the relevant irreducible contributions and helped to spot cancellations between various diagrams. These methods and relations depend neither on heavy baryon formulation, nor on the counting scheme, and can be used in the wide range of chiral EFT studies.

Chapter 3

Pion production operator in chiral EFT with explicit delta

In the standard ChPT, only pions and nucleons are considered as explicit degrees of freedom. Contributions of all higher resonances are viewed as short-range and included in the theory implicitly through the low-energy constants. However, in some particular pion-nucleon processes, the low-energy constants cannot fully capture all relevant physics. In such processes the dynamics related to the low-lying resonances such as $\Delta(1232)$, $N^*(1440)$, $N^*(1535)$ and so on, may become relevant. Out of low-lying resonances, the $\Delta(1232)$ — the lowest excitation of the nucleon — is of particular importance: the delta-nucleon mass difference $\delta = m_\Delta - m_N \simeq 294$ MeV is just 2 times larger than the pion mass. As a consequence, it may become inefficient to absorb effects of the delta resonance into low-energy constants alone.

Already in the study of low-energy pion-nucleon scattering [FM01b, Ber08, KEM07, BKM97] it was found that the delta resonance plays an important role. The explicit inclusion of the delta in pion-nucleon scattering led to a better control over the dynamics and resulted in more natural values of the low-energy constants [KGE12, KEM07]. The latter fact is especially important since it leads to a better convergence of the theory. Thus, the explicit inclusion of the delta resonance in chiral EFT is beneficial for some pion-nucleon processes.

In pion production reactions, the effects of delta-resonance are even more important than in πN-scattering. The reason is that the typical momenta in pion production reactions are about $p \simeq \sqrt{m_\pi m_N} \simeq 360$ MeV, which numerically is even larger than the delta-nucleon mass difference δ. This gives a strong motivation to include delta as an explicit degree of freedom and, in this way, keep all long-range contributions from the delta resonance explicitly.

The impact of the delta resonance on pion production was already studied in chiral EFT with MCS. The latest review of chiral EFT studies can be found in Ref. [BHM14], see also [Han04] for a detailed review of various phenomenological studies and early chiral EFT calculations.

In the first chiral EFT study within the delta-full theory [dRMvK00], the only diagram with an explicit delta considered was a tree-level NLO diagram. It was found to give a small contribution.[1] NLO MCS loop-diagrams with delta were also calculated in the chiral EFT

[1] In the study [dRMvK00], the convolution with $NN \to N\Delta$ wave functions was made using the static approximation for the delta propagator. It was noted in the Ref. [BHH$^+$07] that in order to get realistic results,

Table 3.1: Additional diagrams contributing to the pion production operator up to N^2LO MCS appearing in the theory with explicit delta and a qualitative estimation of their contributions to different pion production channels. The first row shows the MCS order, the second row shows the diagrams which start to contribute at that order, and the last two rows indicate the qualitative contributions of the diagrams to different pion production channels. The notation and expressions for the vertices are given in Appendix B.

MCS order	LO	NLO	N^2LO
diagrams	none	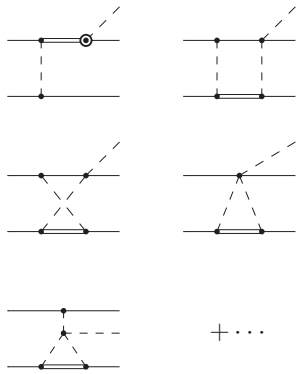	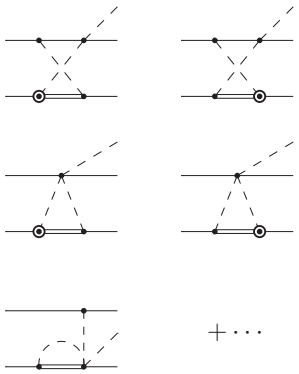
contr. to $pp \to d\pi^+$	0	very small (cancellations and destructive interference) [HK02, BHH$^+$07]	expected to be small relative to large LO from πN-sector [calculated in this work]
contr. to $pp \to pp\pi^0$	0	very small (loops cancel out [HK02], tree-level very small [CFMvK96])	expected to be small but important due to suppression of LO and NLO [calculated in this work]

approach. It was found that the sum of all loop contributions at NLO cancels out [HK02]. This sum, however, contains a remainder, which can be estimated as N^2LO MCS. In the latest hybrid EFT study [BHH$^+$07], it was found that individual NLO tree-level diagrams and the N^2LO remainder (from NLO loops) give moderate (10–15% of LO) contributions to the amplitude, but interfere destructively with each other, see column "NLO" in the Table 3.1. Due to these accidental[2] suppressions at NLO, the contributions of N^2LO start to play the important role. On the other hand, none of genuine irreducible loops at N^2LO, as shown in Table 3.1, was investigated so far. This gives a motivation to calculate N^2LO corrections in the theory with explicit delta.

The delta-resonance-induced contributions listed in the Table 3.1 should be added to the

static approximation is not sufficient and recoil corrections to the delta propagator should be considered.

[2]These kind of suppressions are not related to counting, because individual diagrams are in line with the estimations based on naive dimensional analysis, but the sum is highly suppressed.

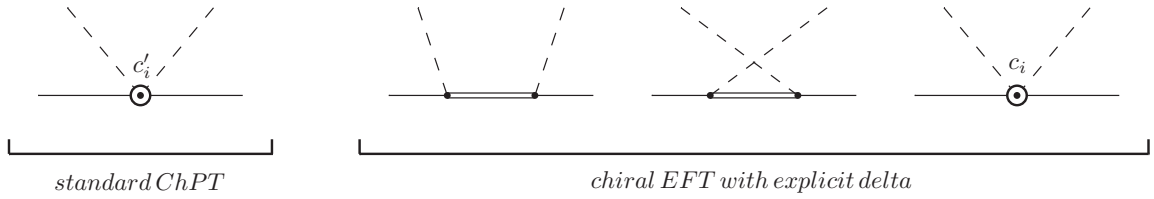

Figure 3.1: Some examples of πN-scattering diagrams governed by the delta-resonance in different formulations of chiral EFT. In the standard ChPT, the effects of delta are considered to be of short range and encoded in LECs c_i'. In the chiral EFT with explicit delta, the effects of delta are included via new diagrams with delta propagators. The values of LECs in the two formulations are different.

pure pion-nucleon contributions from previous chapter (see Table 2.1 there).

In this chapter[3] we perform the full chiral EFT calculation of pion production operators due to explicit delta up-to-and-including $\mathrm{N^2LO}$ in MCS.

To study the long-range contributions of the delta resonance, the standard ChPT is extended to a more general chiral EFT with delta as an explicit degree of freedom [CFMvK96, Hem96, HHK98]. One introduces the delta fields in the theory and writes the most general Lagrangian for interactions of pions, nucleons, and deltas. The outline of this procedure is given in the section 1.3. Practically, the inclusion of explicit delta isobars introduces new terms in the effective Lagrangian. In addition to the terms from standard ChPT, in chiral EFT with explicit delta isobars there are new vertices, which describe pion-nucleon-delta, pion-delta, nucleon-delta, and delta-delta interactions. New vertices also lead to additional Feynman diagrams, which have to be taken into account. Besides the appearance of new diagrams, the inclusion of explicit delta isobars has several specific aspects, which are discussed below.

The explicit inclusion of delta isobars changes the values of low-energy constants, because in the extended chiral EFT the delta resonance is treated explicitly as a dynamic degree of freedom, see Fig. 3.1. One can expect the values of LECs to be more natural in chiral EFT with explicit delta, because significant contributions, which were pushed to LECs in standard ChPT, are now treated dynamically.

In addition, the inclusion of explicit delta isobars affects power counting, because it introduces a new small scale $\delta = m_\Delta - m_N$. For simplicity, in the processes where the only small scale is m_π such as *e.g.* πN-scattering, the new scale δ is associated with this single small scale[4]. In pion production, even without explicit delta, there are already two distinct small scales: m_π and $\sqrt{m_\pi m_N}$. To simplify the estimation procedure, instead of introducing a third small scale, it is reasonable to associate δ with one of the existing scales. In the MCS, the delta-nucleon mass difference δ is associated with $\sqrt{m_\pi m_N}$ [Han04], because numerically δ is closer to $\sqrt{m_\pi m_N}$ than to m_π.

Most of the diagrams with delta excitation can be constructed from the similar pion-nucleon diagrams by substituting nucleon propagators by delta propagators. However, diagrams with delta propagators can be of lower order than similar diagrams with nucleon

[3]The results of this study have been published in [FBE+13].

[4]This allows one to use the standard Weinberg counting with the expansion parameter $\chi_W \simeq m_\pi/\Lambda \simeq \delta/\Lambda$.

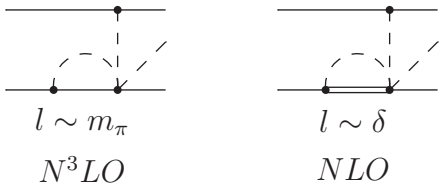

Figure 3.2: Loop diagrams with similar topology but different baryon propagators and, thus, different MCS estimations. The diagram with the delta propagator is of a lower order compared to the one with nucleon propagator, because the loop integral with the delta isobar involves the relatively large scale δ, while the other loop integral involves only small scale m_π.

propagators according to the MCS (see Figure 3.2). To illustrate the difference in counting of pion-nucleon and pion-delta loops, let's recall the estimation procedure for pion-nucleon loops. As discussed in Section 1.4, see also Fig. 1.4, the running momentum in pion-nucleon loop can be either of order m_π or $\sqrt{m_\pi m_N}$ depending on the kinematics and topology of a diagram. In particular, in the loop-integrals with one pion propagator and one (or more) nucleon propagators, the scale $\sqrt{m_\pi m_N}$ does not enter the integral or it can be removed by a shift of variables. Since the only remaining scale in such an integral is m_π, the corresponding diagram is suppressed. In the loop integrals with delta propagator the situation is different. The value δ, which enters the delta propagator, is estimated in the MCS as $\sqrt{m_\pi m_N}$, thus the delta propagator always introduces the relatively large scale $\sqrt{m_\pi m_N}$ to the loop integral, and this scale cannot be removed. Therefore, diagrams with delta propagators in loops can be more important than similar loop diagrams with only nucleon propagators. This is the reason why at $\mathrm{N^2LO}$, there are more diagrams with delta propagators than those with nucleon propagators.

Because in the theory with explicit delta isobar there are more $\mathrm{N^2LO}$ loop diagrams, there are also more LECs that should be renormalized at this order. Unlike to the pion-nucleon case, in the theory with explicit delta isobars, in addition to the five-point $NNNN\pi$ contact terms, also one has to renormalize the pion-nucleon coupling constant g_A and include the nucleon Z-factor Z_N at $\mathrm{N^2LO}$ MCS. This issue is discussed in Section 3.3.1.

Since some diagrams with delta isobars are more important than similar ones with nucleon propagators, it can naively appear that contributions of heavier resonances are more important than the ones of lighter particle. This interpretation, however, is not correct. According to one of the the main principles of EFT, the heavier resonance is, the smaller its impact on low-energy processes. In the limit of infinitely heavy resonance, there are no observable contribution from it at all. The last statement is known as *decoupling theorem* [AC75]. Before carrying out the loop integration and renormalization, it is obvious that contributions of all diagrams with delta propagators vanish in the limit of the very heavy delta ($\delta \to \infty$), because the parameter δ always enters the denominator of the integrand. To keep this property after renormalization, one has to use a proper renormalization scheme. In Section 3.3.1, we describe the regularization scheme required to make all delta contributions vanish in the limit $\delta \to \infty$. For the physical mass of the delta, our explicit calculation shows that the contributions of diagrams with delta excitations are of the same order in magnitude as nucleon ones, which agrees well with the power counting. More precisely, delta contributions turn out to be

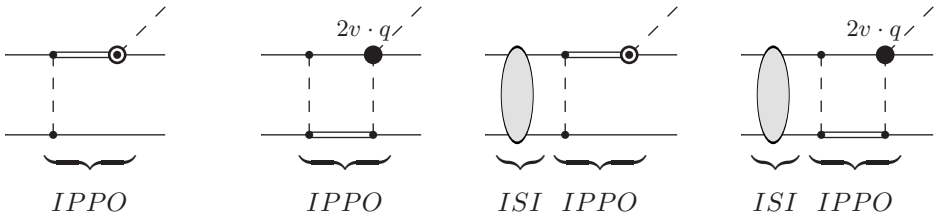

Figure 3.3: One of the ways to formulate the hybrid approach in the theory with explicit delta. The full amplitude receives contributions from the irreducible pion production operators (IPPO) involving internal delta propagators as well as from the convolution of IPPO with the $NN \to NN$ wave functions. ISI stands for initial state interaction of nucleons. Convolution with final state interaction also contributes to the full amplitude, but is not shown. The notation for the vertices is presented in Appendix B.

numerically a bit smaller than the nucleon ones due to spin-isospin factors which are not accounted for in the counting scheme.

This chapter has the following structure. In Section 3.1 we discuss the hybrid approach and the definition of the irreducible operator in the theory with explicit delta. In Sections 3.2 and 3.3 we provide results for tree-level and loop diagrams. We discuss issues of renormalization and decoupling of delta in Section 3.3.1. In section 3.4 we compare long-range contributions from delta loops to the similar contributions from pion-nucleon loops. The summary of our findings is presented in the Section 3.5.

3.1 Reducible diagrams with intermediate delta excitations

To take into account nonperturbative NN interactions in the pion production process, we use the hybrid approach (Section 1.6). To obtain the full amplitude in the hybrid approach, the pion production operator should be convoluted with NN wave functions. In the theory with explicit delta, the hybrid approach should be generalized to take into account additional $NN \to N\Delta$ transitions. There are two common ways to reach this goal, which will be discussed in the next paragraphs.

One way to include delta in the hybrid approach is to consider pion production operators with external nucleons only. In this formulation, delta appears only via an internal propagator inside the production operators. To get the full amplitude, the production operator is convoluted with $NN \to NN$ wave functions in the same way as in the delta-less theory. Exemplary production operators and corresponding contributions to the full amplitude are shown in Fig. 3.3. In this formulation, all off-shell delta effects are treated consistently within chiral EFT, however there are more diagrams to calculate, and some unknown $NN \to N\Delta$ LECs contribute to the production operator.

Another way to include delta in the hybrid approach is to consider pion production *building blocks*, which contain external delta legs, and convolute them with $NN \to N\Delta$ wave functions. Unlike normal pion production operators, building blocks have external deltas and kinematically can never be on-shell. Some examples of building blocks and their contributions to the full amplitude are shown in Fig. 3.4. In this approach, there are less diagrams and

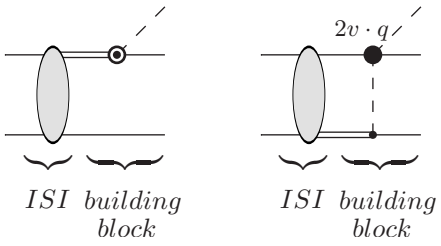

Figure 3.4: Another way to formulate the hybrid approach in the theory with explicit delta. The contribution to the full amplitude is obtained by the convolution of the pion production building block (involving external delta) with the $NN \to N\Delta$ initial state interaction (ISI) wave functions. Similar diagrams with final state interaction are not shown, but should be also included. The notation for the vertices is presented in Appendix B.

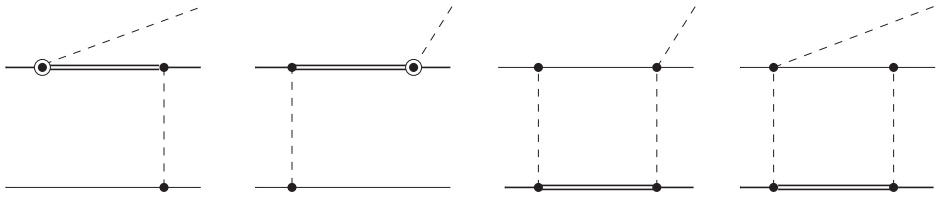

Figure 3.5: Reducible Δ contributions at NLO (first two diagrams) and at $\mathrm{N^2LO}$ (last two).

the $NN \to N\Delta$ LECs do not contribute to the building blocks, but are taken into account in $NN \to N\Delta$ wave functions. The $NN \to N\Delta$ wave functions are obtained through the solution of the coupled-channel problem involving NN and $N\Delta$ interactions. The short range part of the $N\Delta$ interaction (as well as that of NN) is constrained by the fit to NN partial wave amplitudes [ABSW07]. However it is difficult to treat off-shell delta effects consistently when phenomenological $NN \to N\Delta$ wave functions are used.

In this thesis we use the second way and calculate the corresponding building blocks.

Note that the diagrams with $\Delta\Delta$ intermediate states start to contribute to s-wave pion production at $\mathrm{N^3LO}$. Some examples of such diagrams are shown in the Fig. 3.6. Thus, at $\mathrm{N^2LO}$, it is not necessary to consider either building blocks with two external deltas or the corresponding convolution with $NN \to \Delta\Delta$ wave functions.

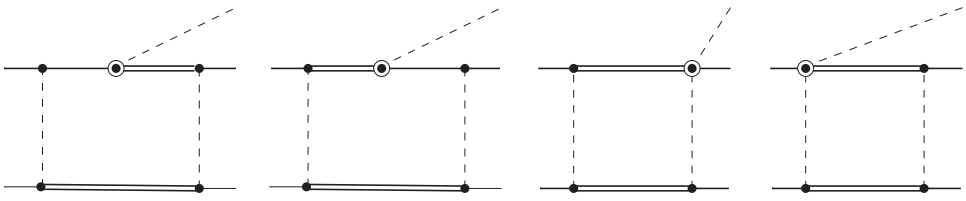

Figure 3.6: Examples of $\mathrm{N^3LO}$ contributions involving $\Delta\Delta$ intermediate states.

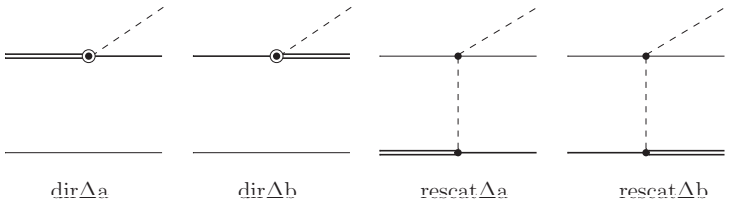

Figure 3.7: Single baryon and rescattering diagrams with Δ contributions which appear as building blocks in the construction of the pion-production amplitude.

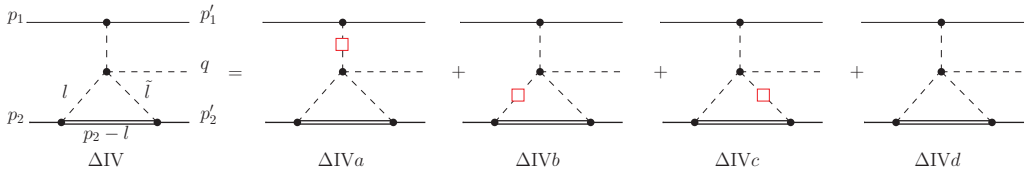

Figure 3.8: An example of the loop diagrams with the explicit Δ. The notation for the vertices is presented in Appendix B.

3.2 Tree-level diagrams with delta-resonance

In this thesis we consider diagrams with intermediate $N\Delta$ state as reducible and calculate only corresponding irreducible tree-level building blocks. In this section we provide expressions for the tree-level building blocks for the pion production amplitude. The corresponding diagrams are shown in Fig. 3.7. We obtain the following expressions:

$$\begin{aligned}
iM_{\mathrm{dir\Delta a}} &= -\frac{g_{\pi N\Delta}}{m_N f_\pi} T_1^a v\cdot q(\mathbb{S}_1\cdot p_1)\delta(\vec{p}_2-\vec{p}_2'),\\
iM_{\mathrm{dir\Delta b}} &= -\frac{g_{\pi N\Delta}}{m_N f_\pi} T_1^{\dagger a} v\cdot q(\mathbb{S}_1^\dagger\cdot p_1')\delta(\vec{p}_2-\vec{p}_2'),\\
iM_{\mathrm{rescat\Delta a}} &= \frac{g_{\pi N\Delta}}{2f_\pi^3} v\cdot q\, i\epsilon^{bac}\tau_1^c T_2^b \frac{1}{k_2^2-m_\pi^2+i0}(\mathbb{S}_2\cdot k_2),\\
iM_{\mathrm{rescat\Delta b}} &= \frac{g_{\pi N\Delta}}{2f_\pi^3} v\cdot q\, i\epsilon^{bac}\tau_1^c T_2^{\dagger b} \frac{1}{k_2^2-m_\pi^2+i0}(\mathbb{S}_2^\dagger\cdot k_2),
\end{aligned} \tag{3.1}$$

where $\delta(\vec{p}_2-\vec{p}_2')$ is a three-dimensional delta-function. These building blocks contain external deltas and cannot be on-shell. To get corresponding contributions to the full amplitude, these blocks must me convoluted with initial or final $NN\to N\Delta$ interactions.

The contributions of these operators to charged pion production ($pp\to d\pi^+$) amplitude are evaluated in Ref. [BHH$^+$07]. It is shown there that contributions to the full amplitude from these building blocks interfere destructively, resulting in a very small total contribution.

3.3 Loop diagrams with delta propagators

Loop diagrams involving delta isobars which contribute to s-wave pion production up to N^{2}LO are shown in Fig. 3.9. In the next paragraphs, we consider the contributions from various groups of these diagrams.

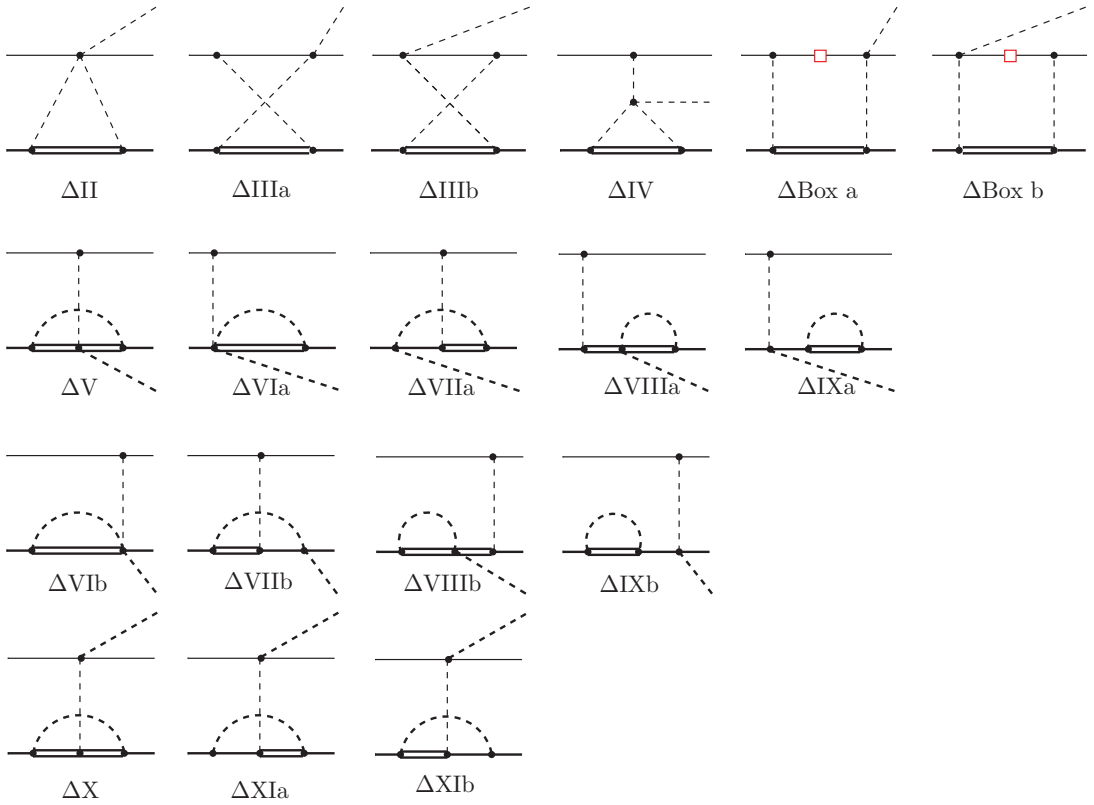

Figure 3.9: Loop diagrams with the delta degree of freedom contributing to s-wave pion production up to N^{2}LO. The notation for the vertices is presented in Appendix B.

In the first row of Fig. 3.9, we have two-pion exchange diagrams with topologies completely analogous to the pion-nucleon g_A^3-graphs from Chapter 2 (see the second row in Fig. 2.6). The two-pion exchange diagrams in the first row of Fig. 3.9 individually start to contribute at NLO. However, these NLO diagrams cancel completely in the sum for the same reason as do the NLO pion-nucleon ones. Again, one can factor out the common structure of these diagrams, and the sum of remaining $\pi N \to \pi\pi N$ subgraphs cancel out. Moreover, N^{2}LO contributions of the diagrams in the first row in Fig. 3.9 also show the cancellation pattern among the diagrams which is completely analogous to the pion-nucleon case. In the first row of Fig. 3.10, we demonstrate graphically this systematic cancellation pattern at NLO and N^{2}LO. It should be mentioned that the diagrams in the first row of Fig. 3.9 also receive corrections from higher-order vertices $\propto 1/m_N$ from $\mathcal{L}_{\pi N}^{(2)}$. Those corrections, however, again cancel completely at N^{2}LO in a full analogy with the cancellations among the corresponding pion-nucleon loop contributions. The net sum of the N^{2}LO diagrams in the first row of Fig. 3.9 receives contributions only from diagrams ΔIIIa and ΔIIIb, where the Weinberg-Tomozawa πN vertices are on-shell, and a remnant of diagram ΔIV, the pion-gauge independent ΔIVd shown in Fig.3.8. In other words, the contributions of the diagrams ΔIVa–c in Fig.3.8 cancel against other diagrams, as indicated in Fig. 3.10, and only ΔIVd with a residual part of the four-pion vertex survives.

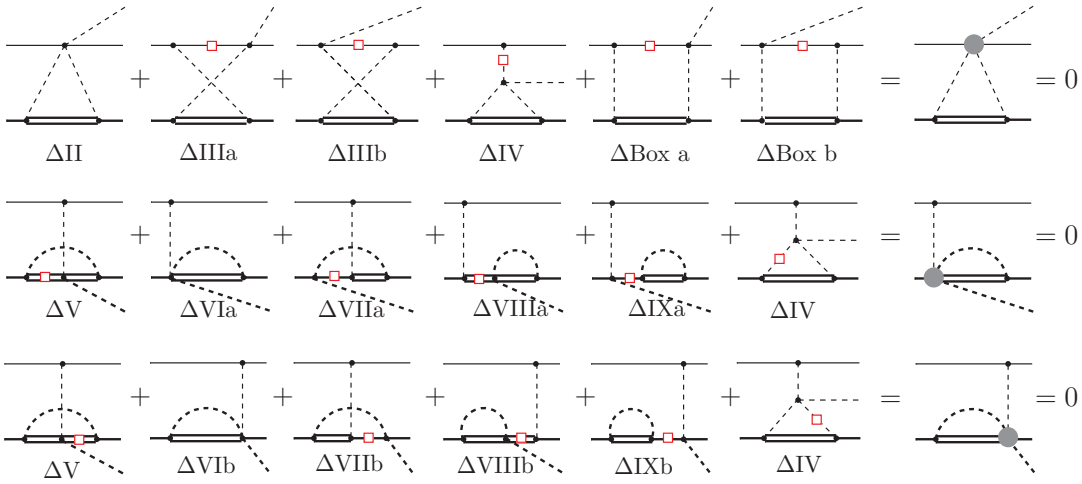

Figure 3.10: Illustration of the cancellation pattern among the Δ-loop contributions for different topologies shown on the l.h.s. of each row. The (red) squares on the nucleon or Δ propagators indicate that for each diagram, this nucleon or Δ propagator cancels against parts of the adjacent πN or $\pi\Delta$ rescattering vertex. The red squares on the pion propagators indicate that for each diagram, the pion propagator cancels against parts of the four-pion vertex expression. These propagator cancellations generate the rightmost effective diagrams in each row, where the effective vertices (blobs) receive contributions from all graphs on the l.h.s. The zero on the very r.h.s. in each row means that the sum of all diagrams on the l.h.s. does not contribute to the s-wave pion production at least up to $\mathrm{N^2LO}$.

In addition, there are several new loop diagrams containing delta propagators, where one effectively has a pion being exchanged between the two nucleons, see diagrams ΔV–ΔXI in Fig. 3.9. Surprisingly, parts of diagrams ΔV–ΔIX in rows two and three also undergo significant cancellations. Again, as illustrated in rows two and three in Fig. 3.10, after the cancellations of the vertex structures with the propagators, some parts of the diagrams ΔV–ΔIX and ΔIV acquire the effective topology of the diagrams ΔVIa and ΔVIb. The net result of such contributions again vanishes at NLO and $\mathrm{N^2LO}$ for s-wave pion production as indicated on the r.h.s. in rows two and three of Fig. 3.10. After the cancellations, only those parts of diagrams ΔV–ΔIX remain, which are proportional to the on-shell part, $2m_\pi$, of the $\pi\Delta - \pi\Delta$ and $\pi N - \pi N$ vertices. Although the dimensional analysis estimate indicates that these residual contributions are naively of $\mathrm{N^2LO}$ in the MCS, most of the $\mathrm{N^2LO}$ amplitude expression vanishes due to the angular integration in the loop. For example, for diagrams ΔVII the numerator of the integrand $\propto 2m_\pi\, \mathbb{S}\cdot(p_1 - p_1')(\mathbb{S}\cdot l)$ is odd with the loop momentum l yielding the vanishing contribution at $\mathrm{N^2LO}$. As a consequence of these cancellations, almost all loop diagrams in rows two and three in Fig. 3.9 do not contribute to the s-wave $\mathrm{N^2LO}$ pion-production amplitude. From the loop diagrams in rows two and three only diagram ΔV yields a non-vanishing $\mathrm{N^2LO}$ contribution. This contribution corresponds to the part of the $\pi\Delta - \pi\Delta$ rescattering vertex proportional to $2v\cdot q$.

Finally, the three one-pion-exchange delta loop diagrams in the last row of Fig. 3.9, which have to be taken into account at $\mathrm{N^2LO}$, contribute only to renormalization of g_A at $\mathrm{N^2LO}$,

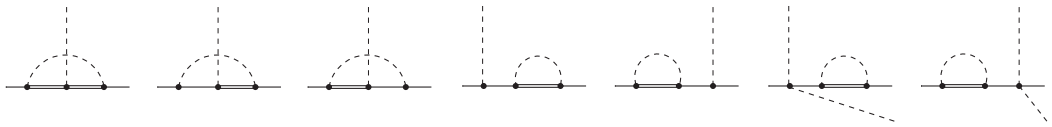

Figure 3.11: Various renormalization diagrams relevant at N^{2}LO. The first three diagrams contribute to renormalization of the πN coupling constant g_A, whereas the last four diagrams lead to the nucleon wave function renormalization in the theory with explicit Δ degrees of freedom.

see the next subsection.

3.3.1 Regularization of UV divergences and renormalization

The loop diagrams with explicit delta are UV-divergent at N^{2}LO. There are two types of contributions: one is related to the divergences in the one-pion-exchange (OPE) diagrams and another one to the divergences in the two-pion-exchange (TPE) diagrams.

Divergences in OPE loop diagrams with explicit delta isobars are of a lower order than in similar pion-nucleon diagrams (see Fig. 3.2 and related discussion in the beginning of this chapter). That is why in the N^{2}LO calculation with explicit deltas, it is necessary to renormalize not only five-point contact term (as in the pion-nucleon theory), but also the pion-nucleon coupling constant and nucleon fields. The corresponding renormalization corrections at order $\delta^2/\Lambda_\chi^2 \sim \chi^2_{\rm MCS}$ were evaluated in Ref. [FMS98, FMMS00] for πN-scattering with explicit Δ using dimensional regularization. We confirmed the results of Ref. [BFHM98, FMS98, FMMS00]:

$$
\begin{aligned}
Z_N &= 1 + 2(d-2) g_{\pi N\Delta}^2 \frac{\delta}{f_\pi^2} J_{\pi\Delta} + \mathcal{O}\left(\frac{m_\pi^2}{\Lambda^2}\right), \qquad (3.2)\\
\mathring{g}_A &= g_A + \frac{10(6+d-4d^2+d^3)}{9(d-1)^2}\, g_1\, g_{\pi N\Delta}^2\, \frac{\delta}{f_\pi^2}\, J_{\pi\Delta} + \frac{16(d-2)}{3(d-1)^2}\, g_A\, g_{\pi N\Delta}^2\, \frac{\delta}{f_\pi^2}\, J_{\pi\Delta} + \mathcal{O}\left(\frac{m_\pi^2}{\Lambda^2}\right),
\end{aligned}
$$

where $\mathring{g}_A$ is the bare axial coupling, $g_{\pi N\Delta} = h_A/2$ and g_1 is the $\pi\Delta\Delta$ coupling constant. The basic integral $J_{\pi\Delta}$ is defined in Appendix D.1, and is estimated in MCS as $\delta/(4\pi)^2$. Since renormalization corrections in Eq. (3.2) are suppressed as $\chi^2_{\rm MCS}$ compared to physical values of g_A and Z_N, they are only important in the LO diagrams. In higher-order diagrams, one can set $\mathring{g}_A = g_A$ and $Z_N = 1$. LO diagrams are discussed in the previous Chapter and include rescattering and direct pion production (See Table 2.1). After substituting the bare LEC $\mathring{g}_A$ and the bare nucleon fields in LO tree-level diagrams in terms of the physical quantities we obtain additional N^{2}LO contributions which, by construction, cancel all divergences in the OPE loop diagrams with delta at N^{2}LO. It is noteworthy that diagrams ΔX and ΔXI in Fig. 3.9 consist solely of divergent parts and cancel out completely after the renormalization of g_A.

After the cancellations discussed in the previous section and the renormalization of g_A, the only nonzero contributions at N^{2}LO emerge from the residual parts of diagrams ΔIII, ΔIV and ΔV. These contributions contain both finite and divergent parts. Most of the remaining divergent parts are eliminated by renormalization of nucleon field. Namely, these divergences

cancel with the corrections to the nucleon Z-factor included in the LO tree-level rescattering diagram Eq. (2.1). The remainder includes a finite part and a divergency which is eliminated by renormalization of the five-point contact term.

The individual non-vanishing contributions of the delta loop diagrams in Fig. 3.9, expressed in terms of four well-known scalar integrals, $J_{\pi\Delta}$, $I_{\pi\pi}$, $J_{\pi\pi\Delta}$, and $J_{\pi\pi N\Delta}$, defined in Appendix D, read

$$\begin{aligned}
iM_{\Delta\mathrm{III(a+b)}} &= i(SI_1)\frac{1}{(d-1)(d-2)}\left\{I_{\pi\pi}-\frac{1}{2}\frac{J_{\pi\Delta}}{\delta}+\delta J_{\pi\pi\Delta}+\frac{1}{4}k_1^2 J_{\pi\pi N\Delta}\right\} \\
&+ i(SI_2)\,\frac{d-2}{d-1}\left\{\frac{1}{2}I_{\pi\pi}-\frac{1}{2}\frac{J_{\pi\Delta}}{\delta}+\frac{1}{2}\delta J_{\pi\pi\Delta}+\frac{1}{4}k_1^2 J_{\pi\pi N\Delta}\right\}, \\
iM_{\Delta\mathrm{IV}} &= i(SI_2)\,\frac{d-2}{d-1}\left\{\left(2-\frac{1}{d-1}+4\,\frac{\delta^2}{k_1^2}\right)I_{\pi\pi}-4\frac{\delta^2}{k_1^2}\frac{J_{\pi\Delta}}{\delta}+\left(2+4\frac{\delta^2}{k_1^2}\right)\delta J_{\pi\pi\Delta}\right\}, \\
iM_{\Delta\mathrm{V}} &= i(SI_2)\,(d-2)\left\{5\frac{\delta^2}{k_1^2}\frac{J_{\pi\Delta}}{\delta}\right\}, \\
iM_{\Delta}^{Z_N} &= i(SI_2)\,(d-2)\left\{-3\frac{\delta^2}{k_1^2}\frac{J_{\pi\Delta}}{\delta}\right\},
\end{aligned} \tag{3.3}$$

where the two spin-isospin operators in Eq.(3.3) are:

$$\begin{aligned}
(SI_1) &= (-i)\frac{g_{\pi N\Delta}^2}{f_\pi^5}g_A\left\{\left(\frac{2}{3}\tau_1^a-\frac{1}{3}\tau_2^a\right)4\,[S_{2\mu},\,S_{2\nu}]\,S_1^\nu k_1^\mu v\cdot q \quad +(1\leftrightarrow 2)\right\}, \\
(SI_2) &= (-i)\frac{g_{\pi N\Delta}^2}{f_\pi^5}g_A\,\frac{i}{3}\left\{(\boldsymbol{\tau}_1\times\boldsymbol{\tau}_2)^a S_1\cdot k_1 v\cdot q \quad +(1\leftrightarrow 2)\right\}.
\end{aligned} \tag{3.4}$$

The four different loop integrals in Eq. (3.3) can be characterized in the following manner. The integral $J_{\pi\pi\Delta}$, Eq. (D.5), contains two pion propagators and a delta propagator whereas the integral $J_{\pi\pi N\Delta}$, Eq. (D.6), has an additional nucleon propagator. Furthermore, we note that both of these integrals are UV finite. Meanwhile, the integrals $J_{\pi\Delta}$ and $I_{\pi\pi}$ contain UV divergences and, similar to the pion-nucleon loops, some of these divergencies can be absorbed by the five-point $NN\to NN\pi$ contact term.

All divergences in TPE loop diagrams with delta are removed by the renormalization of the five-point $NN\to NN\pi$ contact term. However, in a theory containing a "heavy" resonance Δ, it is not sufficient to require just the cancellation of the UV divergent terms with the corresponding LECs. The integrals $J_{\pi\Delta}$ and $I_{\pi\pi}$ in Eq. (3.3), which are multiplied by the factor δ^2/k_1^2, pose an additional problem. Such polynomial behavior would give divergences if the Δ-resonance was infinitely heavy, i.e., in the limit $\delta\to\infty$. Therefore, to find the most natural finite values of the renormalized LECs, the explicit "decoupling" renormalization scheme was introduced [AC75]. In such a scheme, the finite parts of LECs are chosen such that the renormalized contribution from diagrams with Δ loops vanish in the limit $\delta\to\infty$. It is demonstrated in Appendix E that the following combinations of loop

integrals (up to N^{2}LO in MCS) do vanish when $\delta \to \infty$:

$$k_1^2 J_{\pi\pi N\Delta}, \tag{3.5}$$

$$\left(I_{\pi\pi} + \frac{1}{2}\frac{J_{\pi\Delta}}{\delta} + \delta J_{\pi\pi\Delta} + \frac{2}{(4\pi)^2}\right), \tag{3.6}$$

$$\frac{\delta^2}{k_1^2}\left(I_{\pi\pi} + \frac{1}{2}\frac{J_{\pi\Delta}}{\delta} + \delta J_{\pi\pi\Delta} + \frac{2}{(4\pi)^2}\right) - \frac{1}{12}\left(I_{\pi\pi} + \frac{1}{2}\frac{J_{\pi\Delta}}{\delta} + \frac{1}{3}\frac{2}{(4\pi)^2}\right). \tag{3.7}$$

We find that the combination of the two integrals $J_{\pi\Delta}$ and $I_{\pi\pi}$ in Eqs. (3.5)-(3.7), $I_{\pi\pi} + \frac{1}{2\delta}J_{\pi\Delta}$ cancels the UV divergences of the individual integrals as proven at the end of the Appendix E. Hence, Eqs. (3.5)-(3.7) are all UV finite and vanish when $\delta \to \infty$.

Rewriting the sum of the amplitudes $M_{\Delta\mathrm{III(a+b)}}, M_{\Delta\mathrm{IV}}, M_{\Delta\mathrm{V}}$ and $M_\Delta^{Z_N}$ from Eq. (3.3) in terms of the integral combinations (3.5)–(3.7), we obtain the following transition amplitude from the Δ loop diagrams:

$$\begin{aligned}
iM^{\mathrm{N^2LO}}_{\Delta\text{-loops}} &= \frac{g_A g_{\pi N\Delta}^2}{f_\pi^5} v\cdot q\, \tau_+^a \left(i\varepsilon^{\alpha\mu\nu\beta} v_\alpha k_{1\mu} S_{1\nu} S_{2\beta}\right) \\
\times\ & \left\{\frac{2}{9}\left(I_{\pi\pi} + \frac{1}{2}\frac{J_{\pi\Delta}}{\delta} + \delta J_{\pi\pi\Delta} + \frac{2}{(4\pi)^2}\right) + \frac{1}{18}k_1^2 J_{\pi\pi N\Delta} - \left[\frac{2}{3(d-1))}\frac{J_{\pi\Delta}}{\delta}\right] + \tilde{\mathcal{A}}^\Delta_{\mathrm{CT}}\right\} \\
+\ & \frac{g_A g_{\pi N\Delta}^2}{f_\pi^5} v\cdot q\, \tau_\times (S_1+S_2)\cdot k_1 \\
\times\ & \left\{\frac{5}{9}\left(I_{\pi\pi} + \frac{1}{2}\frac{J_{\pi\Delta}}{\delta} + \delta J_{\pi\pi\Delta} + \frac{2}{(4\pi)^2}\right) + \frac{1}{18}k_1^2 J_{\pi\pi N\Delta} - \frac{2}{27}\left(I_{\pi\pi} + \frac{1}{2}\frac{J_{\pi\Delta}}{\delta} + \frac{1}{3}\frac{2}{(4\pi)^2}\right)\right. \\
+\ & \left.\frac{8}{9}\frac{\delta^2}{k_1^2}\left(I_{\pi\pi} + \frac{1}{2}\frac{J_{\pi\Delta}}{\delta} + \delta J_{\pi\pi\Delta} + \frac{2}{(4\pi)^2}\right) - \left[\frac{(d-2)}{3(d-1)}\left(\frac{19}{12}\frac{J_{\pi\Delta}}{\delta} + \frac{5}{(4\pi)^2}\right)\right] + \tilde{\mathcal{B}}^\Delta_{\mathrm{CT}}\right\}.
\end{aligned} \tag{3.8}$$

Additional terms, that do not vanish at the large-δ limit and shown in the square brackets in Eq. (3.8), are short-ranged and are cancelled in the amplitude expression by the parts of the five-point contact terms $\tilde{\mathcal{A}}^\Delta_{\mathrm{CT}}$ and $\tilde{\mathcal{B}}^\Delta_{\mathrm{CT}}$. In other words, the decoupling condition fixes the magnitude of the five-point contact interactions due to the explicit Δ, $\tilde{\mathcal{A}}^\Delta_{\mathrm{CT}}$ and $\tilde{\mathcal{B}}^\Delta_{\mathrm{CT}}$, up to higher order terms. In fact, by defining the five point contact terms as

$$\tilde{\mathcal{A}}^\Delta_{\mathrm{CT}} = \frac{2}{3(d-1)}\frac{J_{\pi\Delta}}{\delta} + O\left(\frac{m_\pi^2}{\delta^2}\right), \tag{3.9}$$

$$\tilde{\mathcal{B}}^\Delta_{\mathrm{CT}} = \frac{(d-2)}{3(d-1)}\left(\frac{19}{12}\frac{J_{\pi\Delta}}{\delta} + \frac{5}{(4\pi)^2}\right) + O\left(\frac{m_\pi^2}{\delta^2}\right), \tag{3.10}$$

we obtain the fully renormalized, finite Δ loops amplitude contribution to s-wave pion pro-

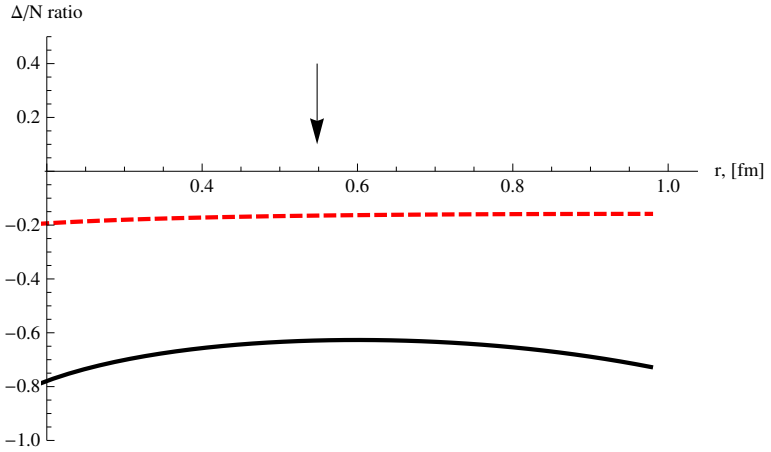

Figure 3.12: The ratio of the long-range contributions of the delta loop diagrams to the similar contributions of the pion-nucleon loop diagrams for different pion production channels. The red dashed curve correspond to the ratio of contributions to the amplitude $\mathcal{A}$ relevant for $pp \to pp\pi^0$ channel, while the black solid curve correspond to the ratio of contributions to the amplitude $\mathcal{B}$ relevant for $pp \to d\pi^+$ channel. The arrow indicates the typical distance relevant for pion production process $r \sim 1/p = 1/\sqrt{m_\pi m_N}$.

duction at N^{2}LO, which satisfies the decoupling condition:

$$
\begin{aligned}
iM^{\mathrm{N^2LO}}_{\Delta\text{-loops}} &= \frac{g_A g^2_{\pi N\Delta}}{f_\pi^5} v\cdot q\,\tau^a_+ \left(i\varepsilon^{\alpha\mu\nu\beta} v_\alpha k_{1\mu} S_{1\nu} S_{2\beta}\right) \\
\times &\left\{\frac{2}{9}\left(I_{\pi\pi} + \frac{1}{2}\frac{J_{\pi\Delta}}{\delta} + \delta J_{\pi\pi\Delta} + \frac{2}{(4\pi)^2}\right) + \frac{1}{18}k_1^2 J_{\pi\pi N\Delta}\right\} \\
+ &\frac{g_A g^2_{\pi N\Delta}}{f_\pi^5} v\cdot q\,\tau_\times (S_1+S_2)\cdot k_1 \\
\times &\left\{\frac{5}{9}\left(I_{\pi\pi} + \frac{1}{2}\frac{J_{\pi\Delta}}{\delta} + \delta J_{\pi\pi\Delta} + \frac{2}{(4\pi)^2}\right) + \frac{1}{18}k_1^2 J_{\pi\pi N\Delta}\right. \\
+ &\left.\frac{8}{9}\frac{\delta^2}{k_1^2}\left(I_{\pi\pi} + \frac{1}{2}\frac{J_{\pi\Delta}}{\delta} + \delta J_{\pi\pi\Delta} + \frac{2}{(4\pi)^2}\right) - \frac{2}{27}\left(I_{\pi\pi} + \frac{1}{2}\frac{J_{\pi\Delta}}{\delta} + \frac{1}{3}\frac{2}{(4\pi)^2}\right)\right\}. \quad (3.11)
\end{aligned}
$$

This expression should be added to the finite s-wave production operators presented in Chapter 2.

3.4 Comparison of the pion-nucleon and delta loop contributions

In Chapter 2 (Section 2.2.5), we argued that the long-range scheme-independent part of the pion-nucleon loops at N^{2}LO is sizable and could resolve the problem with the description of pion production data in the neutral channel, $pp \to pp\pi^0$. We now add the long-ranged

delta contribution and study its importance. First, we note that the spin-isospin structure of the delta loops in Eq. (3.11) is exactly the same as for the pion-nucleon case in Eq. (2.19). Meanwhile, the dimensionless integrals are different, and the coefficients in front of the spin-isospin operators also differ. We want to compare the resulting amplitudes from the nucleon and delta loop diagrams at NN relative distances relevant for pion production, i.e. at $r \sim 1/p \simeq 1/\sqrt{m_\pi m_N}$. In order to separate the long-range scheme-independent contributions of the delta loop expressions from the short-range ones in a transparent manner, we make a Fourier transformation of our expressions. The Fourier transformation of a short-range (constant) contribution gives a δ-function, $\delta(\mathbf{r})$, which does not influence the long-range physics of interest, and we, therefore, ignore this contribution in this section. The Fourier transformation of the long-range part of the loop integrals is evaluated numerically as follows:

$$I(r) = \int \frac{d^3k}{(2\pi)^3} e^{i\mathbf{k}\cdot\mathbf{r}}\, I(k)\, e^{-k^2/\Lambda^2}\,. \tag{3.12}$$

Here, the regulator e^{-k^2/Λ^2} is used in order to minimize the influence of the large momenta in the loop integrals, denoted by $I(k)$ for short. We have verified that for $\Lambda > 2$ GeV this regulator does not affect the results in the long-range region of $r \sim 1/p$. Specifically, we Fourier transform the integral combinations in the curly brackets in Eq. (3.11) (multiplied by $g_A g^2_{\pi N\Delta}$) corresponding to τ_+ (neutral) and $\tau_\times$ (charged) channels. We compare the resulting Fourier transformed amplitudes with the Fourier transformed amplitudes of the corresponding pion-nucleon contributions in Eqs. (2.18) and (2.19), $-2g_A^3 I_{\pi\pi}$ and $(-19/24 g_A^3 + 1/6 g_A) I_{\pi\pi}$, respectively. The ratio of the r-space Δ loop contributions to those of the nucleon is shown in Fig. 3.12. One can see that in the neutral channel, the long-range part of the delta contribution constitutes less than 20% compared to the pion-nucleon loop amplitude. This can be understood by the specific combination of the coefficients for the spin-isospin operator in the case of the delta-resonance amplitude, which results in a suppression by almost one order of magnitude. Therefore, the conclusion of Chapter 2, regarding the importance of the pion-nucleon loops in explaining the neutral pion production, appears to be only slightly modified by the delta loop contributions. Regarding the charged channel, the delta loop contribution to the s-wave pion-production amplitude is almost of the same magnitude (roughly 60%) but of opposite sign compared to the pion-nucleon one. The net loop amplitude from the nucleon and delta loop diagrams is therefore not as important as in the neutral channel.

The pattern that emerged from the loops is, therefore, exactly what is necessary to quantitatively describe the data on both $pp \to pp\pi^0$ and $pp \to d\pi^+$ very near to the threshold: while in the former reaction there persists a huge discrepancy between data and the chiral perturbation theory calculation to NLO, in the latter the description at NLO is already quite good [LBH$^+$06]. In line with this observation we now find that due to large cancellations among the pion-nucleon and the Delta loops, the N^{2}LO corrections from the loops are small in the charged pion channel. On the other hand, this cancellation is by far not that efficient in the neutral pion channel leading to a significant loop contribution. In combination with the observation that in the neutral pion channel the leading order diagrams are suppressed both kinematically and dynamically [Han04], this provides a dynamical reason of why it was so much harder to understand phenomenologically the neutral pion production compared to the charged pion production.

3.5 Chapter summary

In this chapter we have calculated additional tree-level and loop contributions to the N^{2}LO pion production amplitude appearing in the theory with explicit delta isobars. We have shown that the delta resonance provides important long-range contributions to the pion production operator. Such contributions were not considered in the phenomenological models so far. The obtained result has a compact analytical form and does not contain any unknown low-energy constants.

We found numerous cancellations between various loop diagrams. In addition to the cancellations at NLO reported in [HK02], we discovered significant cancellations at N^{2}LO. We found that all cancellations are driven by the same mechanism. Namely, the sum of all point-like[5] $\pi N \to \pi\pi N$ subgraphs gives the vanishing contribution to the s-wave pion production reaction $NN \to NN\pi$. In addition, the sums of all point-like $\pi\Delta \to \pi\pi N$ and $\pi N \to \pi\pi\Delta$ subgraphs do not contribute to s-wave pion production either (see Fig. 3.10).

After carrying out renormalization, our result is finite and consistent with the requirement of the decoupling theorem [AC75], namely, all contributions from diagrams with explicit delta vanish if the mass of the delta is taken to infinity.

The obtained N^{2}LO pion production operators together with the ones from the previous chapter can be convoluted with $NN \to NN$ and $NN \to N\Delta$ interactions and used to calculate various pion production observables. In addition, the compact analytical form makes it easy to use these results as building blocks for more complicated few-nucleon processes.

Finally, the methods which we developed to deal with cancellations between various $NN \to NN\pi$ loop diagrams rely neither on heavy baryon expansion nor on the special power counting scheme and can be used to study other processes within chiral EFT.

[5] *I.e.* subgraphs which contain no propagators or in which all propagators cancel with momentum dependent vertices.

Chapter 4

Charge symmetry breaking in $NN \to NN\pi$

Symmetries play an important role in the particle physics. They allow one to understand the fundamental principles of particle interactions, explain similarities in different reactions, and make predictions for new experiments. Symmetries can be fulfilled to a different degree. There are several symmetries that are satisfied in every known experiment. Such exact symmetries allow one to derive the fundamental conservation laws (*e.g.* four-momentum and total angular momentum conservation). There are also many approximate symmetries, which are not satisfied exactly, but symmetry-breaking contributions are small compared to the symmetric ones. Approximate symmetries allow one to study fine details of particle interactions.

The symmetry breaking pattern of the Standard Model is highly nontrivial. The Lagrangian of QCD possesses an approximate chiral symmetry. This symmetry is spontaneously broken by quark condensate and explicitly broken by nonzero quark masses and electromagnetic (EM) effects. However, if one neglects long-range electromagnetic effects and assumes the masses and charges of up and down quarks to be the same, there remains a subgroup of chiral symmetry which is exact. This remaining subgroup is known as *isospin symmetry* (or *charge independence*)[1]. The isospin symmetry is also explicitly broken. *Isospin violation* (IV) has several sources. The first source is the difference of masses of up and down quarks ($m_u - m_d$). This difference makes the neutron heavier than the proton. The second source are short-range hard-photon exchanges between quarks of different charges. These effects make charged pions heavier than the neutral one, and produce a shift to the nucleon mass which is bigger for protons. The strength of short-range EM IV effects is governed by the difference of the quark charges ($q_u - q_d$). Finally, there are long-range soft-photon-exchanges, which are *e.g.* responsible for Coulomb interaction between protons and produce various IV effects in nuclei.

Which of isospin violation mechanisms dominates a specific observable depends on the particular process. In most processes IV is dominated by electromagnetic effects. In particular, Coulomb interaction typically dominates in systems of several protons, while hard-photon exchanges and effects of pion mass difference dominate in many other systems. There are,

[1] A generalization of the isospin symmetry, when u, d, and s-quarks are assumed to have equal masses is called *flavour symmetry*.

however, some processes, where main isospin violating contributions are produced by strong interaction (*i.e.* by the quark mass difference). Studying strong IV effects is of great importance, since they provide access to the information about the quark mass difference.

To study strong isospin violation it is convenient to consider a special class of IV effects, which is known as *charge symmetry breaking* (CSB) [MNS90, MOS06]. *Charge symmetry* (CS) is an invariance under interchange of up and down quarks. In terms of the rotation in the isospin space, the charge symmetry corresponds to the invariance of the system under 180° rotation along the y-axis, while the isospin symmetry (charge independence) corresponds to invariance under *any* rotation. Isospin symmetry implies charge symmetry, but not the other way round. Isospin violating effects can be either charge symmetry breaking or charge-symmetric. Short-range CSB effects are not invariant under interchange of u and d quarks and thus should be proportional to the odd powers of $m_u - m_d$ or $q_u - q_d$, while charge-symmetric IV effects are invariant under interchange of quarks and proportional to even powers of quark mass/charge difference. The main interest in CSB processes is that they allow to extract information about the quark mass difference more directly, since electromagnetic effects, which typically dominate IV observables, are charge-symmetric and do not contribute to CSB.

Study of CSB effects involves several challenges. First, CSB effects are typically much smaller than charge symmetric ones. From the theoretical side, this requires methods which allow a systematic inclusion of both charge symmetric and CSB effects. From the experimental side, a high-precision measurements and a good control over systematic uncertainties are needed to detect CSB signals. Second, since CSB effects have both strong and electromagnetic origins, which are of comparable importance, it is necessary to have a theory which can systematically describe both kinds of effects. Finally, CSB effects are frequently masked by the long-range Coulomb interaction. Thus, one has to calculate the contributions of soft-photon-exchanges or better consider reactions which do not include the Coulomb interaction at all.

Charge symmetry breaking can be observed in a wide range of systems. The examples are: the mass difference between protons and neutrons, the mass difference between D^0 and D^+ mesons [GHKM08], decays of η-mesons (see [BG07] for a recent two-loop calculation), the scattering length difference in pp and nn scattering (see [MOS06] for a review article), neutron-proton elastic scattering at intermediate energies [ABB$^+$89, ZAB$^+$98, VJK$^+$92], $\rho\omega$ mixing [BCE$^+$85], $\pi\eta$-mixing [CS95], binding energy differences of mirror nuclei [NS69], pion-deuteron scattering [BHH$^+$11b], and neutral pion production reactions such as $dd \to \alpha\pi^0$ [SBA$^+$03] and $pn \to d\pi^0$ [OKH$^+$03].

In this chapter we concentrate on the neutral pion production reaction $pn \to d\pi^0$. In this reaction, CSB manifests itself in the asymmetry of the differential cross section (DCS). Charge symmetry transformation (the interchange of u and d quarks) swaps around proton and neutron in the initial state while keeping the final state invariant. Thus, in a charge symmetric world, the DCS of this reaction would stay invariant under interchange of initial nucleons. In the real world, there is an observable asymmetry in DCS [OKH$^+$03]. This asymmetry carries information about the quark mass difference.

The reaction $pn \to d\pi^0$ has several advantages for studying strong CSB effects. First, there are no long-range Coulomb interaction both in the initial and final states. The only electromagnetic effects contributing are the short-range effects from hard photon exchanges. Since the asymmetry in $pn \to d\pi^0$ is purely CSB effect, the charge-symmetric pion mass

difference doesn't contribute here. Using chiral EFT one can relate various mechanisms responsible for CSB in this reaction with other CSB processes, most notably with the neutron-proton mass difference.

The neutron-proton mass difference is due to strong and electromagnetic interactions [GL82], i.e. $\delta m_N = m_n - m_p = \delta m_N^{\rm str} + \delta m_N^{\rm em}$. As a result of the chiral structure of the QCD Lagrangian, the strength of the CSB pion production operator in $pn \to d\pi^0$ is proportional to a different combination of $\delta m_N^{\rm str}$ and $\delta m_N^{\rm em}$ [vKNM00, MS98] (for related work on isospin violation in pion-nucleon scattering see [FMS99, FM01c, FM01a, HKM09, HKM10]). Thus, the analysis of CSB effects in $pn \to d\pi^0$ may allow one to determine the values of $\delta m_N^{\rm str}$ and $\delta m_N^{\rm em}$ individually. This was stressed and exploited in Ref. [vKNM00] for the first time. Consistency of these important quantities as determined from the reaction $pn \to d\pi^0$, where they control the strength of the isospin violating πN scattering amplitude, with results obtained in Ref.[GL82] from the neutron-proton mass difference itself via the Cottingham sum rule [Cot63], would provide a highly non-trivial test of our current understanding of QCD. It was therefore quite disturbing to find that, using the values for $\delta m_N^{\rm str}$ and $\delta m_N^{\rm em}$ from Ref. [GL82], the leading order calculation of the forward-backward asymmetry [vKNM00] over-predicted the experimental value by about a factor of 3 — a consistent description would call for an agreement with data within the theoretical uncertainty of 15% for this kind of calculation. It was shown in Ref. [GHN$^+$04] that there is no NLO contribution – thus the theoretical uncertainty of a leading order calculation is expected to be of the order of m_π/m_N. The evaluation of certain higher order corrections performed in Ref. [vKNM00] and in a recent study [BM10] did not change the situation noticeably — the significant overestimation of the data persisted.

In this chapter[2] we show that there is one more CSB rescattering operator that contributes at LO. We evaluate this new LO operator and recalculate the LO contribution considered in Ref. [vKNM00] since the numerical evaluation in that work turned out to be incorrect. The complete LO calculation for $pn \to d\pi^0$ reveals a very good agreement with the experimental data. Moreover, the resulting contribution is found to be proportional to $\delta m_N^{\rm str}$ only. Thus, a quantitative understanding of the CSB part of $pn \to d\pi^0$ promises an alternative method of extraction of this important quantity compared to that used in Ref. [GL82].

This chapter is organized as follows. In the next section we introduce the definition of the forward backward asymmetry in $pn \to d\pi^0$ and consider partial amplitudes which contribute to this observable. In Section 4.2 we consider the chiral effective Lagrangian terms, which are relevant for calculation of CSB amplitude. In Section 4.3 we calculate LO CSB pion production operators and full LO CSB amplitude. Finally, in Section 4.4 we discuss the extraction of strong part of the neutron-proton mass difference from the asymmetry data.

4.1 Forward-backward asymmetry and related partial amplitudes

In this section we consider the definition of the forward-backward asymmetry (A_{fb}) of DCS in $pn \to d\pi^0$. We consider partial amplitudes which are relevant for A_{fb} and show that near-threshold pion production asymmetry A_{fb} can be expressed in terms of three partial amplitudes.

[2]The results of this chapter are published in ref. [FBE$^+$09].

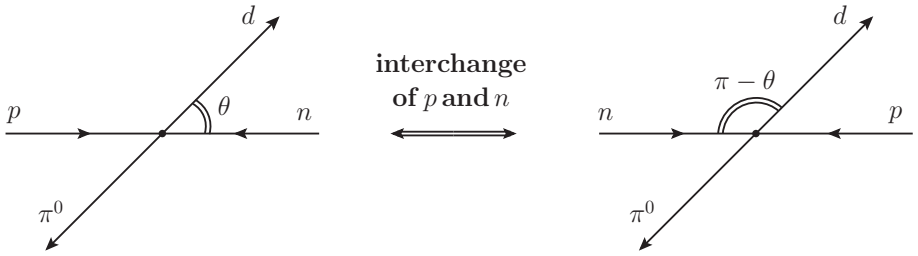

Figure 4.1: The effect of charge symmetry transformation in the $pn \to d\pi^0$ reaction in the center-of-mass system (CMS). Interchanging of protons and neutrons is equivalent to relabeling the angle θ to $\pi - \theta$, where θ is angle in CMS between incident neutron and outgoing deuteron. In a charge symmetric world, the DCS would be symmetric with respect to such transformation. Charge symmetry breaking effects lead to the asymmetry of differential cross section (DCS).

Charge symmetry breaking in the reaction $pn \to d\pi^0$ manifests itself as the asymmetry of DCS in the center-of-mass system (CMS). In the CMS kinematics, the interchange of the proton and neutron is equivalent to the interchange of the angle θ to $\pi - \theta$, where θ is the angle between incident neutron and outgoing deuteron (Fig. 4.1). If charge symmetry were exact, there would be no difference between protons and neutrons, and, thus, the DCS would be symmetric with respect to the interchange $\theta \to \pi - \theta$. However, in nature the charge symmetry is broken and the interchange of p and n leads to an observable difference in the DCS of the $pn \to d\pi^0$ reaction:

$$\frac{d\sigma}{d\Omega}(\theta) \neq \frac{d\sigma}{d\Omega}(\pi - \theta). \tag{4.1}$$

It is convenient to quantify the amount of CSB by considering the integrated forward-backward asymmetry:

$$A_{fb} \equiv \frac{\int_0^{\pi/2} [\frac{d\sigma}{d\Omega}(\theta) - \frac{d\sigma}{d\Omega}(\pi - \theta)] \sin\theta d\theta}{\int_0^{\pi/2} [\frac{d\sigma}{d\Omega}(\theta) + \frac{d\sigma}{d\Omega}(\pi - \theta)] \sin\theta d\theta}. \tag{4.2}$$

This quantity was measured at TRIUMF [OKH$^+$03] and found to be $A_{fb} = (17.2 \pm 8(\text{stat.}) \pm 5.5(\text{sys.})) \times 10^{-4}$. The experiment was performed at the energy very close to the pion production threshold. (The threshold corresponds to the neutron lab. energy of 275.06 MeV, while the experiment was done at 279.5 MeV)

Forward-backward asymmetry stems from a specific angular dependence of DCS. Due to the low energies involved in the process, it is convenient to expand the DCS in terms of Legendre polynomials:

$$\frac{d\sigma}{d\Omega}(\theta) = \sum_{i=0}^{\infty} A_i P_i(\cos\theta) = A_0 + A_1 \cos\theta + A_2 \frac{1}{2}(3\cos^2\theta - 1) + \cdots, \tag{4.3}$$

where A_i are the expansion coefficients, $P_i(\cos\theta)$ are the Legendre polynomials, and the dots stand for higher order terms which can be ignored near threshold. Using the expansion Eq. (4.3) we can rewrite the forward-backward asymmetry Eq. (4.2) as

$$A_{fb} = \frac{A_1}{2A_0}. \tag{4.4}$$

According to Eq.(4.4) only the first two coefficients of the expansion (4.3) are required to describe the forward-backward asymmetry near threshold.

Before considering the partial amplitudes, which contribute to the coefficients A_0 and A_1, we first determine which partial waves are allowed according to selection rules. Due to near-threshold kinematics, only s- and p-waves for outgoing pions contribute. Selection rules take into account conservation of parity, total angular momenta, and the Pauli principle for nucleons. Since isospin symmetry is not exact, the total isospin is not necessary conserved. The total isospin of the final state is always 1 because pion has isospin 1 and deuteron has zero isospin, but the total isospin of initial two nucleons can be either 1 or 0. Both possibilities should be considered.

For conserved total isospin (*i.e.* the isospin of initial nucleons is 1), there are three contributing partial amplitudes:

$$\begin{aligned} M_1 &= M(^3P_1 \to {}^3S_1 s), \\ M_2 &= M(^1S_0 \to {}^3S_1 p), \\ M_3 &= M(^1D_2 \to {}^3S_1 p), \end{aligned} \tag{4.5}$$

where the quantum numbers of the initial and final NN pairs are given in the spectroscopic notation ($^{2S+1}L_J$), while the partial wave of the outgoing pion is denoted by the lowercase letters s and p. The variables M_i denote the scalar quantities which correspond to partial wave projection of the full pion production amplitude[3].

If the total isospin is not conserved (*i.e.* the isospin of initial nucleons is 0) there are four additional partial amplitudes:

$$\begin{aligned} M_4 &= M(^1P_1 \to {}^3S_1 s), \\ M_5 &= M(^3S_1 \to {}^3S_1 p), \\ M_6 &= M(^3D_1 \to {}^3S_1 p), \\ M_7 &= M(^3D_2 \to {}^3S_1 p). \end{aligned} \tag{4.6}$$

Note that the p-wave IV amplitudes M_5–M_7 can be neglected in the LO calculation, because their contribution to A_{fb} turned out to be of a higher order. In addition, in ref. [vKNM00] it was shown that the p-wave CSB amplitudes interfere destructively with each other, and are thus even more suppressed.

We are now in the position to find out which of the allowed partial amplitudes contribute to the coefficients A_0 and A_1. For this we have to consider the general structure of the DCS. To get the DCS one has to compute the absolute value squared of the sum of all partial

[3] Full amplitudes are calculated using the hybrid approach (see. Sec. 1.6). Namely, one calculates pion production operator, takes the partial wave projection of it, and convolutes resulting operator with corresponding NN interactions. Partial wave projections are made following the procedure described in [Len07].

amplitudes, and then take a proper average of the possible initial states and sum over possible final states. The result of this procedure is presented below. Since we are looking for A_0 and A_1, we have to collect the coefficients in front of zeroth and first Legendre polynomial in the expression for DCS.

The value of the coefficient A_0 in terms of the partial amplitudes has the following form:

$$A_0 = \frac{1}{256\pi^2}\frac{|\vec{k}_\pi|}{|\vec{p}_{\rm in}|(m_\pi+m_{\rm deut})^2}\left[4|M_1|^2+2|M_2|^2+\frac{4}{9}|M_3|^2\right], \tag{4.7}$$

where $\vec{p}_{\rm in}$ is the three-momentum of the initial nucleon, $\vec{k}_\pi$ is the three-momentum of the pion, and $m_{\rm deut}$ is the deuteron mass. The contributions of isospin violating amplitudes M_4–M_7 were neglected in Eq. (4.7), since they are much smaller than contributions of isospin conserving amplitudes. The contributions of isospin conserving p-wave amplitudes M_2 and M_3 are also very small near threshold, since they are proportional to the momentum of the outgoing pion, which vanishes at threshold. Thus, for near-threshold pion production, the coefficient A_0 is dominated by the s-wave partial amplitude M_1, with small corrections from p-wave amplitudes M_2 and M_3.

The numerical value of A_0 (at the energy we are interested) can be found using the high accuracy chiral EFT calculation and precise experimental data at threshold. It is customary to write down the total cross section (TCS) $\sigma = 4\pi A_0$ near threshold in the following form:

$$\sigma = \alpha\eta + \beta\eta^3, \tag{4.8}$$

where $\eta = |\vec{k}_\pi|/m_\pi$ is the outgoing pion momentum in units of the pion mass. For the experiment [OKH$^+$03], this value was $\eta = 0.17$. Using Eq. (4.7) one can write:

$$\alpha = \frac{1}{16\pi}\frac{m_\pi}{|\vec{p}_{\rm in}|(m_\pi+m_{\rm deut})^2}\,|M_1|^2, \tag{4.9}$$

$$\beta = \frac{1}{16\pi}\frac{m_\pi}{|\vec{p}_{\rm in}|(m_\pi+m_{\rm deut})^2}\left[\frac{1}{2}\left|\frac{M_2}{\eta}\right|^2+\frac{1}{9}\left|\frac{M_3}{\eta}\right|^2\right]. \tag{4.10}$$

The production operator that gives rise to the amplitude M_1 was calculated in previous two chapters. This production operator should be convoluted with the ISI and FSI, and the relevant contact term at N^{2}LO should be fitted to reproduce TCS data. Alternatively, one can use the experimental value of α which can be extracted with very high accuracy from the lifetime of the pionic deuterium atom [SAA$^+$10, SAA$^+$11]. The result of the extraction is $\sigma(nn\to d\pi^-) = 252^{+5}_{-11}\cdot\eta$ [μb]. To convert it to the cross section of the $pn\to d\pi^0$ reaction we use isospin symmetry: $\sigma(pn\to d\pi^0) = \sigma(nn\to d\pi^-)/2$. Isospin breaking effects in this relation are expected to be of natural size and thus can be neglected in our study. Since we are interested in the cross section slightly above threshold, we also include the contribution of p-waves to A_0. The corresponding coefficient β is defined by partial amplitudes M_2 and M_3. These amplitudes were calculated in Ref. [BEH$^+$09] up-to-and-including N^{2}LO MCS terms. In this reference it was also shown that the contribution of the amplitude M_2 is quite uncertain and much smaller than the one of M_3. Thus, M_2 can be neglected. The total value for the coefficient A_0 near threshold is

$$A_0 = 10.0^{+0.2}_{-0.4}\cdot\eta + (47.8\pm5.7)\cdot\eta^3\,[\mu\text{b}]. \tag{4.11}$$

Let's now consider the coefficient A_1. The leading contribution to the coefficient A_1 is given by the interference of the leading CSB s-wave amplitude M_4 and isospin symmetric p-wave amplitudes M_2 and M_3:

$$A_1 = \frac{1}{256\pi^2}\frac{|\vec{k}_\pi|}{|\vec{p}_{\rm in}|(m_\pi + m_{\rm deut})^2}\left[4{\rm Re}(M_2 M_4^*) + \frac{8}{3}{\rm Re}(M_3 M_4^*)\right]. \tag{4.12}$$

It can be easily shown using power counting discussed in Section 4.2, that the interference of the CSB p-wave amplitudes M_5–M_7 with the charge symmetric s-wave amplitude M_1 is suppressed by two orders in the MCS. Furthermore, the contribution of the amplitude M_2 can be neglected for the same reasons as discussed for coefficient A_0.

We conclude that the forward-backward asymmetry near threshold Eq. (4.4) depends only on coefficients A_0 and A_1. The coefficient A_0 is dominated by isospin conserving amplitudes and is known with high accuracy from experiment and recent chiral EFT calculations. The coefficient A_1 is dominated by the interference of known isospin-conserving amplitude M_3 with isospin violating amplitude M_4. We calculate M_4 in the next sections.

4.2 Isospin violating effective Lagrangian and power counting

In order to calculate isospin violating pion production amplitudes we have to take into account IV terms in the effective Lagrangian and define a counting procedure for those terms. In this section we discuss both topics. We consider how LECs of the IV Lagrangian are related to the hadronic observables such as the pion mass and the neutron-proton mass differences. In addition, we consider a field redefinition procedure, which significantly simplifies the calculation of effects related to the neutron-proton mass difference.

If one neglects quark masses and electromagnetic effects, the Lagrangian of QCD is chirally symmetric. One uses this symmetry to construct the main part of the effective Lagrangian. However, chiral symmetry is not exact in nature. In addition, in order to perform realistic calculations one has to include effects of the nonzero quark masses and electromagnetic effects, which explicitly break charge symmetry. To include these effects, one adds the appropriate chiral symmetry breaking (χSB) terms to the initial chiral-symmetric Lagrangian. The inclusion of χSB terms allows one to describe a broad range of effects from the values of pion masses to tiny CSB effects, such as the neutron-proton mass difference. We consider χSB terms (strong and electromagnetic) and their implications in order to identify the terms responsible for charge symmetry breaking.

Let's consider building blocks which should be used to construct IV Lagrangian. We first discuss how the effects of quark masses are included in the chiral Lagrangian. Strong χSB emerges from the quark mass matrix

$$s = \begin{pmatrix} m_u & 0 \\ 0 & m_d \end{pmatrix} = \frac{m_u + m_d}{2}\,1 + \frac{m_u - m_d}{2}\,\tau_3, \tag{4.13}$$

where 1 is a unity matrix and τ_3 is the third Pauli matrix in the isospin space. The corresponding building block for the effective Lagrangian is

$$\chi_\pm = 2B_0(u^\dagger s u^\dagger \pm u s^\dagger u), \tag{4.14}$$

where the matrix u is defined by Eq. (1.2) and B_0 is a low-energy constant that describes the strength of the light quark condensate $\langle 0|\bar{q}q|0\rangle = -f_\pi^2 B_0(1+\mathcal{O}(m_q))$. From the expression (4.13) one can see that all Lagrangian terms stemming from the quark masses are proportional either to the sum or to the difference of quark masses. Those which are proportional to the sum, are acting identically on particles of any isospin, and thus are isospin conserving. On the other hand, terms proportional to the difference of the quark masses give isospin violating contributions.

To include the short-range electromagnetic interaction of quarks (*i.e.* exchange of virtual photons) in EFT, one includes additional terms in the effective Lagrangian which are proportional to the quark charge matrix:

$$Q_q = \begin{pmatrix} q_u & 0 \\ 0 & q_d \end{pmatrix} = \begin{pmatrix} \frac{2}{3}e & 0 \\ 0 & -\frac{1}{3}e \end{pmatrix}, \tag{4.15}$$

where e is the elementary charge. However, for our study it is more convenient to use the nucleon charge matrix,

$$Q = \begin{pmatrix} q_u+q_u+q_d & 0 \\ 0 & q_u+q_d+q_d \end{pmatrix} = \frac{3}{2}(q_u+q_d)1 + \frac{1}{2}(q_u-q_d)\tau_3, \tag{4.16}$$

which differs from Q_q by a simple transformation $Q = (q_u+q_d)1 + Q_q$. At the order we are working, this transformation does not affect any observables [MS98]. The decomposition (4.16) is similar to the one for the quark mass matrix (4.13). Namely, the first term in the r.h.s. of Eq. (4.16) is invariant under interchange of quarks, while the second term is not and thus can lead to CSB effects. The corresponding building block for the effective Lagrangian reads

$$Q_\pm = \frac{1}{2}(u^\dagger Q u \pm u Q u^\dagger). \tag{4.17}$$

We are now in the position to discuss the IV Lagrangian for mesonic sector. Using the building blocks discussed above, the LO mesonic Lagrangian which accounts for short-range electromagnetic effects as well as for the nonvanishing quark masses can be written as [EGPdR89, MMS97]

$$L^{(2)}_{\gamma^*\pi\pi} = \frac{f_\pi^2}{4}\langle u_\mu u^\mu + \chi_+\rangle + C\langle Q_+^2 - Q_-^2\rangle, \tag{4.18}$$

where C is a low-energy constant, and the angle brackets denote trace in the isospin space. Rewriting the Lagrangian (4.18) in terms of the pion fields, one can derive the LO contribution to the pion mass as well as the leading correction, which is responsible for the difference of the neutral and charged pion masses. The resulting expressions for the pion masses are:

$$\begin{aligned} m^2_{\pi^0} &= B_0(m_u+m_d), \\ m^2_{\pi^\pm} &= B_0(m_u+m_d) + \frac{2}{f_\pi^2}(q_u-q_d)^2 C, \end{aligned} \tag{4.19}$$

where $(q_u - q_d)^2$ can be rewritten[4] as e^2. The main contribution to the pion masses is due to the sum of quark masses, while the difference of pion masses is of electromagnetic origin and proportional to the difference of quark charges squared. One can explicitly see that both effects are invariant under interchange of quarks and are thus charge symmetric. It is notable that the pion mass difference, while being isospin violating effect, is charge symmetric. Thus, at leading order CSB effects do not contribute to the pion mass difference.

Let's consider CSB effects in the pion-nucleon sector. Below we summarize the heavy-baryon Lagrangian terms (up to m_π^2/m_N^2) which are relevant for our study of charge symmetry breaking effects. The relevant effective Lagrangian structures are [MS98, Ste99]

$$\begin{aligned} L_{\gamma^*\pi N} &= \bar{N}\big[iv\cdot D + c_1\langle\chi_+\rangle + c_5(\chi_+ - \langle\chi_+\rangle/2) \\ &\quad + f_\pi^2\left(f_1\langle Q_+^2 - Q_-^2\rangle + f_2\langle Q_+\rangle Q_+ + f_3\langle Q_+\rangle^2\right) \\ &\quad + d_{17}\langle S\cdot u\chi_+\rangle + id_{18}[S\cdot D,\,\chi_-] + id_{19}[S\cdot D, \langle\chi_-\rangle]\big]N, \end{aligned} \tag{4.20}$$

where c_i and d_i are LECs with the dimensions MeV^{-1} and MeV^{-2} respectively. The constant f_π^2 is introduced in order to make electromagnetic LECs f_i of the same dimension as corresponding strong LECs c_i. After rewriting the Lagrangian (4.20) in terms of the pion and nucleon fields, one can collect the terms responsible for the nucleon masses. Including corrections of order of m_π^2/m_N^2, one gets the following expression for the nucleon mass term:

$$\begin{aligned} m_N &= m - 4B_0(m_u+m_d)c_1 - 2B_0(m_u-m_d)c_5\tau_3 \\ &\quad - f_\pi^2 f_1\left(\frac{1}{2}(q_u-q_d)^2 + \frac{9}{2}(q_u+q_d)^2\right) \\ &\quad - f_\pi^2\frac{f_2}{2}\left(9(q_u+q_d)^2 + 3(q_u+q_d)(q_u-q_d)\tau_3\right) - 9f_\pi^2 f_3(q_u+q_d)^2 \\ &= m - 4m_\pi^2 c_1 - 2B_0(m_u-m_d)c_5\tau_3 - e^2 f_\pi^2\left(f_1 + \frac{f_2}{2}(1+\tau_3) + f_3\right), \end{aligned} \tag{4.21}$$

where we used explicit quark charges in the last equality. All terms in Eq. (4.21), which are not proportional to τ_3, just shift the masses of both nucleons and are not directly observable. Two terms which are proportional to τ_3 are responsible for the neutron-proton mass difference. One of them is proportional to $(q_u+q_d)(q_u-q_d)$ and another is proportional to the light quark mass difference $(m_u - m_d)$. It is notable that both terms responsible for the nucleon mass difference are charge symmetry breaking. For simplicity, one can introduce the following notation for the strong and electromagnetic parts of neutron-proton mass difference:

$$\begin{aligned} \delta m_N^{\text{str.}} &\equiv 4B_0(m_u-m_d)c_5, \\ \delta m_N^{\text{e.m.}} &\equiv 3(q_u+q_d)(q_u-q_d)f_\pi^2 f_2 = e^2 f_\pi^2 f_2. \end{aligned} \tag{4.22}$$

In this notation the total neutron-proton mass difference is just the sum of two combinations:

$$m_n - m_p = \delta m_N = \delta m_N^{\text{str.}} + \delta m_N^{\text{e.m.}} \tag{4.23}$$

[4] One can use the values of the quark charges (Eq. (4.15)) to rewrite the sum and the difference of the quark charges in terms of elementary charge *i.e.* $3(q_u+q_d) = e$ and $q_u - q_d = e$. In this form one, however, cannot distinguish CSB terms from charge symmetric ones. To track the terms which are not invariant under interchange of quarks, we keep the notation with explicit quark charges.

The total neutron-proton mass difference δm_N is measured with high precision $\delta m_N = 1.2933322 \pm 0.0000004$ MeV [B$^+$12].

One can rewrite the relevant CSB pion-nucleon Lagrangian (4.20) in terms of the combinations (4.22):

$$L^{\pi N}_{\text{Leading CSB}} = \frac{\delta m_N}{2}\bar{N}\tau_3 N - \frac{\delta m_N^{\text{str.}}}{4f_\pi^2}\bar{N}\boldsymbol{\tau}\cdot\boldsymbol{\pi}\pi_3 N - \frac{\delta m_N^{\text{e.m.}}}{4f_\pi^2}\bar{N}\left(\tau_3\boldsymbol{\pi}^2 - \boldsymbol{\tau}\cdot\boldsymbol{\pi}\pi_3\right)N \qquad (4.24)$$

The first term in the r.h.s. of Eq. (4.24) corresponds to the explicit neutron-proton mass difference, while the remaining two terms correspond to the CSB $\pi N \to \pi N$ vertex. It is notable that strong and electromagnetic contributions to the neutron-proton mass difference can contribute to reactions in different linear combinations. One can thus use CSB in pion-nucleon processes to find these LECs separately.

Inclusion of isospin violating terms in the effective Lagrangian introduces new expansion parameters: the quark mass difference and elementary charge. To make a systematic calculation possible, one has to define a counting procedure for those parameters. Since we are not considering sums of CSB and CS effects (only interference) in our study, we only need to compare CSB amplitudes among themselves. For this reason, we count CSB amplitudes separately from CS ones. The most prominent CSB observables are strong and electromagnetic contributions to the neutron-proton mass difference Eq. (4.22). These two quantities are known from various sources to be of the same order of magnitude [GL82, WLCM12, BOS07, BZD$^+$10]. For this reason we assign both of them to the leading order CSB vertex (LO CSB).

We now want to discuss field redefinitions, which make the calculation of CSB effects much easier. The LO CSB πN Lagrangian (4.24) contains explicitly the neutron-proton mass difference term $\delta m_N \bar{N}\tau_3 N/2$, which produces an important contribution to CSB amplitudes. However, it is not trivial to calculate operators containing such a term, because such operators are typically reducible and Feynman diagram technique cannot be directly applied to calculate them. The calculation of CSB amplitudes can be significantly simplified by performing a field redefinition, which removes this term from the effective Lagrangian and allows one to use the Feynman diagram technique[5]. In order to remove this term one introduces the following redefinitions of the pion and nucleon fields [FvKRT04, EKM08]:

$$\begin{aligned} N &\to \exp\left(i\delta m_N \frac{\tau_3}{2}t\right)N = \cos\left(\frac{1}{2}\delta m_N t\right)N + i\tau_3 \sin\left(\frac{1}{2}\delta m_N t\right)N, \\ \pi_i &\to \cos(\delta m_N t)\pi_i + \sin(\delta m_N t)\epsilon_{ij3}\pi_j + (1-\cos(\delta m_N t))\delta_{i3}\pi_3. \end{aligned} \qquad (4.25)$$

These transformations do not affect observables and most terms in the effective Lagrangian are invariant under transformations (4.25). Only those which contain a time derivative are not invariant and will generate new interactions. The time derivatives contribute to the LO Lagrangian via the building blocks u_μ and Γ_μ. Field redefinition transforms these building blocks in the following way:

$$\begin{aligned} u_\mu &\to u_\mu - \frac{\delta m_N}{f_\pi}v_\mu[\boldsymbol{\tau}\times\boldsymbol{\pi}]_3 + \mathcal{O}(\boldsymbol{\pi}^3), \\ \Gamma_\mu &\to \Gamma_\mu + i\frac{\delta m_N}{2}v_\mu\tau_3 - i\frac{\delta m_N}{4f_\pi^2}v_\mu\left[\boldsymbol{\pi}^2\tau_3 - \boldsymbol{\pi}\cdot\boldsymbol{\tau}\pi_3\right] + \mathcal{O}(\boldsymbol{\pi}^4). \end{aligned} \qquad (4.26)$$

[5] An alternative method to handle explicit neutron-proton mass difference using unitary transformations was discussed in Refs. [EMP05, EM05].

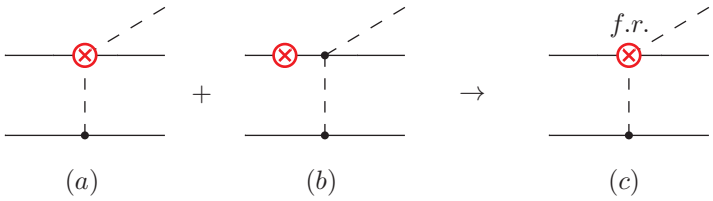

Figure 4.2: LO CSB pion production operators, which contribute to the amplitude M_4 in the reaction $pn \to d\pi^0$, in usual formalism (diagrams a and b) and in the field-redefined theory (diagram c). Diagram (a) corresponds to isospin violation in πN scattering vertex explicitly whereas diagram (b) indicates an isospin-violating contribution due to the neutron-proton mass difference in conjunction with the time-dependent Weinberg–Tomozawa operator. Diagram (c) is the only isospin-violating contribution (at the considered order) in the theory after field redefinition, which removes explicit neutron-proton mass difference. Expressions for vertices can be found in the Appendix B.

The second term in the r.h.s. of Eq. (4.26) cancels the neutron-proton mass difference term exactly, when substituted to the LO HB Lagrangian Eq. (1.20), while the third term generates an additional contribution to CSB $\pi N \to \pi N$ vertex. The LO CSB πN Lagrangian after the field redefinition take the form:

$$L^{\pi N\text{f.r.}}_{\text{Leading CSB}} = -\frac{\delta m_N^{\text{str.}}}{4f_\pi^2}\bar{N}\left[\boldsymbol{\tau}\cdot\boldsymbol{\pi}\pi_3 + ((\boldsymbol{\tau}\times\boldsymbol{\pi})\times\boldsymbol{\pi})_3\right]N. \tag{4.27}$$

It is notable that the LO CSB $\pi N \to \pi N$ vertex is proportional to $\delta m_N^{\text{str.}}$ only, while there is no contribution proportional to $\delta m_N^{\text{e.m.}}$. Since there are no more explicit neutron-proton mass difference terms in the Lagrangian after field redefinition, one can use the Feynman diagram technique to derive all amplitudes.

We are now in position to consider the CSB amplitude M_4 within chiral EFT framework.

4.3 Leading CSB s-wave amplitude

In this section we derive the LO CSB amplitude M_4. We consider relevant CSB pion production operators and convolute them with NN interactions in the ISI and FSI using hybrid approach.

There are two operators contributing to M_4 at leading order Fig. 4.2ab. In order to understand the interplay of diagram (a) and diagram (b) of Fig. 4.2 it is sufficient to focus on the πN rescattering vertex on nucleon 1 (the top one on the Fig. 4.2). From the pion production vertex on nucleon 2 we only keep the isospin structure, for the rest is identical for both diagrams. The relevant part of diagram (a) then reads

$$\hat{I}_{(\text{a})} = -i\frac{\delta m_N^{\text{str}}}{4f_\pi^2}\left(\boldsymbol{\tau}^{(1)}\cdot\boldsymbol{\tau}^{(2)} + \tau_3^{(1)}\tau_3^{(2)}\right) + i\frac{\delta m_N^{\text{em}}}{4f_\pi^2}\left(\boldsymbol{\tau}^{(1)}\cdot\boldsymbol{\tau}^{(2)} - \tau_3^{(1)}\tau_3^{(2)}\right). \tag{4.28}$$

We work at leading order in IV. Since we study an IV transition operator, we may treat the

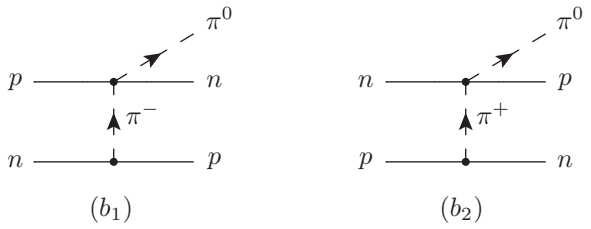

Figure 4.3: Leading-order contributions to isospin violation due to the time-dependent Weinberg-Tomozawa operator in the particle basis.

external nucleons as identical particles[6]. The evaluation of the operator Eq. (4.28) for the isospin violating transition from the isospin zero initial pn state to the isospin zero deuteron state yields

$$\langle I_f = 0|\hat{I}_{(\mathrm{a})}|I_i = 0\rangle = \frac{i}{4f_\pi^2}\, 4\left(\delta m_N^{\mathrm{str}} - \delta m_N^{\mathrm{em}}/2\right) \ . \tag{4.29}$$

This piece represents the complete rescattering contribution included in Refs. [vKNM00, BM10]. Let us now look more closely at diagram (b) of Fig. 4.2. The relevant part of the amplitude for this diagram can be most easily calculated in the particle basis as shown in Fig. 4.3. One gets

$$\langle I_f = 0|\hat{I}_{(\mathrm{b})}|I_i = 0\rangle = -\frac{1}{2}(I_{\mathrm{b}_1} + I_{\mathrm{b}_2}), \tag{4.30}$$

where I_{b_1} and I_{b_2} are the isospin coefficients corresponding to the diagrams (b_1) and (b_2) of Fig. 4.3 and the factor $(-1/2)$ stems from the Clebsch-Gordan coefficients. Note that, since the WT operator involves a time derivative, the corresponding Feynman rule reads

$$V_{WT}^{ab} = \frac{1}{4f_\pi^2}\varepsilon_{abc}\tau_c(q_0 + m_\pi) \ , \tag{4.31}$$

with a, b and c Cartesian pion indices and q_μ the four-momentum of the intermediate pion. Due to the explicit appearance of q_0 in V_{WT}, the final expression for diagram (b) of Fig. 4.2 depends on the neutron–proton mass difference. Indeed, the evaluation of this vertex for the diagrams (b_1) and (b_2) of Fig. 4.3 yields

$$V_{WT} \ = \frac{-i}{4f_\pi^2}\begin{cases} \sqrt{2}\left(\frac{3m_\pi}{2} + \delta m_N\right) & \text{for diagram } (b_1), \\ -\sqrt{2}\left(\frac{3m_\pi}{2} - \delta m_N\right) & \text{for diagram } (b_2). \end{cases} \tag{4.32}$$

Thus, in the isospin violating contribution to Eq. (4.30) the terms $\propto m_\pi$ cancel while those $\propto \delta m_N$ survive. The non-vanishing isospin matrix element for the diagram (b) of Fig. 4.2 amounts to

$$\langle I_f = 0|\hat{I}_{(\mathrm{b})}|I_i = 0\rangle = \frac{i}{4f_\pi^2}\, 2\delta m_N \ . \tag{4.33}$$

[6] This is not the case for the diagram (b), where the mass difference of the external particles plays the essential role.

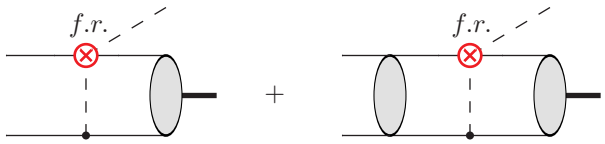

Figure 4.4: Diagrams which contribute to the amplitude M_4 at LO in the hybrid approach. The final state is always a deuteron. Initial nucleons can be either free (left diagram) or nonperturbatively interacting with each other (right diagram).

Adding up the contributions of diagrams (a) and (b) we find that the resulting contribution at LO depends on the quark mass contribution to the nucleon mass difference only — the electromagnetic piece disappears completely:

$$\langle I_f = 0|\hat{I}_{(\mathrm{a})} + \hat{I}_{(\mathrm{b})}|I_i = 0\rangle = \frac{i}{4f_\pi^2}\, 6\,\delta m_N^{\mathrm{str}}. \tag{4.34}$$

In comparison with the expression used previously (cf. Eq. (4.29)), the rescattering operator gets enhanced by about 30%, when standard values $\delta m_N^{\mathrm{str}} = 2$ MeV and $\delta m_N^{\mathrm{em}} = -0.76$ MeV [GL82] are used.

A more elegant way to calculate both LO CSB operators is to perform a field redefinition Eq. (4.25) described in previous section. This redefinition removes the two-point vertex proportional to the neutron-proton mass difference. However, an additional CSB $\pi N \to \pi N$ vertex appears after redefinition (c.f. the third term in Eq. (4.26)). This vertex can be added to the original CSB $\pi N \to \pi N$ vertex, and contributes via rescattering CSB diagram. Thus, in the theory with redefined fields there is only one operator (shown as diagram (c) in Fig. 4.2) due to the Lagrangian density (4.27). After evaluation of the isospin matrix elements in 4.27 one again arrives at 4.34. Thus, the total result in the redefined theory is the same as in original formalism.

For the sake of completeness, we present here the tree-level invariant amplitude M_4^{tree} corresponding to the LO calculation

$$M_4^{\mathrm{tree}} = -i\frac{12m_N^2 g_A}{f_\pi^3}\,\delta m_N^{\mathrm{str}} \int \frac{d\Omega_{p'}}{4\pi}\frac{(\vec{p}\,' - \vec{p})\cdot\hat{p}}{(\vec{p}\,' - \vec{p})^2 + m_\pi^2}, \tag{4.35}$$

where $\vec{p}$ and $\vec{p}\,'$ denote initial and final relative momenta of the two nucleons, respectively, and $\hat{p} = \vec{p}/p$. In the calculation we use $f_\pi = 92.4$ MeV and $g_A = 1.32$ (utilizing the Goldberger-Treiman relation). To get the full amplitude M_4 which enters the observables, M_4^{tree} given above needs to be convoluted with proper NN wave functions in the initial and final states, cf. Appendix A of Ref. [BEH$^+$09] for a detailed description. Ideally, one should use wave functions derived in the same framework, namely ChPT. However, up to now these are only available for energies below the pion production threshold [BvK02, Epe06, EHM09]. We therefore adopt the hybrid approach (see Sec. 1.6) *i.e.* we use transition operators derived within effective field theory and convolute them with realistic NN wave functions [HHJ93].

Since we consider the $pn \to d\pi^0$ reaction, the FSI is always a deuteron. Nucleons in the initial state have two possibilities. They can either be free, or interact with each other. Thus,

the full LO CSB amplitude M_4 in the hybrid approach is defined by two diagrams shown in Fig. 4.4.

We are now in the position to discuss the results for the forward-backward asymmetry within the complete LO calculation. Using the values for the parameters specified above and utilizing the NN wave functions from Ref. [HHJ93], the result can be presented in the form

$$A_{\rm fb}^{\rm LO} = (11.5 \pm 3.5) \times 10^{-4} \, \frac{\delta m_N^{\rm str}}{\rm MeV} \ . \tag{4.36}$$

The LO calculation of the coefficient has a theoretical uncertainty of 15% which is doubled to provide a more conservative estimate. This uncertainty is included in the expression above. We now use the experimental result for $A_{\rm fb}$ [OKH$^+$03] to extract $\delta m_N^{\rm str}$ which yields

$$\delta m_N^{\rm str} = (1.5 \pm 0.8 \ (\text{exp.}) \pm 0.5 \ (\text{th.})) \ \text{MeV} \ , \tag{4.37}$$

where we added the experimental errors in quadrature. This is the final result of our analysis. In the present stage, the uncertainty in the determination of $\delta m_N^{\rm str}$ is dominated by the experimental uncertainty for $A_{\rm fb}$.

In this context let us point out the following: Apart from the additional IV contribution discussed in detail above, there are other reasons why our result deviates from those of Refs. [vKNM00, BM10] already at leading order. The numerical evaluation of the diagram (a) of Fig. 4.2 revealed that the value we obtain is significantly smaller than the one found in Ref. [vKNM00]. It turned out that the result of that work is too large by a factor of 4 due to an error[7]. The discrepancy of our result to that of Ref. [BM10] is an accumulation of various effects. First of all in Ref. [BM10] the isospin conserving s– and p–wave amplitudes are calculated within ChPT up to NLO. Thus, they come with individual uncertainties of 30% and 15%, respectively — the uncertainty for the s–wave appears doubled for this amplitude, since it enters squared in A_0, while the p–wave amplitudes mainly contribute linearly to A_1 — cf. Eqs. (4.4) and (4.12)). In contrast to this we take the s–wave amplitude directly from data, with a negligible uncertainty and for the p–wave amplitudes the results of Ref. [BEH$^+$09], which were calculated to NNLO and are additionally constrained by data. Thus, combining these uncertainties with that for the CSB amplitude in quadrature, a total uncertainty of 50% arises for the result of Ref. [BM10]. In addition, the p–wave amplitude with the $^1S_0$ initial state employed in Ref. [BM10], which amounts to an enhancement of 50% in the isospin-conserving p-wave amplitude in this calculation, is in conflict with the data for $pp \to d\pi^+$, which calls for a negligible contribution of this partial wave [BEH$^+$09]. These effects together — the larger uncertainty of the calculation of Ref. [BM10] as well as the wrong p–wave amplitude — explain the discrepancy between our result and that of Ref. [BM10].

In Ref. [vKNM00] also some higher order contributions were calculated as well, see also [MOS06]. While individually sizeable, the sum of the considered corrections was found to contribute very little to the asymmetry. We re-evaluated these additional pieces and confirmed these findings qualitatively though our results deviate from the ones of Refs. [vKNM00, MOS06] quantitatively. In addition, in Ref. [BM10] some CSB p-wave amplitudes were evaluated. Through an interference with the isospin conserving s-wave, they also contribute to the

[7]Due to inconsistent definitions of f_π in the analytical and numerical calculations the LO contribution evaluated in [vKNM00] is a factor 4 too large. We thank J. Niskanen for his help in solving this issue.

forward–backward asymmetry discussed in this work, however, only at NNLO. It is reassuring that quantitatively these contributions are in line with the power counting estimates given above and thus support our uncertainty estimate.

4.4 Discussion and conclusion

In this chapter we calculated the CSB forward–backward asymmetry for the reaction $pn \to d\pi^0$ to next-to-leading order in the chiral expansion. We showed that the resulting production operator is driven by the contribution to the neutron-proton mass difference which is coming solely from the quark mass difference $\propto \delta m_N^{\rm str}$. Using the TRIUMF measurement of the forward-backward asymmetry [OKH$^+$03] we extracted the value

$$\delta m_N^{\rm str} = 1.5 \pm 0.9 \text{ MeV} \ , \tag{4.38}$$

where the theoretical and experimental uncertainties are added in quadrature. This result is consistent with extractions of the same quantity using Cottingham sum rule [Cot63] in references [GL82, WLCM12] and with lattice simulations [BOS07, BZD$^+$10, dDDF$^+$12]. See table 4.1 for an overview.

Table 4.1: Results of extraction of the strong neutron-proton mass difference using different methods.

$\delta m_N^{\rm str}$ [MeV]	Method	Ref.
1.5 ± 0.9	chiral EFT	this work
2.0 ± 0.3	Cottingham sum rule	[GL82]
2.59(03)(47)	Cottingham sum rule	[WLCM12]
$2.26 \pm 0.57 \pm 0.42 \pm 0.10$	Lattice simulation	[BOS07]
2.51(14)	Lattice simulation	[BZD$^+$10]

We emphasize that the agreement of the various independent extractions provides a highly non-trivial and important test of our understanding of the chiral symmetry and the isospin breaking pattern of QCD.

At present the uncertainty in Eq. (4.38) is dominated by the experimental error bars – an improvement on this side would be very important. Still, a more refined N^{2}LO calculation is also called for since only then one can be confident about the estimated theoretical uncertainty.

Thesis Summary

In this thesis we have studied pion production in nucleon-nucleon collisions near threshold within the heavy baryon chiral EFT framework. The reaction $NN \to NN\pi$ is of great interest since it is the first inelastic channel of NN interaction, it appears as a building block for many hadronic processes, and provides a direct way to study charge symmetry breaking in the Standard Model. The main challenge arising in the chiral EFT study of $NN \to NN\pi$ is the large three-momentum which is transferred between two nucleons in order to produce a pion. To properly incorporate large transferred momenta, the momentum counting scheme (MCS) was used. This power counting scheme properly accounts for the additional scale and allows one to classify various contributions to the $NN \to NN\pi$ transition amplitudes according to their importance. Successful application of MCS to describe s- and p-wave pion production observables in the channels where no accidental cancellations occur provides a strong indication for convergence of the MCS chiral counting. This approach allowed us to calculate pion production operators with high accuracy, including both charge symmetric and charge symmetry breaking amplitudes, and extract strong contribution to the neutron-proton mass difference from the data on differential cross section asymmetry in $pn \to d\pi^0$. We summarize the main results of our study below.

In **Chapter 1** we give a brief summary of the methods used to study pion production in this work. We start with fundamentals of chiral EFT and revise the heavy baryon formulation which is used to include nucleons and delta-isobars. The main part of Chapter 1 is devoted to the momentum counting scheme, which allows one to make accurate estimations of pion production operators. We also discuss the inclusion of nonperturbative NN interactions in the initial and final states.

In **Chapter 2** we construct the high-accuracy pion production operators at threshold in the chiral EFT formulation with only pions and nucleons being explicit degrees of freedom. This operator is an important building block for CSB processes. In addition, such a high accuracy calculation is necessary to understand the mechanisms behind various pion production channels. The results of our investigation are:

- We have evaluated all tree-level and loop diagrams with pions and nucleons as the only explicit degrees of freedom up to and including N^{2}LO. We confirm the full cancellation of all loop diagrams at NLO [HK02, LBH$^+$06].

- We found significant cancellations among the loop diagrams at N^{2}LO. In particular, all loop topologies involving $1/m_N$ corrections to the leading vertices cancel completely, as do the loops involving low-energy constants (LECs) c_i.

- The cancellation of pion-nucleon loops at N^{2}LO is not complete yielding a non-vanishing N^{2}LO contribution.

- We have obtained the fully renormalized result. Using dimensional regularization, all UV divergencies in the loops were absorbed into redefinition of low-energy-constants (LECs) in the Lagrangian at N^{2}LO. At this order, there are only two unknown LECs.

- We have shown that the intermediate-range two-pion-exchange effects give the important contribution to the production operator, in accordance with N^{2}LO MCS estimation.

This questions mechanisms used in phenomenological studies [LR93, HMG94, Hor93, Nis96, HO95, HHR$^+$95, HHKS98], where the data description was obtained, but none of these N^{2}LO loop contributions were considered.

- To calculate loop corrections to the production operator we develop an efficient method based on identification of common structures in Feynman diagrams. This method allows one to identify numerous cancellation between diagrams before carrying out the loop integration. In addition, we derive relations between propagators and momentum-dependent vertices in chiral EFT. These relations allow one to easily identify relevant irreducible contributions and help to spot cancellations between various diagrams. These methods and relations depend neither on heavy baryon formulation, nor on the counting scheme, and can be used in the wide range of chiral EFT studies.

In **Chapter 3** we studied the effect of explicit delta-excitation on pion production at threshold. The main motivation to include delta explicitly is the observation that the excitation energy of the delta is of the same order as transferred momenta required to produce a pion in $NN \to NN\pi$. Explicit inclusion of the delta resonance allows one to better identify the relevant pion production mechanisms and improves convergence of chiral expansion. Below we present the results of our findings.

- We have calculated all additional tree-level and loop contributions to the N^{2}LO pion production amplitude appearing in the theory with explicit delta isobars.

- After carrying out the renormalization our result is finite and consistent with the requirement of the decoupling theorem [AC75]. Namely, all contributions from diagrams with explicit delta would vanish if the mass of the delta were taken to infinity. The obtained result does not contain any unknown low-energy constants.

- We found numerous cancellations between various loop diagrams. In addition to the cancellations at NLO reported in [HK02], we discovered significant cancellations at N^{2}LO.

- While all loops cancel at NLO completely, at N^{2}LO there is a finite remainder of the Δ loop contributions which is of the same order of magnitude as its purely pion-nucleon counter part calculated in Chapter 2. This shows that the delta resonance provides an important intermediate-range two-pion-exchange contribution to the pion production operator. This mechanism so far was not considered in the phenomenological models, where the description of data was obtained using mostly short range mechanisms.

The obtained N^{2}LO pion production operators together with the ones from Chapter 2 can be convoluted with $NN \to NN$ and $NN \to N\Delta$ interactions and used to calculate various pion production observables. In addition, the compact analytical form makes it easy to use these results as building blocks for more complicated few-nucleon processes, such as study of charge symmetry breaking in $pn \to d\pi^0$ and $dd \to \alpha\pi^0$.

In **Chapter 4** we studied pion production in the $pn \to d\pi^0$ channel near threshold. This channel is of exceptional interest since one can directly observe manifestations of charge symmetry breaking effect in the forward-backward asymmetry of the differential cross section. Below we present the summary of our results:

- We have calculated full leading-order charge symmetry breaking pion production operator. We found a new LO contribution which was not considered in previous studies [vKNM00, BM10]. This contribution stems from the energy dependence of the pion-nucleon vertex and explicit proton-neutron mass difference terms in the chiral Lagrangian. We have also recalculated the LO operator considered in previous studies, since there was a numerical mistake in previous calculation.

- We showed that the full LO CSB operator is directly proportional to the strong part of the neutron-proton mass difference $\delta m_N^{\rm str}$.

- We calculated the full LO CSB amplitude, which takes into account nonperturbative nucleon-nucleon interactions in the initial and final states. For this purpose we adopted the hybrid approach, which consists of the convolution of the LO CSB operator with the the initial and final NN wave functions.

- Using full LO CSB amplitude, we calculated the CSB forward–backward asymmetry for the reaction $pn \to d\pi^0$ to leading order in the chiral expansion.

- Using the TRIUMF measurement of the forward-backward asymmetry [OKH$^+$03] we extracted the value

$$\delta m_N^{\rm str} = 1.5 \pm 0.9 \text{ MeV} ,$$

  where the theoretical and experimental uncertainties are added in quadrature. This result is consistent with extractions of the same quantities using Cottingham sum rule [Cot63] in references [GL82, WLCM12] and with lattice simulations [BOS07, BZD$^+$10, dDDF$^+$12]. We emphasize that the agreement of the various independent extractions provides a highly non-trivial and important test of our understanding of the chiral symmetry and the isospin breaking pattern of QCD.

We have calculated CSB pion production operator at leading order in chiral expansion, and since there are no NLO CSB contributions, the accuracy of our result is even higher than LO. However to verify convergence and increase accuracy one has to calculate N^{2}LO CSB corrections. This task is quite challenging since at that order loop diagrams start to contribute. The methods to handle loop integrals, developed in this work, can be useful to efficiently perform such calculation. In addition, our results can be useful in study of charge symmetry breaking in $dd \to \alpha\pi^0$, where both charge symmetric and charge symmetry breaking $NN \to NN\pi$ operators contribute as building blocks. Finally, a combined analysis of CSB in $pn \to d\pi^0$ and $dd \to \alpha\pi^0$ reactions can be used to better restrict low energy constants that appear at higher orders.

Outlook

In this section we outline the directions of future research related to pion production in nucleon-nucleon collisions.

- Isospin-conserving pion production operators calculated in chapters 2 and 3 should be used to calculate observables, most notably, cross sections. Such calculation will allow one to fix the values of five-point $NN \to NN\pi$ LECs, investigate naturalness of these LECs, and make a definitive quantitative conclusion about the role of short- and intermediate-range mechanisms in pion production.

- Calculation of $NN \to NN\pi$ observables requires taking into account nonperturbative interaction of nucleons in the initial and final state. For a long time, there were no chiral-EFT NN wave functions available to make fully consistent chiral EFT calculation possible. (The large transferred momentum between nucleons in pion production makes the construction of such wave function highly nontrivial.) This is why the hybrid approach is typically adopted in studies of $NN \to NN\pi$ reactions. We have also used it in Chapter 4. In the hybrid approach one uses realistic phenomenological wave functions instead of chiral ones, thus, a fully consistent estimation of the uncertainty is not possible. Recent developments in construction of chiral NN wave functions near pion production threshold [Epe14] can allow one to perform a fully consistent chiral EFT study of pion production.

- A full N^{2}LO calculation of CSB $NN \to NN\pi$ amplitudes can be interesting in order to verify the convergence of chiral series for CSB amplitudes and to fix the values of subleading CSB LECs, which can be used to predict other CSB processes.

- One of the most promising applications of the results of this thesis can be theoretical description of charge symmetry breaking in $dd \to \alpha\pi^0$. The corresponding experiment has been done at IUCF [SBA$^+$03] very close to threshold yielding nonvanishing total cross section of this CSB reaction. See Refs. [GHN$^+$04, NFG$^+$06, FMM09] for the first theory study. Moreover, the measurement of this reaction in a wider range of energies is currently ongoing at COSY [A$^+$13].

Appendix A

Lagrangian density

In this Appendix we present the Lagrangian densities relevant for our studies. We use heavy baryon formalism and employ sigma-gauge for pion fields[1]. In this section we list the isospin symmetric terms. Isospin violating terms can be found in the Section 4.2.

A.1 ChPT Lagrangian

The leading order chiral Lagrangian for pion-pion interactions has form:

$$\mathcal{L}^{(2)}_{\pi\pi} = \frac{1}{2}(\partial_\mu \boldsymbol{\pi}\cdot\partial^\mu\boldsymbol{\pi}) - \frac{1}{2}m_\pi^2\boldsymbol{\pi}^2 + \frac{1}{2f_\pi^2}(\boldsymbol{\pi}\cdot\partial^\mu\boldsymbol{\pi})(\boldsymbol{\pi}\cdot\partial_\mu\boldsymbol{\pi}) - \frac{m_\pi^2}{8f_\pi^2}\boldsymbol{\pi}^4 + \cdots\,, \tag{A.1}$$

where $\boldsymbol{\pi}$ denotes tree pion fields in the isospin space, m_π is a pion mass, f_π is a pion decay constant, and dots stand for terms with more than four pion fields.

The leading order pion-nucleon Lagrangian expanded in terms of pion fields reads:

$$\mathcal{L}^{(1)}_{\pi N} = N^\dagger\left[\frac{1}{4f_\pi^2}\boldsymbol{\tau}\cdot(\dot{\boldsymbol{\pi}}\times\boldsymbol{\pi}) + \frac{g_A}{2f_\pi}\boldsymbol{\tau}\cdot\vec{\sigma}\left(\vec{\nabla}\boldsymbol{\pi} + \frac{1}{2f_\pi^2}\boldsymbol{\pi}(\boldsymbol{\pi}\cdot\vec{\nabla}\boldsymbol{\pi})\right)\right]N + \cdots\,, \tag{A.2}$$

where N is nucleon field, g_A is pion nucleon coupling constant, σ and $\boldsymbol{\tau}$ correspond to Pauli matrices in spin and isospin spaces respectively, and dots stand for terms with more than three pion fields.

The NLO pion nucleon Lagrangian has form:

$$\begin{aligned}
\mathcal{L}^{(2)}_{\pi N} = {} & \frac{1}{8m_N f_\pi^2}\left[iN^\dagger\boldsymbol{\tau}\cdot(\boldsymbol{\pi}\times\vec{\nabla}\boldsymbol{\pi})\cdot\vec{\nabla}N + h.c.\right] \\
& -\frac{g_A}{4m_N f_\pi}\left[iN^\dagger\boldsymbol{\tau}\cdot\left(\dot{\boldsymbol{\pi}} + \frac{1}{2f_\pi^2}\boldsymbol{\pi}(\boldsymbol{\pi}\cdot\dot{\boldsymbol{\pi}})\right)\vec{\sigma}\cdot\vec{\nabla}N + h.c.\right] \\
& -\frac{g_A}{8m_N f_\pi^3}N^\dagger\boldsymbol{\pi}\cdot(\vec{\sigma}\cdot\vec{\nabla})(\dot{\boldsymbol{\pi}}\times\boldsymbol{\pi})N \\
& +\frac{1}{f_\pi^2}N^\dagger\Bigg[\left(c_3 + c_2 - \frac{g_A^2}{8m_N}\right)\dot{\boldsymbol{\pi}}^2 - c_3(\vec{\nabla}\boldsymbol{\pi})^2 - 2c_1 m_\pi^2\boldsymbol{\pi}^2 \\
& -\frac{1}{2}\left(c_4 + \frac{1}{4m_N}\right)\varepsilon_{ijk}\varepsilon_{abc}\sigma_k\tau_c\partial_i\pi_a\partial_j\pi_b\Bigg]N + \cdots\,,
\end{aligned} \tag{A.3}$$

[1] See [HW07] for discussion of different gauges.

where m_N denotes the nucleon mass and c_1–c_4 are pion-nucleon low-energy constants.

From the third-order pion-nucleon Lagrangian we only need recoil corrections, which can be enhanced in pion production kinematics. Terms proportional to LECs d_i are of higher order than we consider in this study. The relevant third order Lagrangian terms have form

$$\mathcal{L}^{(3)}_{\pi N} = \bar{N}\mathcal{O}^{(3)}_{\rm fixed}N \ , \tag{A.4}$$

where

$$\begin{aligned}
\mathcal{O}^{(3)}_{\rm fixed} &= \frac{g_A}{8m_N^2}\,[D^\mu,[D_\mu,S{\cdot}u]] - i\,\frac{1}{4m_N^2}\,(v{\cdot}D)^3 \\
&\quad -\frac{g_A}{4m_N^2}\,v\cdot\overleftarrow{D}S{\cdot}u\,v{\cdot}D + \frac{1}{8m_N^2}\left(i\,D^2\,v{\cdot}D + h.c.\right) \\
&\quad -\frac{g_A}{4m_N^2}\left(\{S{\cdot}D, v{\cdot}u\}\,v{\cdot}D + h.c.\right) + \frac{3g_A^2}{64m_N^2}\left(i\langle(v{\cdot}u)^2\rangle\,v{\cdot}D + h.c.\right) \\
&\quad +\frac{1}{32m_N^2}\left(\varepsilon^{\mu\nu\alpha\beta}v_\alpha S_\beta[u_\mu,u_\nu]\,v{\cdot}D + h.c.\right) \\
&\quad -\frac{g_A}{8m_N^2}\left(S{\cdot}u\,D^2 + h.c.\right) - \frac{g_A}{4m_N^2}\left(S\cdot\overleftarrow{D}\,u{\cdot}D + h.c.\right) \\
&\quad +\frac{1+g_A^2+8m_N\,c_4}{16m_N^2}\left(\varepsilon^{\mu\nu\alpha\beta}v_\alpha S_\beta[u_\mu,v{\cdot}u]D_\nu + h.c.\right) \\
&\quad -\frac{g_A^2}{16m_N^2}\left(i\,v{\cdot}u\,u{\cdot}D + h.c.\right) \\
&\quad +i\,\frac{1+8m_N\,c_4}{32m_N^2}\,[v{\cdot}u,[D^\mu,u_\mu]] + \frac{c_2}{2m_N}\left(i\langle v{\cdot}u\,u_\mu\rangle D^\mu + h.c.\right) + \cdots \ .
\end{aligned} \tag{A.5}$$

The building blocks D and u are defined by Eqs. (1.9) and (1.3), operators v and S satisfy the relations (1.16), $[\cdots]$ and $\{\cdots\}$ denote commutator and anticommutator, and $\langle\cdots\rangle$ denotes trace in the isospin space.

A.2 Additional Lagrangian terms in chiral EFT with explicit delta

In this section we present the Lagrangian terms for theory with explicit Delta degree of freedom. These expressions are based on the work by Hemmert *et.al.* [HHK98, Hem96]. Note that we use sigma-gauge for pion field, while Hemmert uses exponential one.

Leading pion-nucleon-delta Lagrangian for $N\Delta\pi$ and $N\Delta\pi\pi\pi$ vertices in heavy baryon formalism with Delta reads

$$\begin{aligned}
\mathcal{L}^{(1)}_{\pi N\Delta} &= -g_{\pi N\Delta}\,\bar{\Psi}_\Delta\,\mathbb{S}^{\dagger\mu}\left(\frac{1}{f_\pi}(\mathbf{T}^\dagger\cdot\partial_\mu\boldsymbol{\pi}) + \frac{1}{2f_\pi^3}(\boldsymbol{\pi}\cdot\partial_\mu\boldsymbol{\pi})(\mathbf{T}^\dagger\cdot\boldsymbol{\pi})\right)N \\
&\quad -g_{\pi N\Delta}\,\bar{N}\left(\frac{1}{f_\pi}(\mathbf{T}\cdot\partial_\mu\boldsymbol{\pi}) + \frac{1}{2f_\pi^3}(\boldsymbol{\pi}\cdot\partial_\mu\boldsymbol{\pi})(\mathbf{T}\cdot\boldsymbol{\pi})\right)\mathbb{S}^\mu\,\Psi_\Delta,
\end{aligned} \tag{A.6}$$

where Ψ_Δ denotes delta field in heavy baryon formulation, $g_{\pi N\Delta}$ is a pion-nucleon-delta coupling constant, and $\mathbb{S}$ and $\mathbf{T}$ are spin and isospin projection operators (see Section 1.3).

The Leading Delta-Delta Lagrangian gives rise to the Delta propagator, $\pi\Delta\Delta$ and $\pi\pi\pi\Delta\Delta$ vertices, and $\pi\pi\Delta\Delta$ vertex

$$\begin{aligned}\mathcal{L}^{(1)}_{\pi\Delta\Delta} &= -\bar{\Psi}_\Delta 1_S\, 1_I\, (i(v\cdot\partial)-\delta)\Psi_\Delta \\ &\quad + g_1\bar{\Psi}_\Delta \mathbb{S}^{\dagger\mu} S^\beta \mathbb{S}_\mu T_i^\dagger \tau^k T_i \left(\frac{\partial_\beta \pi^k}{f_\pi} + \frac{1}{2f_\pi^3}(\boldsymbol{\pi}\cdot\partial_\beta\boldsymbol{\pi})\pi^k\right)\Psi_\Delta \\ &\quad + \frac{1}{4f_\pi^2}\bar{\Psi}_\Delta 1_S\, (\boldsymbol{\pi}\times(v\cdot\partial)\boldsymbol{\pi})^k T_i^\dagger(-2i\epsilon^{ijk}+\tau^k\delta^{ij})T_j\Psi_\Delta, \end{aligned} \tag{A.7}$$

where we use the notation $1_S = \mathbb{S}^{\dagger\mu}\mathbb{S}_\mu$, and $1_I = T_i^\dagger T_i$ for spin and isospin unity-matrices, and δ denotes delta-nucleon mass difference.

Appendix B

Feynman rules

In this Appendix we list vertex functions and propagators corresponding to isospin conserving Lagrangian presented in Appendix A and isospin violating Lagrangian discussed in Chapter 4.

B.1 Pion-pion interactions

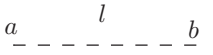

$$= \frac{i\delta^{ab}}{l^2 - m_\pi^2 + i0} \tag{B.1}$$

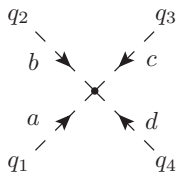

$$= \frac{i}{f_\pi^2}\Big[\delta^{ab}\delta^{cd}\left[(q_1+q_2)^2 - m_\pi^2\right] + \delta^{ac}\delta^{bd}\left[(q_1+q_3)^2 - m_\pi^2\right]$$

$$+\delta^{ad}\delta^{bc}\left[(q_1+q_4)^2 - m_\pi^2\right]\Big] \tag{B.2}$$

Here and in what follows, the letters a–d denote isospin indices.

B.2 Pion-nucleon interactions

Feynman rules from the leading Lagrangian:

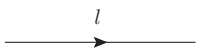

$$= \frac{i}{v\cdot l - \frac{\vec{l}^{\,2}}{2m_N} + i0} \tag{B.3}$$

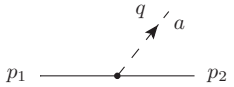

$$= \frac{g_A}{f_\pi} S\cdot q\, \tau^a \tag{B.4}$$

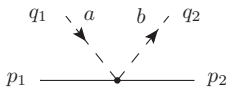

$$= \frac{1}{4f_\pi^2} v\cdot(q_1+q_2)\varepsilon^{abc}\tau^c \tag{B.5}$$

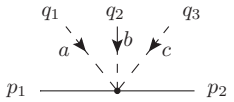

$$= \frac{g_A}{2f_\pi^3}\Big[\tau^a\delta^{bc} S\cdot(q_2+q_3) + \tau^b\delta^{ac} S\cdot(q_1+q_3)$$

$$+\tau^c\delta^{ab} S\cdot(q_1+q_2)\Big] \tag{B.6}$$

Feynman rules from the sub-leading Lagrangian:

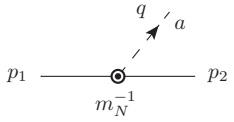

$$= -\frac{g_A}{2m_N f_\pi} S\cdot(p_1+p_2)\, v\cdot q\, \tau^a \tag{B.7}$$

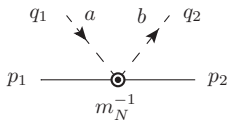

$$= -\frac{1}{8m_N f_\pi^2}\varepsilon^{abc}\tau^c(\vec{p}_1+\vec{p}_2)\cdot(\vec{q}_1+\vec{q}_2) \tag{B.8}$$

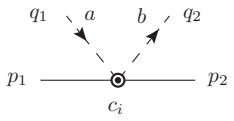

$$= \frac{i\delta^{ab}}{f_\pi^2}[-4c_1 m_\pi^2 + \left(2c_2 - \frac{g_A^2}{4m_N}\right) v\cdot q_1\, v\cdot q_2 + 2c_3 q_1\cdot q_2]$$

$$-\frac{1}{f_\pi^2}\left(2c_4+\frac{1}{2m_N}\right)\varepsilon^{abc}\tau^c[S\cdot q_1, S\cdot q_2] \tag{B.9}$$

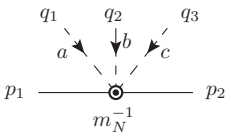

$$= -\frac{ig_A}{4m_N f_\pi^3}\varepsilon^{abc}\Big[v\cdot q_1\, S\cdot(q_2-q_3) + v\cdot q_2\, S\cdot(q_3-q_1)$$

$$+v\cdot q_3\, S\cdot(q_1-q_2)\Big] - \frac{g_A}{4m_N f_\pi^3} S\cdot(p_1+p_2)$$

$$\times\Big[\tau^a\delta^{bc} v\cdot(q_2+q_3) + \tau^b\delta^{ac} v\cdot(q_1+q_3)$$

$$+\tau^c\delta^{ab} v\cdot(q_1+q_2)\Big] \tag{B.10}$$

B.3 Pion-nucleon-delta interactions

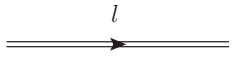

$$= \frac{-i}{v\cdot l - \delta - \frac{\vec{l}^2}{2m_N} + i0} \tag{B.11}$$

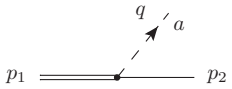

$$= \frac{g_{\pi N\Delta}}{f_\pi}\mathbb{S}^\dagger\cdot q\, T^{\dagger a} \tag{B.12}$$

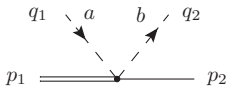

$$= 0 \tag{B.13}$$

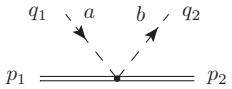

$$= -\frac{1}{4f_\pi^2}T^{\dagger i}v\cdot(q_1+q_2)\varepsilon^{abc}(\tau^c\delta^{ij}-2i\varepsilon^{ijc})T^j \tag{B.14}$$

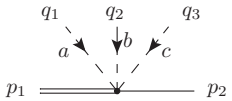

$$= \frac{g_{\pi N\Delta}}{2f_\pi^3}\Big[T^{\dagger a}\delta^{bc}\mathbb{S}^\dagger\cdot(q_2+q_3)+T^{\dagger b}\delta^{ac}\mathbb{S}^\dagger\cdot(q_1+q_3)$$

$$+T^{\dagger c}\delta^{ab}\mathbb{S}^\dagger\cdot(q_1+q_2)\Big] \tag{B.15}$$

B.4 Charge symmetry breaking interactions

Feynman rules for isospin violating pion-nucleon scattering before (Eq. (4.24)) and after (Eq. (4.27)) field redefinition:

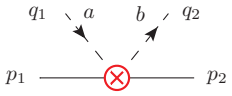

$$= \frac{i}{4f_\pi^2}\left[(\delta m_N^{\text{str.}}-\delta m_N^{\text{e.m.}})(\tau_a\delta_{b3}+\tau_b\delta_{a3})+\delta m_N^{\text{e.m.}}2\delta_{ab}\tau_3\right] \tag{B.16}$$

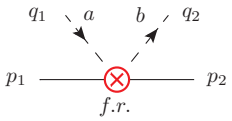

$$= \frac{i}{2f_\pi^2}\delta m_N^{\text{str.}}\,(\tau_a\delta_{b3}+\tau_b\delta_{a3}-\tau_3\delta_{ab}) \tag{B.17}$$

Appendix C

Relations between leading vertices and propagators in chiral EFT

In this Appendix we describe relations between leading $\pi\pi \to \pi\pi$ and $\pi N \to \pi N$ vertices and pion and nucleon propagators respectively. Such relations can significantly simplify calculation of Feynman diagrams. The idea which allow such simplification is to rewrite a vertex as a sum of several terms proportional to the inverse propagators and some remaining term. The advantage of such transformation is that the terms, which are proportional to inverse propagators, usually give zero contribution to the full amplitude. Depending on the state of the particle corresponding to the inverse propagator, there can be two scenarios. If the particle is on-shell then its inverse propagator is zero and the whole structure proportional to it does not contribute. If the particle is off-shell then there exists also a normal propagator attached to the vertex. This normal propagator cancels with the inverse propagator from the vertex and a new structure emerges. Such structure typically exactly cancels with similar structures form other Feynman diagrams.

C.1 Pion propagator and the leading $\pi\pi \to \pi\pi$ vertex

We start with the relation between the leading $\pi\pi \to \pi\pi$ vertex and a pion propagator. The leading $\pi\pi \to \pi\pi$ vertex in the kinematics of Figure C.1 has the form:

$$V_{\pi\pi\to\pi\pi} = \frac{i}{f_\pi^2}\left\{\delta^{ab}\delta^{cd}\left[(l-q)^2 - m_\pi^2\right] + \delta^{ac}\delta^{bd}\left[(\tilde{l}+q)^2 - m_\pi^2\right] + \delta^{ad}\delta^{bc}\left[(k_1-q)^2 - m_\pi^2\right]\right\}.$$

This expression can be rewritten as:

$$\begin{aligned} V_{\pi\pi\to\pi\pi} \;=\; & \frac{i}{f_\pi^2}\Big\{\delta^{ab}\delta^{cd}\left[l^2 - m_\pi^2\right] + \delta^{ac}\delta^{bd}\left[\tilde{l}^{\,2} - m_\pi^2\right] + \delta^{ad}\delta^{bc}\left[k_1^2 - m_\pi^2\right] + \\ & + \delta^{ab}\delta^{cd}\left[-2l\cdot q + q^2\right] + \delta^{ac}\delta^{bd}\left[2\tilde{l}\cdot q + q^2\right] + \delta^{ad}\delta^{bc}\left[-2k_1\cdot q + q^2\right]\Big\}. \end{aligned} \tag{C.1}$$

The first three terms in this expression are proportional to inverse pion propagators. Contributions corresponding to those terms cancel with other Feynman diagrams.

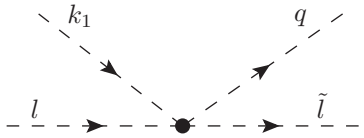

Figure C.1: Kinematics of pion-pion scattering.

C.2 Nucleon propagator and the Weinberg–Tomozawa vertex

In this section we discuss the relation between the leading-order $\pi N \to \pi N$ vertex (so called Weinberg–Tomozawa vertex) and the nucleon propagator. We will first derive this relation in the covariant formulation and then consider it in the heavy-baryon formulation.

C.2.1 Covariant formulation

Let us consider the leading-order covariant $\pi N \to \pi N$ vertex. In the kinematics shown in Figure C.2, the Feynman-rule corresponding to the leading relativistic $\pi N \to \pi N$ vertex reads:

$$V^{\rm cov.}_{\pi N\to\pi N} = \frac{1}{4f_\pi^2}\epsilon_{abc}\tau^c(\not{k}_2 + \not{q}). \tag{C.2}$$

We can exclude k_2 from this expression using the four-momentum conservation ($k_2 = q - P_1 + P_1'$), and add and subtract a nucleon mass. The resulting identity reads:

$$\begin{aligned} V^{\rm cov.}_{\pi N\to\pi N} &= \frac{1}{4f_\pi^2}\epsilon_{abc}\tau^c(2\not{q} - \not{P}_1 + \not{P}_1') \\ &= \frac{1}{4f_\pi^2}\epsilon_{abc}\tau^c(2\not{q} - (\not{P}_1 - m_N) + (\not{P}_1' - m_N)). \end{aligned} \tag{C.3}$$

This identity shows that the leading $\pi N \to \pi N$ vertex can be rewritten as a sum of three terms: the first one is proportional to the outgoing pion momentum ($2\not{q}$), and the remaining two are proportional to the inverse propagators of the initial and final nucleons. If one or both nucleons are on-shell, then the corresponding inverse propagators give zero contribution due to equations of motion. If the nucleon is off-shell, the corresponding inverse propagator cancels with the normal nucleon propagator and the resulting structure usually gives zero in the sum with similar structures from other diagrams.

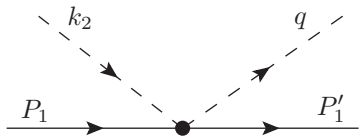

Figure C.2: Kinematics of pion-nucleon scattering in the covariant formulation. The symbols P_1 and P_1' denote full covariant momenta of the nucleon.

Note that the leading $\pi\Delta \to \pi\Delta$ vertex differs from the leading $\pi N \to \pi N$ vertex only by spin-isospin structure and the value of the baryon mass. Thus, the decomposition discussed in this section applies to it in the exactly same way.

C.2.2 Heavy-baryon formulation

Let's now discuss the relation between the WT vertex and the nucleon propagator in the heavy baryon formulation. For simplicity we use the following notation:

$$(\vec{a}\cdot\vec{b}) := (v\cdot a)(v\cdot b) - a\cdot b \qquad \text{and} \qquad \vec{a}^{\,2} := (v\cdot a)^2 - a^2, \tag{C.4}$$

where a and b are four-vectors.

Before considering the relation between the WT vertex and the nucleon propagator, it is instructive to consider nucleon propagator and the on-shell condition in heavy baryon formulation.

In the heavy baryon formulation the four-momentum of the nucleon is decomposed as $P_\mu = v_\mu m_N + p_\mu$, with $v^2 = 1$. Thus, the residual nucleon momentum p doesn't include the nucleon mass. In such formulation, the on-shell condition $P^2 = m_N^2$ turns into $p^2 + 2m_N\, v\cdot p = 0$. Using notation (C.4) we get the exact on-shell condition in the heavy baryon formulation

$$v\cdot p - \frac{\vec{p}^{\,2}}{2m_N} + \frac{(v\cdot p)^2}{2m_N} = 0. \tag{C.5}$$

By expressing $v\cdot p$ from the first term and recursively substituting it to the last term, we get the approximate on-shell condition up-to $1/m_N^3$:

$$v\cdot p - \frac{\vec{p}^{\,2}}{2m_N} + \frac{(v\cdot p)\,\vec{p}^{\,2}}{4m_N^2} - \frac{(v\cdot p)^2\,\vec{p}^{\,2}}{8m_N^3} + \mathcal{O}\left(\frac{1}{m_N^4}\right) = 0. \tag{C.6}$$

The left hand side of this expression corresponds to the inversed nucleon propagator in the heavy baryon formulation.

The Feynman rule for the leading WT vertex in the heavy baryon formalism can be rewritten as:

$$V^{\mathrm{HB,LO}}_{\pi N\to\pi N} = \frac{1}{4f_\pi^2}\epsilon_{abc}\tau^c\, v\cdot(k_2+q) = \frac{1}{4f_\pi^2}\epsilon_{abc}\tau^c\,\left[2v\cdot q - v\cdot p + v\cdot p'\right], \tag{C.7}$$

where in the last equation we used the four-momentum conservation $k_2 = q - p_1 + p_1'$ to exclude k_2. The resulting structure in the r.h.s. of (C.7) is very similar to that in covariant formulation (C.3). The first term is proportional to the outgoing pion momentum, while the second and the third terms are the inverses of the heavy baryon nucleon propagators at leading order in $1/m_N$-expansion.

For our study the $1/m_N$ corrections to the leading pion-nucleon vertex are important both in tree-level and in loop diagrams. The decomposition of the pion-nucleon vertex can be easily generalized to include the $1/m_N$ corrections. The sum of Feynman rules for the leading WT vertex and its $1/m_N$ correction is

$$\begin{aligned} V^{\mathrm{HB,LO}+m_N^{-1}}_{\pi N\to\pi N} &= \frac{1}{4f_\pi^2}\epsilon_{abc}\tau^c\, v\cdot(k_2+q) - \frac{1}{4f_\pi^2}\epsilon_{abc}\tau^c\frac{1}{2m_N}(\vec{p}_1+\vec{p}_1')\cdot(\vec{k}_2+\vec{q}) = \\ &= \frac{1}{4f_\pi^2}\epsilon_{abc}\tau^c\left[2v\cdot q - \frac{2\vec{q}\cdot(\vec{p}_1+\vec{p}_1')}{2m_N} - \left(v\cdot p_1 - \frac{\vec{p}_1^{\,2}}{2m_N}\right) + \left(v\cdot p_1' - \frac{\vec{p}_1'^{\,2}}{2m_N}\right)\right], \end{aligned} \tag{C.8}$$

where we again used the momentum conservation to exclude k_2. The structure remains the same. The first two terms in the square brackets in Eq. (C.8) are proportional to the outgoing pion momentum, and the rest two are inversed nucleon propagators with corresponding $1/m_N$ corrections.

For some N^{2}LO tree-level diagrams in our study we will need to consider $1/m_N^2$ corrections to the leading pion-nucleon vertex. The identity is derived exactly the same way as previous two. The final expression for the Feynman rule for the leading $\pi N \to \pi N$ vertex with recoil corrections up-to-and-including $1/m_N^2$ reads:

$$\begin{aligned} V_{\pi N\to\pi N}^{\mathrm{HB,LO}+m_N^{-2}} &= \frac{1}{4f_\pi^2}\epsilon_{abc}\tau^c\left\{v\cdot(k_2+q)-\frac{1}{2m_N}(\vec{p}_1+\vec{p}_1')\cdot(\vec{k}_2+\vec{q})\right. \\ &\quad +\frac{1}{2m_N^2}\left(\frac{1}{2}v\cdot(k_2+q)\left[(v\cdot p_1)^2+(v\cdot p_1')^2+(v\cdot p_1)(v\cdot p_1')\right]\right. \\ &\quad \left.\left.-\frac{1}{4}\left[(p_1^2+p_1'^2)v\cdot(k_2+q)+v\cdot(p_1+p_1')\,(p_1+p_1')\cdot(k_2+q\,)\right]\right)\right\} \\ &= \frac{1}{4f_\pi^2}\epsilon_{abc}\tau^c\left[2v\cdot q-\frac{2\vec{q}\cdot(\vec{p}_1+\vec{p}_1')}{2m_N}+\frac{v\cdot q\,(\vec{p}_1^{\,2}+\vec{p}_1'^2)}{4m_N^2}+\frac{\vec{q}\cdot(\vec{p}_1+\vec{p}_1')\,v\cdot(p_1+p_1')}{4m_N^2}\right. \\ &\quad \left.-\left(v\cdot p_1-\frac{\vec{p}_1^{\,2}}{2m_N}+\frac{v\cdot p_1\,\vec{p}_1^{\,2}}{4m_N^2}\right)+\left(v\cdot p_1'-\frac{\vec{p}_1'^2}{2m_N}+\frac{v\cdot p_1'\vec{p}_1'^2}{4m_N^2}\right)\right]. \end{aligned} \tag{C.9}$$

Again, the last two terms are proportional to the inversed nucleon propagators with the $1/m_N$ and $1/m_N^2$ corrections.

Appendix D

Basic integrals

D.1 Definitions and analytic expressions for various integrals

In this subsection we give the explicit definitions of the common dimensionless loop integrals used in this work. The first integral $J_{\pi\Delta} = \mu^\epsilon J_0(-\delta)$ where μ is the dimension-regularization scale and the integral $J_0(-\delta)$ is defined in Ref. [BKM95].

$$\begin{aligned}
\frac{1}{\delta} J_{\pi\Delta}(\delta) &= \frac{\mu^\epsilon}{i\delta} \int \frac{d^{4-\epsilon} l}{(2\pi)^{4-\epsilon}} \frac{1}{(l^2 - m_\pi^2 + i0)(-v\cdot l - \delta + i0)} \\
&= 4L + \frac{(-2)}{(4\pi)^2}\left[-1 + \log\left(\frac{\mu^2}{m_\pi^2}\right)\right] \\
&\quad + \frac{4}{(4\pi)^2}\left[-1 + \frac{\sqrt{1-y-i0}}{\sqrt{y}}\left[-\frac{\pi}{2} + \arctan\left(\frac{\sqrt{y}}{\sqrt{1-y-i0}}\right)\right]\right], \qquad \text{(D.1)} \\
I_{\pi\pi}(k_1^2) &= \frac{\mu^\epsilon}{i} \int \frac{d^{4-\epsilon} l}{(2\pi)^{4-\epsilon}} \frac{1}{(l^2 - m_\pi^2 + i0)((l+k_1)^2 - m_\pi^2 + i0)} \\
&= -2L - \frac{1}{(4\pi)^2}\left[\log\left(\frac{m_\pi^2}{\mu^2}\right) - 1 + 2F_1\left(\frac{k_1^2}{m_\pi^2}\right)\right], \qquad \text{(D.2)}
\end{aligned}$$

where

$$F_1(x) = \frac{\sqrt{4-x-i0}}{\sqrt{x}} \arctan\left(\frac{\sqrt{x}}{\sqrt{4-x-i0}}\right), \qquad \text{(D.3)}$$

$$L = \frac{1}{(4\pi)^2}\left[-\frac{1}{\epsilon} + \frac{1}{2}\left(\gamma_E - 1 - \log(4\pi)\right)\right], \qquad \text{(D.4)}$$

and the variables x, y are defined via $x = k_1^2/m_\pi^2$, $y = \delta^2/m_\pi^2$.

Further, the integrals in Eqs. (D.5) and (D.6) can be reduced to simple one-dimensional

integrals which can be calculated numerically.

$$\delta J_{\pi\pi\Delta} = \delta\frac{\mu^\epsilon}{i}\int\frac{d^{4-\epsilon}l}{(2\pi)^{4-\epsilon}}\frac{1}{(l^2-m_\pi^2+i0)((l+k_1)^2-m_\pi^2+i0)(-v\cdot l-\delta+i0)}, \quad \text{(D.5)}$$

$$k_1^2 J_{\pi\pi N\Delta} = k_1^2\frac{\mu^\epsilon}{i}\int\frac{d^{4-\epsilon}l}{(2\pi)^{4-\epsilon}}\Big[\frac{1}{(l^2-m_\pi^2+i0)((l+k_1)^2-m_\pi^2+i0)} \times\frac{1}{(-v\cdot l+i0)(-v\cdot l-\delta+i0)}\Big]. \quad \text{(D.6)}$$

It is also convenient to define finite, scale-independent parts of $J_{\pi\Delta}$ and $I_{\pi\pi}$ in which the divergency L and the $\log(m_\pi/\mu)$ terms are removed. The finite contributions $J_{\pi\Delta}^{finite}$ and $I_{\pi\pi}^{finite}$ will be used in the subsequent section.

$$I_{\pi\pi} = -2L-\frac{1}{(4\pi)^2}\log\left(\frac{m_\pi^2}{\mu^2}\right)+I_{\pi\pi}^{finite}, \quad \text{(D.7)}$$

$$I_{\pi\pi}^{finite} = \frac{1}{(4\pi)^2}\left(1-2\frac{\sqrt{4-x-i0}}{\sqrt{x}}\arctan\left(\frac{\sqrt{x}}{\sqrt{4-x-i0}}\right)\right), \quad \text{(D.8)}$$

$$\frac{1}{\delta}J_{\pi\Delta} = 4L+\frac{2}{(4\pi)^2}\log\left(\frac{m_\pi^2}{\mu^2}\right)+\frac{1}{\delta}J_{\pi\Delta}^{finite}, \quad \text{(D.9)}$$

$$\frac{1}{\delta}J_{\pi\Delta}^{finite} = \frac{4}{(4\pi)^2}\left[-\frac{1}{2}+\frac{\sqrt{1-y-i0}}{\sqrt{y}}\left[-\frac{\pi}{2}+\arctan\left(\frac{\sqrt{y}}{\sqrt{1-y-i0}}\right)\right]\right]. \quad \text{(D.10)}$$

From the expressions above it is easy to obtain the important relation, which is used in the analysis of the integral combinations, relevant for our study

$$I_{\pi\pi}+\frac{1}{2\delta}J_{\pi\Delta} = I_{\pi\pi}^{finite}+\frac{1}{2\delta}J_{\pi\Delta}^{finite}. \quad \text{(D.11)}$$

Appendix E

Combinations of basic integrals in the limit $\delta \to \infty$

In this subsection we discuss the behavior of the integral combinations, see Eqs. (3.5)–(3.7), relevant for loop-diagrams considered in this work. While the integrals $I_{\pi\pi}$ and $J_{\pi\Delta}$ have analytic expressions for any δ, the integral $J_{\pi\pi\Delta}$ can be done analytically only in the limit $\delta \to \infty$. Using the dispersive analysis, one finds the asymptotic expression for $\delta J_{\pi\pi\Delta}$ when $\delta \to \infty$

$$\begin{aligned}(4\pi)^2\delta J_{\pi\pi\Delta} &= 2\log\left[\frac{m_\pi}{2\delta}\right] - 1 - (4\pi)^2 I_{\pi\pi}^{finite} + \frac{1}{36\delta^2}\Big((36m_\pi^2 - 6k_1^2)\log\left[\frac{m_\pi}{2\delta}\right] \\ &\quad -k_1^2 + 6m_\pi^2 + (3k_1^2 - 12m_\pi^2)(4\pi)^2 I_{\pi\pi}^{finite}\Big) + O\left(\frac{1}{\delta^3}\right). \end{aligned} \tag{E.1}$$

Note that to get the MCS terms relevant at N^{2}LO, one ignores m_π^2 compared to k_1^2 in the last two lines of the expression above.

Using the expression above, Eq. (D.11) and the expansion of $J_{\pi\Delta}^{finite}$ for large δ

$$\frac{(4\pi)^2}{\delta} J_{\pi\Delta}^{finite} = -4\log\left[\frac{m_\pi}{2\delta}\right] - 2 + \frac{m_\pi^2}{\delta^2}\left(2\log\left[\frac{m_\pi}{2\delta}\right] - 1\right) + O\left(\frac{1}{\delta^4}\right), \tag{E.2}$$

one obtains

$$\left(I_{\pi\pi} + \delta J_{\pi\pi\Delta} + \frac{1}{2}\frac{J_{\pi\Delta}}{\delta} + \frac{2}{(4\pi)^2}\right) = O\left(\frac{1}{\delta^2}\right). \tag{E.3}$$

Thus, this combination vanishes in the limit $\delta \to \infty$.

Analogously, one finds

$$\begin{aligned}&\frac{\delta^2}{k_1^2}\left(I_{\pi\pi} + \delta J_{\pi\pi\Delta} + \frac{1}{2}\frac{J_{\pi\Delta}}{\delta} + \frac{2}{(4\pi)^2}\right) - \frac{1}{12}\left(I_{\pi\pi} + \frac{1}{2}\frac{J_{\pi\Delta}}{\delta} + \frac{1}{3}\frac{2}{(4\pi)^2}\right) \\ &= \frac{m_\pi^2}{3k_1^2}\left(6\log\left[\frac{m_\pi}{2\delta}\right] - 1 - I_{\pi\pi}^{finite}\right) + O\left(\frac{1}{\delta^2}\right). \end{aligned} \tag{E.4}$$

This combination vanishes in the limit $\delta \to \infty$ up to higher order terms. To make it vanishing also at higher order one would need to extend the calculation and keep the so far neglected higher order terms.

Finally, the integral $J_{\pi\pi N\Delta}$ obviously vanishes at large δ

$$J_{\pi\pi N\Delta} = \frac{1}{\delta}(J_{\pi\pi\Delta} - J_{\pi\pi N}), \tag{E.5}$$

where $J_{\pi\pi N} = J_{\pi\pi\Delta}(\delta = 0)$.

Appendix F

Evaluation of the individual pion-nucleon diagrams

F.1 Evaluation of the individual g_A^3-diagrams

In this appendix we derive the NLO and N^{2}LO expressions for individual two-pion exchange diagrams shown in Fig. 2.6 under restriction that the outgoing pion is produced in s-wave. The kinematics is defined in Fig. 2.7.

F.1.1 Diagram II

Diagram II shown in Fig. 2.6 is straightforward to evaluate. The operator $A^{abc}_{g_A^3}$ of Eq. (2.5) in this case arises from a three-pion one-nucleon vertex whose explicit form can be found in Eqs. (A.2), (A.3). The diagram II yields the contribution

$$\begin{aligned} iM_{\rm II} &= \int\frac{d^4l}{(2\pi)^4}\,B_2(l,\tilde{l})\;\tau_2^c\tau_2^b\;\frac{g_A}{2f_\pi^3}\Big\{[\tau_1^a\delta^{bc}S_1\cdot(-l+\tilde{l})+\tau_1^b\delta^{ac}S_1\cdot(q+\tilde{l})+\tau_1^c\delta^{ab}S_1\cdot(q-l)] \\ &\quad -\frac{1}{2m_N}i\varepsilon^{abc}[v\cdot qS_1\cdot(-l-\tilde{l})-v\cdot lS_1\cdot(\tilde{l}-q)+v\cdot\tilde{l}S_1\cdot(q+l)] \\ &\quad -\frac{1}{2m_N}S_1\cdot(p_1+p_1')[\tau_1^a\delta^{bc}v\cdot(-l+\tilde{l})+\tau_1^b\delta^{ac}v\cdot(q+\tilde{l})+\tau_1^c\delta^{ab}v\cdot(q-l)]\Big\}, \end{aligned}$$

where $B_2(l,\tilde{l})$ is defined in Eq. (2.6). Contracting isospin indices and ignoring all p-wave terms ($\propto S_1\cdot q$) and higher-order s-wave terms $\propto v\cdot q/m_N\simeq m_\pi/m_N$ we find

$$\begin{aligned} iM_{\rm II} &= \frac{g_A}{4f_\pi^3}\int\frac{d^4l}{(2\pi)^4}\,B_2(l,\tilde{l})\Big\{-(S_1\cdot l)[4\tau_+ + 4\tau_- - 2\tau_\times]+(S_1\cdot\tilde{l})[4\tau_+ + 4\tau_- + 2\tau_\times] \\ &\quad +\left[-\frac{S_1\cdot l}{2m_N}v\cdot\tilde{l}+\frac{S_1\cdot\tilde{l}}{2m_N}v\cdot l\right](2\tau_+ - 2\tau_-) \\ &\quad +\frac{S_1\cdot(p_1+p_1')}{2m_N}[v\cdot l(4\tau_+ + 4\tau_- - 2\tau_\times)-v\cdot\tilde{l}(4\tau_+ + 4\tau_- + 2\tau_\times)]\Big\}, \end{aligned}$$

where the integrand in the first line starts to contribute at NLO while that in the last two lines gives N^{2}LO contribution.

F.1.2 Diagram IIIa

The crossed box diagram, Type IIIa, shown in Fig. 2.6 has a more complicated structure. In this diagram the operator $A^{abc}_{g_A^3}$ consists of a $\pi N \to \pi N$ scattering vertex, a nucleon propagator and a πNN-vertex. Again we only need to include the contributions from the leading and subleading chiral Lagrangian in the vertices. We also include the nucleon recoil correction in the nucleon propagator. This diagram gives the following expression

$$\begin{aligned} iM_{\rm IIIa} &= \int\frac{d^4l}{(2\pi)^4}\,B_2(l,\tilde{l})\;\tau_2^c\tau_2^b\;\frac{1}{4f_\pi^2}\varepsilon^{bad}\tau_1^d\left(v\cdot(l+q)-\frac{(\vec{p}_1+\vec{p}_1'-\vec{\tilde{l}})\cdot(\vec{l}+\vec{q})}{2m_N}\right)\\ &\quad\times\frac{i}{p_{10}-\tilde{l}_0-\frac{(\vec{p}_1-\vec{\tilde{l}})^2}{2m_N}+i0}\frac{g_A}{f_\pi}\tau_1^c\left(S_1\cdot\tilde{l}-\frac{S_1\cdot(2p_1-\tilde{l})v\cdot\tilde{l}}{2m_N}\right). \end{aligned} \tag{F.1}$$

We have ignored here the subleading c_i-contributions to the $\pi N \to \pi N$ rescattering vertex since they are suppressed in the momentum counting scheme due to the negligible kinetic energy of the outgoing pion with $q \simeq (m_\pi, \vec{0})$. We will rewrite the $\pi N \to \pi N$ vertex expression in the integrand above in a way similar to the rearrangement in Eq. (C.8)

$$\begin{aligned} &v\cdot(l+q)-\frac{(\vec{p}_1+\vec{p}_1'-\vec{\tilde{l}})\cdot(\vec{l}+\vec{q})}{2m_N}=\\ &=-\left(p_{10}-\tilde{l}_0-\frac{(\vec{p}_1-\vec{\tilde{l}})^2}{2m_N}\right)+2q_0-\frac{2\vec{q}\cdot(\vec{p}_1+\vec{p}_1'-\vec{\tilde{l}})}{2m_N}, \end{aligned} \tag{F.2}$$

where we used that $v\cdot p_1' = p_{10}' \simeq \vec{p}_1'^{\,2}/2m_N$. The first term on the second line of Eq. (F.2) is identical to the nucleon propagator in Eq. (F.1) and will give a factor of -1 when inserted into Eq. (F.1). This factor of -1 together with the lowest-order contribution of the πNN-vertex, $S_1\cdot\tilde{l}$, give the NLO contribution of diagram IIIa. The last term in the second line of Eq. (F.2) contribute to an outgoing p-wave pion and is ignored in this paper. The $2q_0$ term in Eq. (F.2) will contribute to the N^{2}LO amplitude. We next use the relation $\tilde{l} = l + p_1 - p_1' - q$ in the πNN-vertex and in the nucleon propagator. We ignore $p_{10}' \sim q_0 \sim m_\pi$ contributions and the recoil correction in the propagator which are of a higher order. Carrying out the isospin algebra we get:

$$\begin{aligned} iM_{\rm IIIa} &= \frac{g_A}{4f_\pi^3}\int\frac{d^4l}{(2\pi)^4}\,B_2(l,\tilde{l})\Big\{(S_1\cdot\tilde{l})+\frac{S_1\cdot l}{2m_N}(v\cdot\tilde{l})\\ &\quad-\frac{S_1\cdot(p_1+p_1')}{2m_N}(v\cdot\tilde{l})-\left(\frac{2v\cdot q}{-v\cdot l+i0}\right)\left(S_1\cdot\tilde{l}\right)\Big\}[2\tau_+-\tau_\times]. \end{aligned}$$

The first term in the curly bracket starts to contribute at NLO. The remaining three terms contribute to N^{2}LO.

F.1.3 Diagram IIIb

Diagram IIIb (Fig. 2.6) has a structure similar to diagram IIIa. We proceed along the same lines as for the two previous diagrams and obtain the following contribution:

$$iM_{\rm IIIb} = \int\frac{d^4l}{(2\pi)^4}\,B_2(l,\tilde{l})\;\tau_2^c\tau_2^b(-1)\frac{g_A}{f_\pi}\tau_1^b\left(S_1\cdot l-\frac{S_1\cdot(2p_1'-l)v\cdot l}{2m_N}\right)$$
$$\times\frac{i}{p_{10}'-l_0-\frac{(\vec{p}_1'-\vec{l})^2}{2m_N}+i0}\frac{1}{4f_\pi^2}\varepsilon^{cad}\tau_1^d\left(v\cdot(-\tilde{l}+q)-\frac{(\vec{p}_1+\vec{p}_1'-\vec{l})\cdot(-\vec{\tilde{l}}+\vec{q})}{2m_N}\right).$$

Using the on-shell condition for the incoming nucleon with $p_{10}=\vec{p}_1^{\,2}/2m_N$, we rewrite the $\pi N\to\pi N$ vertex in a way similar to what was done for diagram IIIa

$$v\cdot(-\tilde{l}+q)-\frac{(\vec{p}_1+\vec{p}_1'-\vec{l})\cdot(-\vec{\tilde{l}}+\vec{q})}{2m_N}=$$
$$=\left(p_{10}'-l_0-\frac{(\vec{p}_1'-\vec{l})^2}{2m_N}\right)+2q_0-\frac{2\vec{q}\cdot(\vec{p}_1+\vec{p}_1'-\vec{l})}{2m_N}\,. \qquad \text{(F.3)}$$

Using the relation $2q_0=2v\cdot q$ and keeping only terms appropriate at the order we are working we obtain:

$$iM_{\rm IIIb} = \frac{g_A}{4f_\pi^3}\int\frac{d^4l}{(2\pi)^4}\,B_2(l,\tilde{l})\Big\{(S_1\cdot l)+\frac{S_1\cdot\tilde{l}}{2m_N}(v\cdot l)$$
$$-\frac{S_1\cdot(p_1+p_1')}{2m_N}(v\cdot l)+\left(\frac{2v\cdot q}{-v\cdot l+i0}\right)(S_1\cdot l)\Big\}[-2\tau_+-\tau_\times].$$

The first term in the curly bracket starts to contribute at NLO. The remaining three terms contribute to $\mathrm{N^2LO}$.

F.1.4 Diagram IV

Diagram IV (Fig. 2.6) has an operator $A^{abc}_{g_A^3}$ containing a four-pion vertex, a pion propagator and one πNN-vertex. We keep the leading and next-to-leading order in the πNN-vertex and obtain

$$iM_{\rm IV} = \int\frac{d^4l}{(2\pi)^4}\,B_2(l,\tilde{l})\;\tau_2^c\tau_2^b\left(\frac{g_A}{f_\pi}\right)\tau_1^d\left(S_1\cdot k_1-\frac{S_1\cdot(p_1+p_1')v\cdot k_1}{2m_N}\right)\frac{i}{k_1^2-m_\pi^2+i0}$$
$$\times\frac{i}{f_\pi^2}\left\{\delta^{ab}\delta^{cd}\left[(l-q)^2-m_\pi^2\right]+\delta^{ac}\delta^{bd}\left[(\tilde{l}+q)^2-m_\pi^2\right]+\delta^{ad}\delta^{bc}\left[(k_1-q)^2-m_\pi^2\right]\right\}.$$

The four-pion vertex is rewritten as a sum of six terms

$$\frac{i}{f_\pi^2}\left\{\delta^{ab}\delta^{cd}\left[(l-q)^2-m_\pi^2\right]+\delta^{ac}\delta^{bd}\left[(\tilde{l}+q)^2-m_\pi^2\right]+\delta^{ad}\delta^{bc}\left[(k_1-q)^2-m_\pi^2\right]\right\}=$$
$$=\frac{i}{f_\pi^2}\Big\{\delta^{ab}\delta^{cd}\left[l^2-m_\pi^2\right]+\delta^{ac}\delta^{bd}\left[\tilde{l}^2-m_\pi^2\right]+\delta^{ad}\delta^{bc}\left[k_1^2-m_\pi^2\right]+$$
$$+\delta^{ab}\delta^{cd}\left[-2l\cdot q+q^2\right]+\delta^{ac}\delta^{bd}\left[2\tilde{l}\cdot q+q^2\right]+\delta^{ad}\delta^{bc}\left[-2k_1\cdot q+q^2\right]\Big\}. \qquad \text{(F.4)}$$

The contributions from the first two terms on the r.h.s. of Eq. (F.4) are of a higher order. The reason is that each term cancels a corresponding pion propagator in the operator $B_2(l,\tilde{l})$. When one pion propagator in $B_2(l,\tilde{l})$ is eliminated, the large momentum, like $\vec{k}_1$ or $\vec{p}_1$, of this reaction is no longer part of the loop integral which, consequently, only contributes at a higher order than what is considered in this Thesis. Keep in mind that $v\cdot k_1$, $v\cdot p_1$ and $v\cdot p_2$ are all of the order m_π, whereas, $|\vec{k}_1|\sim p=\sqrt{m_\pi m_N}$. The third term cancels the pion propagator $k_1^2-m_\pi^2+i0$ and will contribute at NLO and higher order in our counting. The last three terms in Eq. (F.4) start contributing from N^{2}LO.

Using $k_1=\tilde{l}-l+q$, dropping terms contributing to outgoing p-wave pions and carrying out the spin and isospin algebra we find:

$$\begin{aligned} iM_{\rm IV} &= \frac{g_A}{4f_\pi^3}\int\frac{d^4l}{(2\pi)^4}\,B_2(l,\tilde{l})\Bigg\{\left[(S_1\cdot l)-(S_1\cdot\tilde{l})+\frac{S_1\cdot(p_1+p_1')}{2m_N}\left(-v\cdot l+v\cdot\tilde{l}\right)\right]6(\tau_+ +\tau_-)\\ &\quad +(S_1\cdot k_1)\left[\frac{(l+\tilde{l})\cdot q}{k_1^2-m_\pi^2+i0}\right](-8\tau_\times)\Bigg\}. \end{aligned}$$

The first two terms in the first square bracket are NLO contributions. The remaining two terms are N^{2}LO terms.

F.1.5 Box diagram a

In the expression for the Box a diagram (Fig. 2.6) we again rewrite the pion-nucleon rescattering vertex as a sum of two terms similar to what we did for the Type-III diagrams. One of the new terms will cancel nucleon propagator yielding an irreducible NLO contribution. In contrast to the derivation of the amplitude for the Type-III graphs, we here do not consider the contribution from the term with the (remaining) nucleon propagator since it is reducible and thus included in the initial NN state interaction. Using again that the sum of the two lowest orders contribute to the vertices, we obtain from the box a diagram:

$$\begin{aligned} iM_{\rm Box\ a} &= \int\frac{d^4l}{(2\pi)^4}\,B_2(l,\tilde{l})\;\tau_2^c\tau_2^b\left(\frac{1}{4f_\pi^2}\right)\varepsilon^{cad}\tau_1^d\left(v\cdot(-\tilde{l}+q)-\frac{(\vec{p}_1+\vec{p}_1'+\vec{l})\cdot(-\vec{\tilde{l}}+\vec{q})}{2m_N}\right)\\ &\quad\times\frac{i}{l_0+p_{10}-\frac{(\vec{p}_1+\vec{l})^2}{2m_N}}(-1)\frac{g_A}{f_\pi}\tau_1^b\left(S_1\cdot l-\frac{S_1\cdot(2p_1+l)v\cdot l}{2m_N}\right). \end{aligned} \tag{F.5}$$

To rewrite the expression in the pion-nucleon rescattering vertex we again use that that p_1' is on-shell, i.e. $p_{10}'=\vec{p}_1'^{\,2}/2m_N$. The $\pi N\to\pi N$ vertex is rewritten as

$$\begin{aligned} &v\cdot(-\tilde{l}+q)-\frac{(\vec{p}_1+\vec{p}_1'+\vec{l})\cdot(-\vec{\tilde{l}}+\vec{q})}{2m_N}=\\ &=-\left(l_0+p_{10}-\frac{(\vec{p}_1+\vec{l})^2}{2m_N}\right)+2q_0-\frac{2\vec{q}\cdot(\vec{p}_1+\vec{p}_1'+\vec{l})}{2m_N}\,. \end{aligned}$$

The first term on the r.h.s. of the above expression is identical to the nucleon propagator and will give a factor of -1 when inserted into Eq. (F.5). The last term is a p-wave pion contribution and is ignored. Also the $2q_0$-term does not need to be taken into account as it

corresponds to a reducible contribution. Using $2p_1 + l = \tilde{l} + (p_1 + p_1') + q$, ignoring the p-wave pion terms, and evaluating the spin and isospin structures, we find:

$$iM^{\text{irred.}}_{\text{Box a}} = \frac{g_A}{4f_\pi^3}\int\frac{d^4l}{(2\pi)^4}\,B_2(l,\tilde{l})\Big\{-(S_1\cdot l) + \frac{S_1\cdot\tilde{l}}{2m_N}(v\cdot l) + \frac{S_1\cdot(p_1+p_1')}{2m_N}(v\cdot l)\Big\}[2\tau_- + \tau_\times].$$

F.1.6 Box diagram b

The Box b diagram given in Fig. 2.6 is very similar to the Box a diagram and the evaluation procedure is similar. We consider again only the irreducible contribution. The diagram gives:

$$\begin{aligned} iM_{\text{Box b}} &= \int\frac{d^4l}{(2\pi)^4}\,B_2(l,\tilde{l})\;\tau_2^c\tau_2^b\left(\frac{g_A}{f_\pi}\right)\tau_1^c\left(S_1\cdot\tilde{l} - \frac{S_1\cdot(2p_1'+\tilde{l})v\cdot\tilde{l}}{2m_N}\right) \\ &\quad\times\frac{i}{p_{10}' + \tilde{l}_0 - \frac{(\vec{p}_1'+\vec{\tilde{l}})^2}{2m_N}}\,\frac{1}{4f_\pi^2}\varepsilon^{bad}\tau_1^d\left(v\cdot(l+q) - \frac{(\vec{p}_1+\vec{p}_1'+\vec{\tilde{l}})\cdot(\vec{l}+\vec{q})}{2m_N}\right). \quad \text{(F.6)} \end{aligned}$$

Again, rewriting the pion-nucleon rescattering vertex using that p_1 is on shell, $p_{10} = \vec{p}_1^{\,2}/2m_N$ leads to :

$$\begin{aligned} &v\cdot(l+q) - \frac{(\vec{p}_1+\vec{p}_1'+\vec{\tilde{l}})\cdot(\vec{l}+\vec{q})}{2m_N} = \\ &= \left(p_{10}' + \tilde{l}_0 - \frac{(\vec{p}_1'+\vec{\tilde{l}})^2}{2m_N}\right) + 2q_0 - \frac{2\vec{q}\cdot(\vec{p}_1+\vec{p}_1'+\vec{\tilde{l}})}{2m_N}\,. \quad \text{(F.7)} \end{aligned}$$

The first factor on the r.h.s. of the Eq. (F.7), when coupled with the nucleon propagator in Eq. (F.6), yields a factor of 1 while the $2q_0$-term in Eq. (F.7) produces a reducible contribution included in the final NN state interaction. Using the relation $2p_1' + \tilde{l} = l + (p_1 + p_1') - q$, ignoring terms leading to outgoing p-wave pions and carrying out the spin and isospin algebra leads to:

$$iM^{\text{irred.}}_{\text{Box b}} = \frac{g_A}{4f_\pi^3}\int\frac{d^4l}{(2\pi)^4}\,B_2(l,\tilde{l})\Big\{(S_1\cdot\tilde{l}) - \frac{S_1\cdot l}{2m_N}(v\cdot\tilde{l}) - \frac{S_1\cdot(p_1+p_1')}{2m_N}(v\cdot\tilde{l})\Big\}[2\tau_- - \tau_\times].$$

Like the final expression for the Box a diagram, the first term starts at NLO and the next two terms are the N^{2}LO contributions to the amplitude.

F.2 Evaluation of the individual g_A-diagrams

In this appendix we derive the expression for two-pion exchange diagram linear in g_A for s-wave pions produced. The final expressions for the diagrams contain N^{2}LO contributions. The kinematics is defined in Fig. 2.8.

F.2.1 The "Football" diagram

The two pion propagators are tied together in pion-nucleon scattering vertices at both nucleons. Since this loop diagram involve just pion propagators, we have an extra symmetry factor 1/2 associated with the boson loop. The "football" diagram shown in Fig. 2.6 gives the following expression:

$$\begin{aligned} iM_{\rm F} &= \frac{1}{2}\int\frac{d^4l}{(2\pi)^4}\,D_2(l,\tilde{l})\;\varepsilon^{cby}\tau_2^y\left(\frac{g_A}{2f_\pi^3}\right) \\ &\quad\times\Big\{[\tau_1^a\delta^{bc}S_1\cdot(-l+\tilde{l})+\tau_1^b\delta^{ac}S_1\cdot(q+\tilde{l})+\tau_1^c\delta^{ab}S_1\cdot(q-l)] \\ &\quad-\frac{1}{2m_N}i\varepsilon^{abc}[v\cdot qS_1\cdot(-l-\tilde{l})-v\cdot lS_1\cdot(\tilde{l}-q)+v\cdot\tilde{l}S_1\cdot(q+l)] \\ &\quad-\frac{1}{2m_N}S_1\cdot(p_1+p_1')[\tau_1^a\delta^{bc}v\cdot(-l+\tilde{l})+\tau_1^b\delta^{ac}v\cdot(q+\tilde{l})+\tau_1^c\delta^{ab}v\cdot(q-l)]\Big\}. \end{aligned}$$

After performing some spin and isospin algebra, dropping terms corresponding to the outgoing p-wave pion and/or higher-order corrections we obtain

$$\begin{aligned} iM_{\rm F} &= i\frac{g_A}{8f_\pi^3}\int\frac{d^4l}{(2\pi)^4}\,D_2(l,\tilde{l})\Big\{\Big[(S_1\cdot l)+(S_1\cdot\tilde{l})\Big](-2\tau_\times) \\ &\quad+\left[\frac{S_1\cdot l}{2m_N}(v\cdot\tilde{l})-\frac{S_1\cdot\tilde{l}}{2m_N}(v\cdot l)\right](2\tau_+-2\tau_-)+\frac{S_1\cdot(p_1+p_1')}{2m_N}\Big[v\cdot l+v\cdot\tilde{l}\Big](2\tau_\times)\Big\}. \end{aligned} \tag{F.8}$$

The obtained result requires some clarification. Looking naively at the first line in Eq. (F.8), one may conjecture that this diagram starts to contribute already at NLO. Indeed, assuming $l_0\sim|\vec{l}|\sim p$, the dimensional analysis gives

$$\frac{p}{f_\pi^3}\cdot\frac{1}{f_\pi^2p^3}\cdot\frac{p^4}{(4\pi)^2}\sim\frac{1}{f_\pi^3}\frac{p^2}{m_N^2}$$

where the three terms on the l.h.s. stand for the $\pi\pi\pi NN$-vertex, the estimate of $D(l,\tilde{l})$ as follows from Eq. (2.13) and the integral measure, in order. Above we also used that $(4\pi f_\pi)^2\simeq m_N^2$. On the other hand, a more careful analysis shows that the first line of the integral in Eq. (F.8), which appears at NLO, is

$$iM_{\rm F}=\tau_\times\,\frac{g_A}{16f_\pi^5}\int\frac{d^4l}{(2\pi)^4}\,\frac{2l_0}{(l_0^2-\vec{l}^{\,2}+i0)(l_0^2-\vec{\tilde{l}}^{\,2}+i0)}\Big[(S_1\cdot l)+(S_1\cdot\tilde{l})\Big],$$

where we have used that $l_0\sim|\vec{l}|\sim p\gg m_\pi$ to drop all subleading contributions including the $1/m_N$ terms in the curly bracket of the integrand. This last integral, however, vanishes when integrating over l_0 because the numerator of the integrand is an odd function of l_0 whereas the denominator is an even one. The next-higher order contributions in Eq. (F.8) do not vanish. They scale as m_π/p and p/m_N compared to NLO and thus emerge at N^{2}LO. Following the same lines, one can show that also the other diagrams of g_A-topology start to contribute at N^{2}LO.

F.2.2 Diagram Ia

The double-scattering diagram Ia shown in Fig. 2.6 gives the following expression

$$iM_{\rm Ia} = \int\frac{d^4l}{(2\pi)^4}\,D_2(l,\tilde{l})\varepsilon^{cby}\tau_2^y\left(\frac{1}{4f_\pi^2}\right)\varepsilon^{bad}\tau_1^d\left(v\cdot(l+q)-\frac{(\vec{p}_1+\vec{p}_1'-\vec{\tilde{l}})\cdot(\vec{l}+\vec{q})}{2m_N}\right)$$
$$\times\frac{i}{p_{10}-\tilde{l}_0-\frac{(\vec{p}_1-\vec{\tilde{l}})^2}{2m_N}+i0}\left(\frac{g_A}{f_\pi}\right)\tau_1^c\left(S_1\cdot\tilde{l}-\frac{S_1\cdot(2p_1-\tilde{l})v\cdot\tilde{l}}{2m_N}\right).$$

In the $\pi N\to\pi N$ rescattering vertex (off nucleon 1) we included the leading WT vertex contribution together with its recoil correction. However, we dropped the subleading c_i-terms in this vertex since they are of higher order. The $\pi N\to\pi N$ vertex expression is rewritten the same way as for diagram IIIa, shown in Eq. (F.2).

Using that $p_{10}'=\vec{p}_1'^{\,2}/2m_N$, collecting the spin structures and performing the isospin algebra we get:

$$iM_{\rm Ia} = i\frac{g_A}{8f_\pi^3}\int\frac{d^4l}{(2\pi)^4}\,D_2(l,\tilde{l})\Big\{-(S_1\cdot l)-(S_1\cdot\tilde{l})-\frac{S_1\cdot l}{2m_N}\left(v\cdot\tilde{l}\right)+\frac{S_1\cdot\tilde{l}}{2m_N}(v\cdot l)$$
$$+\frac{S_1\cdot(p_1+p_1')}{2m_N}\left[v\cdot l+v\cdot\tilde{l}\right]+\frac{4v\cdot q}{-v\cdot l+i0}\left(S_1\cdot\tilde{l}\right)\Big\}(\tau_+-\tau_--\tau_\times).$$

This amplitude starts to contribute at N^{2}LO, see discussion in Appendix F.2.1 for more details.

F.2.3 Diagram Ib

The double-scattering diagram Ib in Fig. 2.6 gives an initial expression:

$$iM_{\rm Ib} = \int\frac{d^4l}{(2\pi)^4}\,D_2(l,\tilde{l})\varepsilon^{cby}\tau_2^y(-1)\frac{g_A}{f_\pi}\tau_1^b\left(S_1\cdot l-\frac{S_1\cdot(2p_1'-l)v\cdot l}{2m_N}\right)$$
$$\times\frac{i}{p_{10}'-l_0-\frac{(\vec{p}_1'-\vec{l})^2}{2m_N}+i0}\frac{1}{4f_\pi^2}\varepsilon^{cad}\tau_1^d\left(v\cdot(-\tilde{l}+q)-\frac{(\vec{p}_1+\vec{p}_1'-\vec{l})\cdot(-\vec{\tilde{l}}+\vec{q})}{2m_N}\right).$$

Again, the $\pi N\to\pi N$ vertex is rewritten as sum of two terms as for diagram IIIb, see Eq. (F.3). We follow the simplifications discussed for diagram IIIb, and use that $p_{10}=\vec{p}_1^{\,2}/(2m_N)$. Using again $l\to-\tilde{l}$ etc. to simplify the integrals containing the function $D_2(l,\tilde{l})$, collecting spin structures and performing the isospin algebra we get:

$$iM_{\rm Ib} = i\frac{g_A}{8f_\pi^3}\int\frac{d^4l}{(2\pi)^4}\,D_2(l,\tilde{l})\Big\{(S_1\cdot l)+(S_1\cdot\tilde{l})-\frac{S_1\cdot l}{2m_N}\left(v\cdot\tilde{l}\right)+\frac{S_1\cdot\tilde{l}}{2m_N}(v\cdot l)$$
$$-\frac{S_1\cdot(p_1+p_1')}{2m_N}\left[v\cdot l+v\cdot\tilde{l}\right]+\frac{4v\cdot q}{-v\cdot l+i0}\left(S_1\cdot l\right)\Big\}[\tau_+-\tau_-+\tau_\times].$$

This amplitude also starts to contribute at N^{2}LO, see comment in Appendix F.2.1 for more details.

F.2.4 The "Mini-Football" diagram

The contribution of the "mini-football" diagram in Fig. 2.6 can be written as

$$\begin{aligned} iM_{\rm mF} &= \frac{1}{2}\int\frac{d^4l}{(2\pi)^4}\,D_2(l,\tilde{l})\;\varepsilon^{cby}\tau_2^y\left(\frac{g_A}{f_\pi}\right)\tau_1^d\left(S_1\cdot k_1-\frac{S_1\cdot(p_1+p_1')v\cdot k_1}{2m_N}\right)\frac{i}{k_1^2-m_\pi^2+i0} \\ &\quad\times\frac{i}{f_\pi^2}\left\{\delta^{ab}\delta^{cd}\left[(l-q)^2-m_\pi^2\right]+\delta^{ac}\delta^{bd}\left[(\tilde{l}+q)^2-m_\pi^2\right]+\delta^{ad}\delta^{bc}\left[(k_1-q)^2-m_\pi^2\right]\right\}. \end{aligned}$$

The four-pion vertex can be rewritten as a sum of six terms

$$\begin{aligned} &\frac{i}{f_\pi^2}\left\{\delta^{ab}\delta^{cd}\left[(l-q)^2-m_\pi^2\right]+\delta^{ac}\delta^{bd}\left[(\tilde{l}+q)^2-m_\pi^2\right]+\delta^{ad}\delta^{bc}\left[(k_1-q)^2-m_\pi^2\right]\right\}= \\ &=\frac{i}{f_\pi^2}\Big\{\delta^{ab}\delta^{cd}\left[l^2-m_\pi^2\right]+\delta^{ac}\delta^{bd}\left[\tilde{l}^2-m_\pi^2\right]+\delta^{ad}\delta^{bc}\left[k_1^2-m_\pi^2\right] \\ &+\delta^{ab}\delta^{cd}\left[-2l\cdot q+q^2\right]+\delta^{ac}\delta^{bd}\left[2\tilde{l}\cdot q+q^2\right]+\delta^{ad}\delta^{bc}\left[-2k_1\cdot q+q^2\right]\Big\}. \end{aligned}$$

Following the arguments outlined in the derivation of the contribution from diagram IV, see the discussion below Eq. (F.4), most terms either contribute to outgoing p-wave pions or higher orders in the chiral expansion. The final result reads:

$$iM_{\rm mF}=i\frac{g_A}{8f_\pi^3}\int\frac{d^4l}{(2\pi)^4}\,D_2(l,\tilde{l})\,(S_1\cdot k_1)\left\{\frac{q\cdot(l+\tilde{l})}{k_1^2-m_\pi^2+i0}\right\}(8\tau_\times).$$

This amplitude starts to contribute at $\mathrm{N^2LO}$.

Appendix G

Expressions for loop-integrals

In this Appendix we provide expressions for loop integrals required to calculate the transition amplitude at $\mathrm{N^2LO}$. Using dimensional regularization and integration procedure described in Appendix E of Ref. [PMR93], we obtained the following results:

$$\frac{1}{i}\int\frac{d^4l}{(2\pi)^4}\frac{v\cdot(l+\tilde{l})S_1\cdot(l+\tilde{l})}{(l^2-m_\pi^2+i0)(\tilde{l}^2-m_\pi^2+i0)(-v\cdot l+i0)}\simeq 0, \tag{G.1}$$

$$\frac{1}{i}\int\frac{d^4l}{(2\pi)^4}\frac{v\cdot(l+\tilde{l})}{(l^2-m_\pi^2+i0)(\tilde{l}^2-m_\pi^2+i0)(-v\cdot l+i0)}\simeq -2J(k_1^2), \tag{G.2}$$

$$\frac{1}{i}\int\frac{d^4l}{(2\pi)^4}\frac{v\cdot(l+\tilde{l})\,q\cdot(l+\tilde{l})}{(l^2-m_\pi^2+i0)(\tilde{l}^2-m_\pi^2+i0)}\simeq 2k_1^2(v\cdot q)\left[-\frac{1}{6}J(k_1^2)-\frac{1}{9}\frac{1}{(4\pi)^2}\right], \tag{G.3}$$

$$\frac{1}{i}\int\frac{d^4l}{(2\pi)^4}\frac{(S_2\cdot\tilde{l})\,(S_2\cdot l)\,S_1\cdot(l+\tilde{l})}{(l^2-m_\pi^2+i0)(\tilde{l}^2-m_\pi^2+i0)(-v\cdot l+i0)^2}\simeq -i\varepsilon^{\mu\nu\alpha\beta}k_{1\mu}S_{1\nu}v_\alpha S_{2\beta}J(k_1^2), \tag{G.4}$$

$$\frac{1}{i}\int\frac{d^4l}{(2\pi)^4}\frac{(S_2\cdot\tilde{l})\,(S_2\cdot l)}{(l^2-m_\pi^2+i0)(\tilde{l}^2-m_\pi^2+i0)(-v\cdot l+i0)^2}\simeq \frac{3}{4}J(k_1^2)-\frac{1}{(4\pi)^2}, \tag{G.5}$$

$$\frac{1}{i}\int\frac{d^4l}{(2\pi)^4}\frac{(S_2\cdot\tilde{l})\,(S_2\cdot l)\,q\cdot(l+\tilde{l})}{(l^2-m_\pi^2+i0)(\tilde{l}^2-m_\pi^2+i0)(-v\cdot l+i0)}\simeq v\cdot q\frac{k_1^2}{2}\left[-\frac{5}{12}J(k_1^2)+\frac{1}{18}\frac{1}{(4\pi)^2}\right], \tag{G.6}$$

where integral $J(k_1^2)$ is given by Eq. (2.11), and only the leading loop contributions for the s-wave pion in MCS are kept.

Acknowledgments

At the end of this thesis, I would like to express my gratitude towards all those people who helped me in various ways during the work on this thesis.

First of all, I would like to thank Prof. Dr. Evgeny Epelbaum for his continuous support and encouragement during this work. I am also thankful to him for arranging various travels and for making many useful comments on this manuscript.

I would like to thank Dr. Vadim Baru for great collaboration and support during all periods of my work. I appreciate his enthusiasm in teaching me a lot of different topics from violation of isospin in the Standard Model to returning heavy topspins in table tennis. I would also like to thank him for numerous useful comments on this manuscript.

I am grateful to my collaborators: Prof. Alexander Kudryavtsev, Dr. Christoph Hanhart, Prof. Fred Myhrer, Dr. Hermann Krebs, Dr. Johann Haidenbauer, Prof. Dr. Ulf.-G. Meißner, Dr. Alexey Nefediev and Dr. Yulia S. Kalashnikova for numerous fruitful discussions and enjoyable collaboration.

I want to say 'thank you' to Julia, Jan, Bart and all members of the Institut für Theoretische Physik II of the Ruhr-Universität Bochum for warm and friendly atmosphere.

I would like to thank the members of Institut für Kernphysik (Theorie) of the Forschungszentrum Jülich, where a part this thesis was done.

I want to thank the organizers of Hadron Physics Summer School, Les Nabis School on Amplitude Analysis in Modern Physics, and Student Training Days on Data analysis for fun and educative events.

I am grateful to Prof. Koji Harada for inviting me to visit Kyushu University. I want to thank him, Dr. Hirofumi Kubo and Takuya Minakuchi for their kind hospitality during my stay in Fukuoka.

Finally, I am sincerely grateful to my parents and all my family for their support and warm encouragement during all stages of this work.

Bibliography

[A+13] P. Adlarson et al., *Investigation of the $dd \to {}^3He n\pi^0$ reaction with the FZ Jülich WASA-at-COSY facility*, Phys.Rev. **C88** (2013), no. 1, 014004.

[ABB+89] R. Abegg, D. Bandyopadhyay, J. Birchall, E. Cairns, G. Coombes, et al., *Charge Symmetry Breaking in np Elastic Scattering at 477-MeV*, Phys.Rev. **D39** (1989), 2464.

[ABSW07] R. Arndt, W. Briscoe, I. Strakovsky, and R. Workman, *Updated analysis of NN elastic scattering to 3-GeV*, Phys.Rev. **C76** (2007), 025209.

[AC75] T. Appelquist and J. Carazzone, *Infrared Singularities and Massive Fields*, Phys.Rev. **D11** (1975), 2856.

[APM01] S.-i. Ando, T.-S. Park, and D.-P. Min, *Threshold $pp \to pp\pi^0$ up to one loop accuracy*, Phys.Lett. **B509** (2001), 253–262.

[AS+03] S. AbdEl Samad et al., *Study of the reaction $pp \to pp\pi^0$ within 10-MeV above the threshold*, Eur.Phys.J. **A17** (2003), 595–606.

[B+12] J. Beringer et al., *Review of Particle Physics (RPP)*, Phys.Rev. **D86** (2012), 010001.

[BBH+00] S. R. Beane, P. F. Bedaque, W. C. Haxton, D. R. Phillips, and M. J. Savage, *From hadrons to nuclei: Crossing the border*.

[BCE+85] L. Barkov, A. Chilingarov, S. Eidelman, B. Khazin, M. Y. Lelchuk, et al., *Electromagnetic Pion Form-Factor in the Timelike Region*, Nucl.Phys. **B256** (1985), 365–384.

[BEH+09] V. Baru, E. Epelbaum, J. Haidenbauer, C. Hanhart, A. Kudryavtsev, et al., *p-wave pion production from nucleon-nucleon collisions*, Phys.Rev. **C80** (2009), 044003.

[Ber08] V. Bernard, *Chiral Perturbation Theory and Baryon Properties*, Prog.Part.Nucl.Phys. **60** (2008), 82–160.

[BFHM98] V. Bernard, H. W. Fearing, T. R. Hemmert, and U.-G. Meißner, *The form-factors of the nucleon at small momentum transfer*, Nucl.Phys. **A635** (1998), 121–145.

[BG07] J. Bijnens and K. Ghorbani, $\eta \to 3\pi$ *at Two Loops In Chiral Perturbation Theory*, JHEP **0711** (2007), 030.

[BHH+07] V. Baru, J. Haidenbauer, C. Hanhart, A. E. Kudryavtsev, V. Lensky, et al., *Progress in* $NN \to NN\pi$, eConf **C070910** (2007), 128.

[BHH+11a] V. Baru, C. Hanhart, M. Hoferichter, B. Kubis, A. Nogga, et al., *Precision calculation of the* π^- *deuteron scattering length and its impact on threshold* πN *scattering*, Phys.Lett. **B694** (2011), 473–477.

[BHH+11b] V. Baru, C. Hanhart, M. Hoferichter, B. Kubis, A. Nogga, et al., *Precision calculation of threshold* $\pi^- d$ *scattering,* πN *scattering lengths, and the GMO sum rule*, Nucl.Phys. **A872** (2011), 69–116.

[BHM14] V. Baru, C. Hanhart, and F. Myhrer, *Effective Field Theory calculations of* $NN \to NN\pi$, Int.J.Mod.Phys. **E23** (2014), 1430004.

[BK99] R. Baur and J. Kambor, *Generalized heavy baryon chiral perturbation theory*, Eur.Phys.J. **C7** (1999), 507–524.

[BKM95] V. Bernard, N. Kaiser, and U.-G. Meißner, *Chiral dynamics in nucleons and nuclei*, Int.J.Mod.Phys. **E4** (1995), 193–346.

[BKM97] V. Bernard, N. Kaiser, and U.-G. Meißner, *Aspects of chiral pion-nucleon physics*, Nucl.Phys. **A615** (1997), 483–500.

[BL99] T. Becher and H. Leutwyler, *Baryon chiral perturbation theory in manifestly Lorentz invariant form*, Eur.Phys.J. **C9** (1999), 643–671.

[BM10] D. R. Bolton and G. A. Miller, *Charge Symmetry Breaking in the* $np \to d\pi^0$ *reaction*, Phys.Rev. **C81** (2010), 014001.

[BM11] D. R. Bolton and G. A. Miller, *Impulse approximation in nuclear pion production reactions: absence of a one-body operator*, Phys.Rev. **C83** (2011), 064003.

[Bol11] D. R. Bolton, *Charge Symmetry Breaking and Nuclear Pion Production Reactions*, Ph.D. thesis, University of Washington, 2011.

[BOS07] S. R. Beane, K. Orginos, and M. J. Savage, *Strong-isospin violation in the neutron-proton mass difference from fully-dynamical lattice QCD and PQQCD*, Nucl.Phys. **B768** (2007), 38–50.

[BvK02] P. F. Bedaque and U. van Kolck, *Effective field theory for few nucleon systems*, Ann.Rev.Nucl.Part.Sci. **52** (2002), 339–396.

[BZD+10] T. Blum, R. Zhou, T. Doi, M. Hayakawa, T. Izubuchi, et al., *Electromagnetic mass splittings of the low lying hadrons and quark masses from 2+1 flavor lattice QCD+QED*, Phys.Rev. **D82** (2010), 094508.

[CFMvK96] T. D. Cohen, J. L. Friar, G. A. Miller, and U. van Kolck, *The $pp \to pp\pi^0$ reaction near threshold: A Chiral power counting approach*, Phys.Rev. **C53** (1996), 2661–2673.

[CGL01] G. Colangelo, J. Gasser, and H. Leutwyler, *$\pi\pi$ scattering*, Nucl.Phys. **B603** (2001), 125–179.

[Cot63] W. Cottingham, *The neutron proton mass difference and electron scattering experiments*, Annals Phys. **25** (1963), 424–432.

[CS95] S. Coon and M. Scadron, *Universality of $\Delta I = 1$ meson mixing and charge symmetry breaking*, Phys.Rev. **C51** (1995), 2923–2931.

[D$^+$12] S. Dymov et al., *Differential cross section and analysing power of the quasi-free $pn \to \{pp\}_s\pi^-$ reaction at 353 MeV*, Phys.Lett. **B712** (2012), 375–380.

[D$^+$13] S. Dymov et al., *Measurement of spin observables in the quasi-free $np \to \{pp\}_s\pi^-$ reaction at 353 MeV*, Phys.Rev. **C88** (2013), no. 1, 014001.

[dDDF$^+$12] G. de Divitiis, P. Dimopoulos, R. Frezzotti, V. Lubicz, G. Martinelli, et al., *Isospin breaking effects due to the up-down mass difference in Lattice QCD*, JHEP **1204** (2012), 124.

[DKMS99] V. Dmitrasinovic, K. Kubodera, F. Myhrer, and T. Sato, *A Next-to-next-to leading order $pp \to pp\pi^0$ transition operator in chiral perturbation theory*, Phys.Lett. **B465** (1999), 43–54.

[dRMvK00] C. da Rocha, G. Miller, and U. van Kolck, *The $NN \to NN\pi^+$ reaction near threshold in a chiral power counting approach*, Phys.Rev. **C61** (2000), 034613.

[EGM98] E. Epelbaum, W. Gloeckle, and U.-G. Meißner, *Nuclear forces from chiral Lagrangians using the method of unitary transformation. 1. Formalism*, Nucl.Phys. **A637** (1998), 107–134.

[EGM05] E. Epelbaum, W. Glockle, and U.-G. Meißner, *The Two-nucleon system at next-to-next-to-next-to-leading order*, Nucl.Phys. **A747** (2005), 362–424.

[EGPdR89] G. Ecker, J. Gasser, A. Pich, and E. de Rafael, *The Role of Resonances in Chiral Perturbation Theory*, Nucl.Phys. **B321** (1989), 311.

[EHM09] E. Epelbaum, H.-W. Hammer, and U.-G. Meißner, *Modern Theory of Nuclear Forces*, Rev.Mod.Phys. **81** (2009), 1773–1825.

[EKL$^+$13] E. Epelbaum, H. Krebs, T. A. Lähde, D. Lee, and U.-G. Meißner, *Viability of Carbon-Based Life as a Function of the Light Quark Mass*, Phys.Rev.Lett. **110** (2013), no. 11, 112502.

[EKL$^+$14] E. Epelbaum, H. Krebs, T. A. Lähde, D. Lee, U.-G. Meißner, et al., *Ab initio calculation of the spectrum and structure of ^{16}O*, Phys.Rev.Lett. **112** (2014), 102501.

[EKLM11] E. Epelbaum, H. Krebs, D. Lee, and U.-G. Meißner, *Ab initio calculation of the Hoyle state*, Phys.Rev.Lett. **106** (2011), 192501.

[EKM08] E. Epelbaum, H. Krebs, and U.-G. Meißner, *Delta-excitations and the three-nucleon force*, Nucl.Phys. **A806** (2008), 65–78.

[EM05] E. Epelbaum and U.-G. Meißner, *Isospin-violating nucleon-nucleon forces using the method of unitary transformation*, Phys.Rev. **C72** (2005), 044001.

[EMP05] E. Epelbaum, U.-G. Meißner, and J. Palomar, *Isospin dependence of the three-nucleon force*, Phys.Rev. **C71** (2005), 024001.

[ENG+02] E. Epelbaum, A. Nogga, W. Gloeckle, H. Kamada, U.-G. Meißner, et al., *Three nucleon forces from chiral effective field theory*, Phys.Rev. **C66** (2002), 064001.

[Epe06] E. Epelbaum, *Few-nucleon forces and systems in chiral effective field theory*, Prog.Part.Nucl.Phys. **57** (2006), 654–741.

[Epe14] E. Epelbaum, personal communication, 2014.

[FBE+09] A. Filin, V. Baru, E. Epelbaum, J. Haidenbauer, C. Hanhart, et al., *Extraction of the strong neutron-proton mass difference from the charge symmetry breaking in $pn \to d\pi^0$*, Phys.Lett. **B681** (2009), 423–427.

[FBE+12] A. Filin, V. Baru, E. Epelbaum, H. Krebs, C. Hanhart, et al., *Pion production in nucleon-nucleon collisions in chiral effective field theory: next-to-next-to-leading order contributions*, Phys.Rev. **C85** (2012), 054001.

[FBE+13] A. Filin, V. Baru, E. Epelbaum, C. Hanhart, H. Krebs, et al., *Pion production in nucleon-nucleon collisions in chiral effective field theory with Delta(1232)-degrees of freedom.*

[FM01a] N. Fettes and U.-G. Meißner, *Complete analysis of pion nucleon scattering in chiral perturbation theory to third order*, Nucl.Phys. **A693** (2001), 693–709.

[FM01b] N. Fettes and U.-G. Meißner, *Pion-nucleon scattering in an effective chiral field theory with explicit spin 3/2 fields*, Nucl.Phys. **A679** (2001), 629–670.

[FM01c] N. Fettes and U.-G. Meißner, *Towards an understanding of isospin violation in pion nucleon scattering*, Phys.Rev. **C63** (2001), 045201.

[FMM09] A. Fonseca, R. Machleidt, and G. Miller, *Nucleon-nucleon charge symmetry breaking and the dd $\to$ alpha pi0 reaction*, Phys.Rev. **C80** (2009), 027001.

[FMMS00] N. Fettes, U.-G. Meißner, M. Mojzis, and S. Steininger, *The Chiral effective pion nucleon Lagrangian of order p^4*, Annals Phys. **283** (2000), 273–302.

[FMS98] N. Fettes, U.-G. Meißner, and S. Steininger, *Pion-nucleon scattering in chiral perturbation theory. 1. Isospin symmetric case*, Nucl.Phys. **A640** (1998), 199–234.

[FMS99] N. Fettes, U.-G. Meißner, and S. Steininger, *On the size of isospin violation in low-energy pion-nucleon scattering*, Phys.Lett. **B451** (1999), 233–240.

[FvKRT04] J. L. Friar, U. van Kolck, M. Rentmeester, and R. Timmermans, *The Nucleon-mass difference in chiral perturbation theory and nuclear forces*, Phys.Rev. **C70** (2004), 044001.

[GHKM08] F.-K. Guo, C. Hanhart, S. Krewald, and U.-G. Meißner, *Subleading contributions to the width of the $D_{s0}^*(2317)$*, Phys.Lett. **B666** (2008), 251–255.

[GHN+04] A. Gardestig, C. Horowitz, A. Nogga, A. Fonseca, C. Hanhart, et al., *Survey of charge symmetry breaking operators for $dd \to \alpha\pi^0$*, Phys.Rev. **C69** (2004), 044606.

[GL82] J. Gasser and H. Leutwyler, *Quark Masses*, Phys.Rept. **87** (1982), 77–169.

[GL84] J. Gasser and H. Leutwyler, *Chiral Perturbation Theory to One Loop*, Annals Phys. **158** (1984), 142.

[Gol61] J. Goldstone, *Field Theories with Superconductor Solutions*, Nuovo Cim. **19** (1961), 154–164.

[GP06] A. Gardestig and D. R. Phillips, *Using chiral perturbation theory to extract the neutron-neutron scattering length from $\pi^- d \to nn\gamma$*, Phys.Rev. **C73** (2006), 014002.

[GQN09] D. Gazit, S. Quaglioni, and P. Navratil, *Three-Nucleon Low-Energy Constants from the Consistency of Interactions and Currents in Chiral Effective Field Theory*, Phys.Rev.Lett. **103** (2009), 102502.

[GSS88] J. Gasser, M. Sainio, and A. Svarc, *Nucleons with Chiral Loops*, Nucl.Phys. **B307** (1988), 779.

[GW73] D. J. Gross and F. Wilczek, *Ultraviolet Behavior of Nonabelian Gauge Theories*, Phys.Rev.Lett. **30** (1973), 1343–1346.

[Han04] C. Hanhart, *Meson production in nucleon-nucleon collisions close to the threshold*, Phys.Rept. **397** (2004), 155–256.

[Hem96] T. R. Hemmert, *Heavy baryon chiral perturbation theory with light Deltas*, Ph.D. thesis, University of Massachusetts Amherst, 1996.

[HHH+98] C. Hanhart, J. Haidenbauer, M. Hoffmann, U.-G. Meißner, and J. Speth, *The Reactions $pp \to pp\pi^0$ and $pp \to d\pi^+$ at threshold: The Role of the isoscalar πN scattering amplitude*, Phys.Lett. **B424** (1998), 8–14.

[HHJ93] J. Haidenbauer, K. Holinde, and M. B. Johnson, *A Coupled channel potential for nucleons and deltas*, Phys.Rev. **C48** (1993), 2190–2200.

[HHK98] T. R. Hemmert, B. R. Holstein, and J. Kambor, *Chiral Lagrangians and delta(1232) interactions: Formalism*, J.Phys. **G24** (1998), 1831–1859.

[HHKS98] C. Hanhart, J. Haidenbauer, O. Krehl, and J. Speth, *Role of the Delta isobar in the reaction $NN \to NN\pi$ near threshold*, Phys.Lett. **B444** (1998), 25–31.

[HHKS00] C. Hanhart, J. Haidenbauer, O. Krehl, and J. Speth, *Polarization phenomena in the reaction $NN \to NN\pi$ near threshold*, Phys.Rev. **C61** (2000), 064008.

[HHR+95] C. Hanhart, J. Haidenbauer, A. Reuber, C. Schutz, and J. Speth, *The Reaction $pp \to pp\pi^0$ near threshold*, Phys.Lett. **B358** (1995), 21–26.

[HK02] C. Hanhart and N. Kaiser, *Complete next-to-leading order calculation for pion production in nucleon-nucleon collisions at threshold*, Phys.Rev. **C66** (2002), 054005.

[HKM09] M. Hoferichter, B. Kubis, and U.-G. Meißner, *Isospin breaking in the pion-nucleon scattering lengths*, Phys.Lett. **B678** (2009), 65–71.

[HKM10] M. Hoferichter, B. Kubis, and U.-G. Meißner, *Isospin Violation in Low-Energy Pion-Nucleon Scattering Revisited*, Nucl.Phys. **A833** (2010), 18–103.

[HMG94] C. Horowitz, H. Meyer, and D. K. Griegel, *Role of heavy meson exchange in pion production near threshold*, Phys.Rev. **C49** (1994), 1337–1346.

[HO95] E. Hernandez and E. Oset, *Off-shell πN amplitude and the $pp \to pp\pi^0$ reaction near threshold*, Phys.Lett. **B350** (1995), 158–162.

[Hor93] C. Horowitz, *Role of heavy meson exchange in near threshold $NN \to d\pi$*, Phys.Rev. **C48** (1993), 2920–2925.

[HvKM00] C. Hanhart, U. van Kolck, and G. Miller, *Chiral three nucleon forces from p-wave pion production*, Phys.Rev.Lett. **85** (2000), 2905–2908.

[HW07] C. Hanhart and A. Wirzba, *Remarks on $NN \to NN\pi$ beyond leading order*, Phys.Lett. **B650** (2007), 354–361.

[JM91] E. E. Jenkins and A. V. Manohar, *Baryon chiral perturbation theory using a heavy fermion Lagrangian*, Phys.Lett. **B255** (1991), 558–562.

[KEM07] H. Krebs, E. Epelbaum, and U.-G. Meißner, *Nuclear forces with Delta-excitations up to next-to-next-to-leading order. I. Peripheral nucleon-nucleon waves*, Eur.Phys.J. **A32** (2007), 127–137.

[KGE12] H. Krebs, A. Gasparyan, and E. Epelbaum, *Chiral three-nucleon force at N^4LO I: Longest-range contributions*, Phys.Rev. **C85** (2012), 054006.

[KR66] D. Koltun and A. Reitan, *Production and absorption of S-wave pions at low energy by two nucleons*, Phys.Rev. **141** (1966), 1413–1418.

[Kra90] A. Krause, *Baryon Matrix Elements of the Vector Current in Chiral Perturbation Theory*, Helv.Phys.Acta **63** (1990), 3–70.

[KSMK09] Y. Kim, T. Sato, F. Myhrer, and K. Kubodera, *Two-pion-exchange and other higher-order contributions to the $pp \to pp\pi^0$ reaction*, Phys.Rev. **C80** (2009), 015206.

[LBE+07] V. Lensky, V. Baru, E. Epelbaum, C. Hanhart, J. Haidenbauer, et al., *Neutron-neutron scattering length from the reaction $\gamma d \to \pi^+ nn$ employing chiral perturbation theory*, Eur.Phys.J. **A33** (2007), 339–348.

[LBH+05] V. Lensky, V. Baru, J. Haidenbauer, C. Hanhart, A. E. Kudryavtsev, et al., *Precision calculation of $\gamma d \to \pi^+ nn$ within chiral perturbation theory*, Eur.Phys.J. **A26** (2005), 107–123.

[LBH+06] V. Lensky, V. Baru, J. Haidenbauer, C. Hanhart, A. E. Kudryavtsev, et al., *Towards a field theoretic understanding of $NN \to NN\pi$*, Eur.Phys.J. **A27** (2006), 37–45.

[LBH+07] V. Lensky, V. Baru, J. Haidenbauer, C. Hanhart, A. E. Kudryavtsev, et al., *Dispersive and absorptive corrections to the pion-deuteron scattering length*, Phys.Lett. **B648** (2007), 46–53.

[Len07] V. Lensky, *Elastic and Inelastic Pion Reactions on Few Nucleon Systems*, Ph.D. thesis, Bonn University, 2007.

[LR93] T. Lee and D. Riska, *Short range exchange contributions to the cross-section for $pp \to pp\pi^0$ near threshold*, Phys.Rev.Lett. **70** (1993), 2237–2240.

[ME11] R. Machleidt and D. Entem, *Chiral effective field theory and nuclear forces*, Phys.Rept. **503** (2011), 1–75.

[MHN+92] H. Meyer, C. Horowitz, H. Nann, P. Pancella, S. Pate, et al., *Total cross-section for $p + p \to p + p + \pi^0$ close to threshold*, Nucl.Phys. **A539** (1992), 633–661.

[MMS97] U.-G. Meißner, G. Muller, and S. Steininger, *Virtual photons in SU(2) chiral perturbation theory and electromagnetic corrections to $\pi\pi$ scattering*, Phys.Lett. **B406** (1997), 154–160.

[MNS90] G. Miller, B. Nefkens, and I. Slaus, *Charge symmetry, quarks and mesons*, Phys.Rept. **194** (1990), 1–116.

[MOS06] G. A. Miller, A. K. Opper, and E. J. Stephenson, *Charge symmetry breaking and QCD*, Ann.Rev.Nucl.Part.Sci. **56** (2006), 253–292.

[MS98] U.-G. Meißner and S. Steininger, *Isospin violation in pion nucleon scattering*, Phys.Lett. **B419** (1998), 403–411.

[NFG+06] A. Nogga, A. Fonseca, A. Gardestig, C. Hanhart, C. Horowitz, et al., *Realistic few-body physics in the $dd \to \alpha\pi^0$ reaction*, Phys.Lett. **B639** (2006), 465–470.

[Nis78] J. Niskanen, *The Differential Cross-Section and Polarization in $pp \to d\pi^+$*, Nucl.Phys. **A298** (1978), 417–451.

[Nis96] J. Niskanen, *Comment on 'Role of heavy meson exchange in near threshold $NN \to d\pi$'*, Phys.Rev. **C53** (1996), 526–528.

[Nis99] J. Niskanen, *Isospin breaking in the reaction $np \to d\pi^0$ at threshold*, Few Body Syst. **26** (1999), 241–249.

[NS69] J. Nolen, Jr. and J. Schiffer, *Coulomb energies*, Ann.Rev.Nucl.Part.Sci. **19** (1969), 471–526.

[OKH+03] A. Opper, E. J. Korkmaz, D. Hutcheon, R. Abegg, C. Davis, et al., *Charge symmetry breaking in $np \to d\pi^0$*, Phys.Rev.Lett. **91** (2003), 212302.

[ORvK94] C. Ordóñez, L. Ray, and U. van Kolck, *Nucleon-nucleon potential from an effective chiral Lagrangian*, Phys.Rev.Lett. **72** (1994), 1982–1985.

[ORvK96] C. Ordóñez, L. Ray, and U. van Kolck, *The Two nucleon potential from chiral Lagrangians*, Phys.Rev. **C53** (1996), 2086–2105.

[Pic95] A. Pich, *Chiral perturbation theory*, Rept.Prog.Phys. **58** (1995), 563–610.

[PMM+96] B. Park, F. Myhrer, J. Morones, T. Meissner, and K. Kubodera, *Chiral perturbation approach to the $pp \to pp\pi^0$ reaction near threshold*, Phys.Rev. **C53** (1996), 1519–1531.

[PMR93] T.-S. Park, D.-P. Min, and M. Rho, *Chiral dynamics and heavy fermion formalism in nuclei. 1. Exchange axial currents*, Phys.Rept. **233** (1993), 341–395.

[Pol73] H. D. Politzer, *Reliable Perturbative Results for Strong Interactions?*, Phys.Rev.Lett. **30** (1973), 1346–1349.

[RS41] W. Rarita and J. Schwinger, *On a theory of particles with half integral spin*, Phys.Rev. **60** (1941), 61.

[SAA+10] T. Strauch, F. Amaro, D. Anagnostopoulos, P. Buhler, D. Covita, et al., *Precision determination of the $d\pi \to NN$ transition strength at threshold*, Phys.Rev.Lett. **104** (2010), 142503.

[SAA+11] T. Strauch, F. Amaro, D. Anagnostopoulos, P. Buhler, D. Covita, et al., *Pionic deuterium*, Eur.Phys.J. **A47** (2011), 88.

[SBA+03] E. Stephenson, A. Bacher, C. Allgower, A. Gardestig, C. Lavelle, et al., *Observation of the charge symmetry breaking $d + d \to {}^4He + \pi^0$ reaction near threshold*, Phys.Rev.Lett. **91** (2003), 142302.

[Sch03] S. Scherer, *Introduction to chiral perturbation theory*, Adv.Nucl.Phys. **27** (2003), 277.

[SGS04] M. R. Schindler, J. Gegelia, and S. Scherer, *Infrared regularization of baryon chiral perturbation theory reformulated*, Phys.Lett. **B586** (2004), 258–266.

[SLMK97] T. Sato, T. Lee, F. Myhrer, and K. Kubodera, *Chiral perturbation theory and the $pp \to pp\pi^0$ reaction near threshold*, Phys.Rev. **C56** (1997), 1246–1255.

[SS12] S. Scherer and M. R. Schindler, *A primer for chiral perturbation theory*, Springer Berlin Heidelberg, 2012.

[Ste99] S. Steininger, *Reelle und virtuelle Photonen in chiraler Störungstheorie*, Ph.D. thesis, Bonn University, 1999.

[T+12] D. Tsirkov et al., *Differential cross section and analysing power of the $pp \to \{pp\}_s\pi^0$ reaction at 353 MeV*, Phys.Lett. **B712** (2012), 370–374.

[VJK+92] S. Vigdor, W. Jacobs, L. Knutson, J. Sowinski, C. Bloch, et al., *Charge symmetry breaking in n (polarized) p (polarized) scattering at 183-MeV*, Phys.Rev. **C46** (1992), 410–448.

[vKMR96] U. van Kolck, G. Miller, and D. Riska, *Meson exchange and pion rescattering contributions to the cross-section for $pp \to pp\pi^0$*, Phys.Lett. **B388** (1996), 679–685.

[vKNM00] U. van Kolck, J. Niskanen, and G. Miller, *Charge symmetry violation in $pn \to d\pi^0$ as a test of chiral effective field theory*, Phys.Lett. **B493** (2000), 65–72.

[Wei79] S. Weinberg, *Phenomenological Lagrangians*, Physica **A96** (1979), 327.

[Wei90] S. Weinberg, *Nuclear forces from chiral Lagrangians*, Phys.Lett. **B251** (1990), 288–292.

[Wei91] S. Weinberg, *Effective chiral Lagrangians for nucleon-pion interactions and nuclear forces*, Nucl.Phys. **B363** (1991), 3–18.

[Wei92] S. Weinberg, *Three body interactions among nucleons and pions*, Phys.Lett. **B295** (1992), 114–121.

[WLCM12] A. Walker-Loud, C. E. Carlson, and G. A. Miller, *The Electromagnetic Self-Energy Contribution to $M_p - M_n$ and the Isovector Nucleon Magnetic Polarizability*, Phys.Rev.Lett. **108** (2012), 232301.

[ZAB+98] J. Zhao, R. Abegg, A. Berdoz, J. Birchall, J. Campbell, et al., *Precision measurement of charge symmetry breaking in np elastic scattering at 347-MeV*, Phys.Rev. **C57** (1998), 2126–2141.

Lebenslauf

Arseniy Filin

Persönliches
Geboren am 24. April 1986
in Moskau, Russland
Ledig

Studium und Ausbildung

seit 10/2012	Institut für Theoretische Physik II, Ruhr-Universität Bochum Doktorand
09/2007 – 07/2009	Moskauer Ingenieur-Physikalisches Institut (Staatliche Universität) Institut für Theoretische Kernphysik Magister in der Fachrichtung "Angewandte Mathematik und Physik"
09/2003 – 07/2007	Moskauer Ingenieur-Physikalisches Institut (Staatliche Universität) Institut für Theoretische Kernphysik Bakkalaureus in der Fachrichtung "Angewandte Mathematik und Physik"
09/1993 – 06/2003	Schulbesuch in Tschernogolowka, Moskauer Gebiet, Russland

Berufliche Erfahrung

seit 04/2011	Institut für Theoretische Physik II, Ruhr-Universität Bochum Wissenschaftlicher Mitarbeiter
12/2009 – 03/2011	Helmholtz-Institut für Strahlen- und Kernphysik, Universität Bonn Wissenschaftlicher Mitarbeiter
10/2008 – 07/2009	Institut für Kernphysik (IKP-3), FZ Jülich Studentische Hilfskraft

Publikationsliste

1. A. A. Filin, V. Baru, E. Epelbaum, C. Hanhart, H. Krebs and F. Myhrer, "Pion production in nucleon-nucleon collisions in chiral effective field theory with Delta(1232)-degrees of freedom," Phys. Rev. C **88** (2013) 064003.
2. V. Baru, E. Epelbaum, A. A. Filin, C. Hanhart, U.-G. Meißner and A. V. Nefediev, "Quark mass dependence of the X(3872) binding energy," Phys. Lett. B **726** (2013) 537.
3. A. A. Filin, V. Baru, E. Epelbaum, H. Krebs, C. Hanhart, A. E. Kudryavtsev and F. Myhrer, "Pion production in nucleon-nucleon collisions in chiral effective field theory: next-to-next-to-leading order contributions," Phys. Rev. C **85** (2012) 054001.

4. V. Baru, A. A. Filin, C. Hanhart, Yu. S. Kalashnikova, A. E. Kudryavtsev and A. V. Nefediev, "Three-body $D\bar{D}\pi$ dynamics for the X(3872)," Phys. Rev. D **84** (2011) 074029.

5. A. A. Filin, "Charge symmetry breaking in $pn \to d\pi^0$," Int. J. Mod. Phys. A **26** (2011) 592.

6. A. A. Filin, A. Romanov, V. Baru, C. Hanhart, Yu. S. Kalashnikova, A. E. Kudryavtsev, U.-G. Meißner and A. V. Nefediev, "Comment on 'Possibility of Deeply Bound Hadronic Molecules from Single Pion Exchange'," Phys. Rev. Lett. **105** (2010) 019101.

7. A. Filin, V. Baru, E. Epelbaum, J. Haidenbauer, C. Hanhart, A. E. Kudryavtsev and U.-G. Meißner, "Extraction of the strong neutron-proton mass difference from the charge symmetry breaking in $pn \to d\pi^0$," Phys. Lett. B **681** (2009) 423.

Bochum, 14. April 2014